

# A Permian fish reveals widespread distribution of neopterygian-like jaw suspension

T. Argyriou<sup>1,2,3,4\*</sup>, S. Giles<sup>5,6</sup>, M. Friedman<sup>6,7</sup>

<sup>1</sup>Current Address: Department of Earth and Environmental Sciences, Paleontology & Geobiology, Ludwig-Maximilians-Universität München, München, Germany

<sup>2</sup>Current Address: GeoBio-Center, Ludwig-Maximilians-Universität München, München, Germany

<sup>3</sup>Paleontological Institute and Museum, University of Zurich, Switzerland

<sup>4</sup>CR2P, MNHN-CNRS-Sorbonne Université, Muséum National d'Histoire Naturelle, Paris, France

<sup>5</sup>School of Geography, Earth and Environmental Sciences, University of Birmingham, UK

<sup>6</sup>Research associate, The Natural History Museum, London, UK

<sup>7</sup>Museum of Paleontology and Department of Earth and Environmental Sciences, University of Michigan, USA

## Abstract

The actinopterygian crown group (comprising all living ray-finned fishes) originated by the end of the Carboniferous. However, most late Paleozoic taxa are stem actinopterygians, and broadly resemble stratigraphically older taxa. The early Permian †*Brachydegma caelatum* is notable for its three-dimensional preservation and past phylogenetic interpretations as a nested member of the neopterygian crown. Here, we use computed microtomography to redescribe †*Brachydegma*, uncovering an unanticipated combination of primitive (e.g., aortic canal; immobile maxilla) and derived (e.g., differentiated occipital ossifications; posterior stem of parasphenoid; two accessory hyoidean ossifications; double jaw joint) dermal and endoskeletal features relative to most other Paleozoic actinopterygians. Some of these features were previously thought to be restricted to the neopterygian crown. The precise phylogenetic position of †*Brachydegma* is unclear, with placements either on the

polypterid stem, or as an early-diverging stem neopterygian. However, our analyses decisively reject previous placements of †*Brachydegma* in the neopterygian crown. Critically, we demonstrate that key-endoskeletal components of the hyoid portion of the suspensorium of crown neopterygians appeared deeper in the tree than previously thought.

## Introduction

Living ray-finned fishes (Actinopterygii) include three lineages: the early diverging Cladistia (bichirs and reedfish, 14 spp.), the Chondrostei (sturgeons and paddlefishes, 27 spp.), and the markedly speciose Neopterygii (Holostei [gars and bowfin], 8 spp. + Teleostei, ~32,000 spp.) (Nelson et al., 2016). Molecular and fossil evidence suggests that these lineages diverged in the Devonian–Carboniferous interval, with an early Carboniferous divergence age estimate being more likely (Broughton et al., 2013; Near et al., 2013; Giles et al., 2017). A number of key characters supporting relationships amongst major living actinopterygian groups relate to internal parts of the skeleton, and ambiguities in the relationships of some extinct lineages to these extant radiations might reflect limited information on endoskeletal traits in fossils. The majority of phylogenetic analyses incorporating extant and Palaeozoic-Mesozoic ray-fins have traditionally recovered cladistians, the extant sister lineage to all other living actinopterygians, as branching deep within a Devonian radiation (Patterson, 1982; Gardiner, 1984; Long, 1988; Gardiner and Schaeffer, 1989; Gardiner et al., 1996; Coates, 1999; Gardiner et al., 2005; Xu et al., 2014, but see Cloutier and Arratia, 2004; Mickle et al., 2009). More recently, the hypothesis of †scanilepids as stem-cladistians (Giles et al., 2017) has led to a major revision of early ray-fin relationships, with the notable result that almost all Devonian-Permian and many Triassic taxa fall on the actinopterygian stem. Notwithstanding analyses that recover cladistians as a deep Devonian radiation, surprisingly few Paleozoic taxa [e.g., †*Platysomus* (Moy-Thomas and Dyne, 1938), †eurynotiforms (Sallan and Coates, 2013; Friedman et al., 2018), †*Discoserra* (Lund, 2000; Hurley et al., 2007), †*Ebenaqua* (Campbell and Phuoc, 1983), †*Acentrophorus* (Gill, 1923; Gardiner, 1960; Patterson, 1973)] have been resolved or verbally placed within the actinopterygian



50 crown (Cloutier and Arratia, 2004; Hurley et al., 2007; Xu et al., 2014; Giles et al., 2017; Argyriou et  
51 al., 2018; Latimer and Giles, 2018), and knowledge of the endoskeleton of these taxa is rudimentary at  
52 best.

53 Features of the hyoid arch bear on the relationships of living actinopterygian lineages (Patterson, 1973,  
54 1982; Véran, 1988; Gardiner et al., 1996). Each extant lineage has a distinctive geometry and  
55 arrangement of the hyoid skeleton, with major differences relating to the size and number of elements  
56 between the dorsal and ventral components of the arch. The presence of a single element linking the  
57 dorsal (hyomandibula) and ventral (ceratohyal) components characterizes cladistians (Allis, 1922;  
58 Jollie, 1984; Claeson et al., 2007). Two intermediate elements are present in chondrosteans (Grande  
59 and Bemis, 1991; Hilton et al., 2011) and neopterygians (Patterson, 1973; Grande and Bemis, 1998;  
60 Grande, 2010; Arratia, 2013). In halecomorphs, these ossifications are arranged in a sub-parallel  
61 manner, with one of these articulating with the lower jaw and forming the so-called double jaw joint  
62 (Patterson, 1973, 1982; Grande and Bemis, 1998). A single accessory element has been described for  
63 the majority of Devonian–Triassic non-neopterygian actinopterygians (e.g. †*Mimipiscis* [Gardiner,  
64 1984]; †*Coccocephalichthys* [Poplin and Véran, 1996]; †*Pteronisculus* [Nielsen, 1942];  
65 †*Australosomus* [Nielsen, 1949]; †*Gogosardina* [Choo et al., 2009])). However, Véran (1988)  
66 indicated the presence of two elements in some Triassic–Jurassic non-neopterygian taxa, such as  
67 †*Boreosomus reuterskioldi* and †*Ptycholepis bollensis*. Two intermediary elements, geometrically  
68 arranged in a manner similar to that of halecomorphs, are unambiguously present in the Early Triassic  
69 †parasemionotids (Patterson, 1973, 1982; Olsen, 1984; Gardiner et al., 1996; but see Arratia, 2013 for  
70 a possible similar geometry in early teleosts), as well as younger extinct groups, like †pycnodonts  
71 (Nursall and Maisey, 1987; Gardiner et al., 1996; Kriwet, 2005). These patterns have inspired two  
72 interpretive models for the evolution and homology of hyoid arch elements. Patterson (1982) proposed  
73 that a single intermediate element represented the primitive actinopterygian condition, but this was  
74 subsequently disputed by Véran (1988) who countered that two elements are plesiomorphic for the  
75 group. There are a number of challenges to distinguishing between these hypotheses, not least the  
76 difficulty in interpreting incomplete and poorly preserved fossils, a lack of detailed descriptions for

77 articulated and in-situ fossil hyoid arches, and also the varying degrees of mineralization of these  
78 elements in vivo. Accessory hyoid elements represent a key source of anatomical support for  
79 actinopterygian relationships, but there is a profound lack of information for these features in all but a  
80 handful of Paleozoic and early Mesozoic taxa (Patterson, 1973, 1982; Olsen, 1984; Véran, 1988;  
81 Gardiner et al., 1996; Gardiner et al., 2005).

82 Previous research on the endoskeletal anatomy of fossil actinopterygians has mostly focused on  
83 generalized Devonian–Carboniferous forms (Poplin, 1974; Gardiner, 1984; Poplin and Véran, 1996;  
84 Coates, 1999; Hamel and Poplin, 2008; Giles et al., 2015a; Giles et al., 2015b; Pradel et al., 2016), or  
85 both generalized and anatomically specialized Triassic taxa (Nielsen, 1942, 1949; Patterson, 1975;  
86 Olsen, 1984; Giles et al., 2017; Argyriou et al., 2018; Latimer and Giles, 2018). The Permian is an  
87 important link between the stem-actinopterygian dominated Devonian–Carboniferous and the  
88 neopterygian-rich faunas of Triassic and younger strata. However, the Permian also represents a major  
89 knowledge gap for all aspects of actinopterygian biology (Hurley et al., 2007; Friedman and Sallan,  
90 2012; Sallan, 2014), including endoskeletal structure (for partially preserved examples see Aldinger,  
91 1937; Dunkle, 1946; Jessen, 1972; Figueroa et al., 2019).

92 †*Brachydegma caelatum* is one of the few Permian ray-fins represented by three-dimensional cranial  
93 material, and constitutes a key taxon in debates on patterns and timing of major divergences within  
94 actinopterygian phylogeny (Hurley et al., 2007; Near et al., 2012; Broughton et al., 2013; Xu et al.,  
95 2014; Giles et al., 2017; summarized in Fig. 1). Known only from two specimens (Figs. 2–4;  
96 Appendix Fig. 1) from the Cisuralian (early Permian) Red Beds of Texas, USA (Dunkle, 1939),  
97 †*Brachydegma* has been previously interpreted exclusively through external examination of the type  
98 specimen, leading to radically divergent phylogenetic interpretations (Fig. 1). †*Brachydegma* was  
99 initially aligned with anatomically generalized groups of uncertain monophyly that likely represent  
100 stem actinopterygians (†elonichthyids [Dunkle, 1939] or †acrolepidids [Schaeffer, 1973]), but a later  
101 reappraisal identified it as a halecomorph, predating previous fossil-based minima for the age of the  
102 neopterygian crown and the split between holostean and teleostean lineages by roughly 30 Ma (Hurley  
103 et al., 2007). Subsequent assessments (Fig. 1) challenged the halecomorph (Near et al., 2012; Xu et al.,

2014) or even total-group neopterygian (Broughton et al., 2013; Giles et al., 2017) affinities of †*Brachydegma*. None, however, provided new anatomical data for the specimens.

Here we use computed microtomography (μCT) to reveal, for the first time, the character-rich anatomy of the braincase, mandibular and hyoid arches, branchial skeleton, pectoral girdle and the anterior portion of the axial skeleton of †*Brachydegma* (Appendix Fig. 2), with the goal of informing the phylogenetic position of this enigmatic taxon. We find that, unlike other known Palaeozoic ray-fins, the internal anatomy of †*Brachydegma* bears a number of unexpected specializations and character combinations. Critically, the hyoid arch anatomy of †*Brachydegma* indicates a more complicated evolution of accessory hyoid elements and their involvement in jaw suspension than is currently appreciated. Moreover, †*Brachydegma* presents the first —almost complete and largely articulated— model of branchial anatomy in a Permian actinopterygian, as well as a rare example of pectoral and axial endoskeletal structure from the latter part of the Paleozoic.

## Results

### Systematic paleontology:

Actinopterygii sensu Goodrich 1930

†*Brachydegma caelatum* Dunkle 1939

**Material:** Museum of Comparative Zoology (Harvard University) MCZ VPF 6503, †*Brachydegma caelatum*, holotype, slightly compressed laterally, preserving cranial and anterior postcranial skeleton; MCZ VPF 6504, †*Brachydegma caelatum*, paratype, dorsoventrally compressed, with dermal skeleton eroded away, but preserving internal cranial and aspects of anterior postcranial skeleton.

**Locality and geological background:** Both specimens of †*Brachydegma* come from the stratigraphically oldest deposits of the northern part of the Clear Fork Formation (formerly recognized as the Arroyo Formation; see Nelson et al., 2013), Indian Creek, Baylor County, Texas (Dunkle, 1939). The Clear Fork formation has been biostratigraphically dated to the North American

‘Leonardian’ Stage, which largely overlaps with the late Kungurian (Stage range: 283.5–273.01 Ma)–early Roadian (Stage range: 273.01–266.9 Ma) interval of the late Cisuralian (Nelson et al., 2013). The Clear Fork Formation is characterized by ferruginous, calcitic–sandy, terrigenous facies (Dunkle, 1939; Olson, 1989; Nelson et al., 2013), broadly assigned to coastal floodplain environments (Nelson et al., 2013). The accompanying vertebrate fauna includes †xenacanth, lungfishes, and tetrapods, including the †pelycosaur †*Dimetrodon* (Olson, 1989).

**Revised diagnosis:** Actinopterygian characterized by the following unique combination of characters: occiput comprising three separate ossifications; absence of a dermal basipterygoid process; parasphenoid reaching posterior to the ventral otic fissure; lateral dorsal aortae extending along the ventral surface of parasphenoid; immobile maxilla in broad connection with the palate; coronoid process absent or greatly reduced; at least three suborbitals; at least two ‘accessory opercles’ below dermohyal; independently ossified symplectic and interhyal with sub-parallel arrangement.

#### **Exoskeletal cranial anatomy.**

We provide a re-description of †*Brachydegma caelatum*, mostly based on the better-preserved type specimen MCZ VPF 6503. We present detailed photographs and illustrations (Figs 2–4). For previous interpretations see Dunkle (1939) and Hurley et al. (2007). We only refer to the paratype MCZ VPF 6504 when it shows features absent from the type specimen. Our anatomical interpretations are in broad agreement with the original description (Dunkle, 1939), and are largely based on direct observations of the fossils, since superficial ossifications were not possible to reconstruct from the  $\mu$ CT data (Appendix Fig. 2). Many parts of the external anatomy are badly fractured or preserved. This is particularly the case for the rostral area of the holotype, where individual bones have been subject to varying interpretations by past authors. The dermal ossifications of the skull are externally ornamented with densely packed and often anastomosing vermiform ridges.

*Skull roof.* The rostrum and the anterior part of the skull roof are incompletely preserved. A fragmentary bone bearing a conical tooth represents a fragment of the likely paired premaxilla. The frontals are longer than wide, with their posteroventral margin bearing an indentation for the insertion

of the dermopterotics. The parietals are quadrangular, and the midline suture between the bilateral counterparts of the frontals and parietals anastomoses. Each parietal bears a lateral extension that inserts into the body of the adjacent dermopterotic. There is no independent accessory parietal as suggested by Dunkle (Dunkle, 1939). The dermopterotics are longer than wide. The left dermopterotic appears divided in two parts (dpt, Figs 2–4), but this reflects a combination of breakage and the lateral process of the associated parietal. On the right side of the skull, the anterior and posterior portions of the dermopterotic are clearly connected by a ventral bridge of bone and unambiguously constitute a single ossification, in contrast to the separate intertemporal and supratemporal of many Devonian and some Carboniferous actinopterygians (Gardiner, 1984; Gardiner and Schaeffer, 1989). A pair of lateromedially elongate lateral extrascapulars lie posterior to the parietals.

*Circumorbital, cheek and operculogular ossifications:* The canal-bearing dermosphenotic (postorbital in Dunkle, 1939 and Hurley et al., 2007) is sub-rectangular, with a posterior ramus. Its anterior end is fragmented, but it likely did not reach far anteriorly above the orbit. We recognize a triangular area of bone on both sides of the skull, framed by the dermopterotic posteriorly, the frontal dorsomedially, and the dermosphenotic ventrolaterally. This region was interpreted as a dermosphenotic by Dunkle (1939) and Hurley et al. (2007), but it shows no obvious signs of pores for a sensory canal. Three infraorbitals (named here as infraorbital, jugal, lachrymal) surround the posterior and ventral margins of the orbit, with the lachrymal bearing a possible anterior thickening. The dislocated canal-bearing element situated immediately dorsal to the lachrymal on the right side of the type specimen is a putative antorbital. Another, more elongate canal-bearing bone is present on the left side of the specimen in association with the tooth-bearing fragment of the premaxilla. Previously identified as an antorbital (Hurley et al., 2007), it is best identified as a nasal (na, Figs 3–4) based on the presence of an ascending arm and a possible narial notch. Another possible nasal, or alternatively a fragment of the rostral shield, is present in the paratype, but in a very poorly preserved state (Appendix Fig. 1). At least two supraorbitals must have been present, as evidenced by corresponding sockets on the right frontal. At least three anamestic suborbitals arranged in a dorsoventral series separate the infraorbitals from the preopercle. A supramaxilla is absent. The preopercle is taller than wide, and sits almost

upright in the cheek. It bears an overlap area for the maxilla, shown clearly on the right side of the skull where the two bones have pulled away from each other. The pronounced ventral limb of the preopercle connects to a small quadratojugal. Three additional dorsoventrally arranged anamestic bones separate the preopercle from the opercular series, on the right side of the type specimen (Fig. 2). The dorsal-most constitutes the unfused dermohyal, and the ventral two represent accessory opercles. The latter are broadly comparable to those of the †‘acrolepidids’ sensu lato (Aldinger, 1937; Nielsen, 1942). The opercle is rhomboidal and is of almost equal size to the more quadrate subopercle. At least eight branchiostegal rays are present. The two lateral gulars are rostrocaudally elongate and underlie the posterior half of the lower jaw. The median gular is longer than wide, and of subequal length to the lateral gulars.

*Shoulder girdle:* The dermal skeleton of the pectoral girdle is largely preserved on the right side of the type specimen. The posttemporal is subquadrate and seems to form an anterolateral ramus, likely excluding the extrascapular from the lateral margin of the skull roof. An additional dermal ossification lies ventral to the posttemporal, but is partially obscured by it. We identify this triangular ossification as a presupracleithrum. The supracleithrum is ovoidal and larger than the posttemporal, reaches further posteriorly than the cleithrum, and forms a strongly convex and serrated posterior margin. The postcleithra are poorly-preserved, but appear to have been three to four in number. This series includes the ‘accessory’ postcleithrum of Hurley et al. (Hurley et al., 2007). Fringing fulcra line the anterior margin of the pectoral fin.

## **Endoskeletal anatomy.**

*Braincase and parasphenoid:* The braincase comprises several ossifications, with large gaps presumably filled by cartilage in life. Three distinct ossifications contribute to the occipital region (boc, exo, Fig. 5): a basioccipital and a pair of exoccipitals, comparable to non-teleost neopterygians (Patterson, 1975; Grande and Bemis, 1998; Grande, 2010). The anterior margin of the occiput is well demarcated, likely indicating an unmineralized oticooccipital fissure. The basioccipital projects

posteriorly and encloses a short endoskeletal aortic canal. The exoccipitals form the dorsal margin of the notochordal opening and surround the foramen magnum. Lateral to the foramen magnum, the exoccipitals expand posteriorly, and anteriorly flare laterally, forming possible craniospinal processes. Unlike in many crown neopterygians (Patterson, 1975; Grande and Bemis, 1998; Grande, 2010), the exoccipitals do not enclose the vagus nerve. The otic capsules are poorly preserved and lie within an area of low contrast in both specimens, rendering them impossible to interpret from the scans. The sphenoid ossification is partially preserved in the paratype, and exhibits a deep, paired posterior myodome (osph, pmy, Fig. 5F,G). The interorbital septum forms as a thick median pillar. There is no median optic foramen, with the optic nerves entering each orbit separately. Identification of accessory nerve and venous foramina is difficult in both specimens. It is thus not possible to confidently determine whether features such as spiracular canals or endoskeletal basiptyergoid processes were present.

The parasphenoid (psp, Fig. 5) underlies most of the braincase, extending far posterior to the ventral fissure but terminating before reaching the back of the braincase. A similar condition is present in all crown actinopterygians (Allis, 1922; Patterson, 1975; Olsen, 1984; Hilton et al., 2011; Giles et al., 2017), †saurichthyids (Argyriou et al., 2018), and several Paleozoic forms of uncertain affinity (e.g., †platysomids [Moy-Thomas and Dyne, 1938], †eurynotiforms [Friedman et al., 2018], and †*Sphaerolepis* [Stamberg, 1991]). The lateral dorsal aortae of †*Brachydegma* exit the basicranium and extend along the ventral surface of the parasphenoid, divided by a median keel. The posterodorsally directed ascending processes are well-developed and bear a spiracular groove. A dermal basiptyergoid process is absent. The parasphenoid appears to be edentulous, but this may be an artefact of preservation or lack of contrast. The presence of a buccohypophyseal canal could not be ascertained. The anterior process of the parasphenoid, anterior to the orbitosphenoid region of the braincase, exhibits a posterodorsally–anteroventally directed groove on each side (apal, Fig. 5A,C,F,H). These grooves either transmitted the parabasal canals, or were employed in the articulation of the palate, as in e.g., polypterids and sarcopterygians (Lemberg et al., 2021).

234 *Palate and associated ossifications:* The dermal and endoskeletal palate of †*Brachydegma* (Fig. 6A–E,  
235 H,J) is deep along most of its length, with a convex, imperforate dorsal margin. Processes for  
236 articulation with the braincase and parasphenoid are not apparent. Ventrally, the palate forms a broad  
237 flange that abuts the prominent medial shelf of the maxilla (mxhl, vpl, Fig. 6C–E,K). This indicates a  
238 strong connection between the two, rendering maxillary kinesis impossible. A reinforced lateral palatal  
239 (ectopterygoid) process forms the anterior border of the adductor notch of the palate, and abuts the  
240 maxilla. Dermal palatal bones are difficult to separate in tomograms, but appear to comprise multiple  
241 ossifications. A long and broad accessory vomer lies along the medial surface of the anterior half of  
242 the palate. The quadrate is located posteroventrally and bears two small articular condyles and a gentle  
243 posterior groove. A dorsolateral flange on the palate, slightly anterior to the level of the jaw  
244 articulation, is the only trace of the metapterygoid, and seems to resemble the metapterygoid process  
245 of neopterygians (Olsen, 1984; Arratia and Schultze, 1991). An autopalatine has not been located in  
246 either specimen and was probably not mineralized in life. An ossified labial element is present near the  
247 ventral opening of the mandibular adductor chamber, in both sides of the type specimen (calg, lbe, Fig.  
248 6A,F,G). The one of the right side is more completely preserved, and is approximately tear-shaped and  
249 perforated, resembling the ones found in e.g., †*Boreosomus reuterskioldi* and †*Ptycholepis bollensis*  
250 (Véran, 1996).

251 *Hyoid arch:* The hyomandibula (Fig. 7A–E) forms rather broad and distinct dorsal and ventral limbs,  
252 is perforate, and appears to bear a short and broad opercular process. An unfused dermohyal sits on the  
253 lateral surface of the dorsal limb of the hyomandibula. On the left side of the holotype, two accessory  
254 hyoid elements are preserved, in close association with the ventral tip of the hyomandibula (ih, sy,  
255 Figs. 8A–E), and are aligned subparallel to one another. We identify the anterior ossification as a  
256 symplectic and the posterior ossification as an interhyal based on their position, morphology, and  
257 relationship with other ossifications (see discussion). The symplectic is subquadrangular, and  
258 articulates with the anteroventral tip of the hyomandibula (syf, Fig. 8B). Its anterior surface forms a  
259 keel, which likely fit in a groove on the posterior surface of the quadrate (qdgr, Fig. 8B). The  
260 anteroventral tip of the symplectic forms a thickening, or condyle, which inserts in a facet on the



261 posterior surface of the articular; its posteroventral tip is produced as a thin, ventrally directed process,  
262 which contacts the posterior surface of the articular (cnd, vpsy?, Fig. 8C–E). A faint groove on the  
263 anterodorsal face is likely for the passage of the afferent mandibular artery (afmd, Fig. 8C–E). A  
264 similar groove is present in some †parasemionotids (NHMD 74424 A; Fig. 8F–I), and the putative  
265 symplectic of †*Pteronisculus* (Fig. 8J–M). The presence of this feature in the latter is congruent with  
266 previous observations made by Véran on the putative symplectics of stem actinopterygians (Véran,  
267 1988). The more posterior of the two elements present in †*Brachydegma*, identified as an interhyal, is  
268 rod-shaped, and articulates with the posteroventral tip of the hyomandibula. Only the more robust,  
269 anterior ossification (symplectic) is apparent on the left side of the type specimen (Fig. 7A,B). The  
270 region between the hyomandibula and ceratohyal is poorly preserved in the paratype and thus the  
271 presence of accessory elements cannot be determined (Appendix Fig. 2F). The contact between the  
272 symplectic and articular—a double jaw joint—as well as the sub-parallel arrangement of the  
273 symplectic and the interhyal resemble that of crown neopterygians, such as †parasemionotids (Stensiö,  
274 1932; Patterson, 1973; Olsen, 1984; Fig. 8F–I), †*Parapholidophorus* (Arratia, 2013), as well as  
275 †pycnodonts (Nursall and Maisey, 1987; Gardiner et al., 1996; Kriwet, 2005). A single, laterally  
276 grooved, plate-like ceratohyal is ossified on each side of the hyoid arch of †*Brachydegma* (Figs. 7E,  
277 9A).

278 *Branchial skeleton:* The branchial skeleton of the type specimen is nearly complete (Fig. 9), although  
279 the pharyngobranchials are somewhat disarticulated and shifted from their life positions. We have  
280 attempted to reconstruct the branchial series, but the identification and positioning of the  
281 suprapharyngobranchials remains somewhat speculative. The branchial skeleton of †*Brachydegma*  
282 exhibits the common motif of five ossified branchial arches. One or two basibranchials are preserved  
283 (bb/bh?, bb, Fig. 9C,E). The anteriormost and smallest of the two exhibits a subtriangular cross  
284 section; it could alternatively constitute a dislocated basihyal, similar to that of e.g., †*Pteronisculus*  
285 (Nielsen, 1942). The second (or only) basibranchial is subtriangular in cross section, and exhibits a flat  
286 dorsal surface. This element is constricted at mid-length. Five ceratobranchials are present (cb1–5, Fig.  
287 9). The first four ceratobranchials are curved. Their posteroventral surface is grooved, whereas

288 anterodorsally they accommodate a series of small, multicuspid rakers. The fifth ceratobranchial is  
289 reduced to a tiny rod-like structure. The dorsal bones of the gill arches are partially disarticulated. The  
290 first three epibranchials (ep1–3, Fig. 9) bear uncinat processes, with the first two being particularly  
291 well-developed, like in e.g., †*Australosomus* (Nielsen, 1949). The uncinat processes of the second  
292 and third epibranchials are oriented medially. The fourth epibranchial is short and wide and forms a  
293 long and thin anterior process, and a laterally expanded plate supporting the passage of the efferent  
294 branchial artery. No expanded toothplates are associated with the epibranchials. The first  
295 infrapharyngobranchial is rod-shaped and edentulous. The element tentatively identified as the first  
296 suprapharyngobranchial is hooked, possibly engulfing its corresponding efferent arterial vessel. The  
297 second infrapharyngobranchial is wider and plate-like, and bears putative teeth on its ventral surface.  
298 The second suprapharyngobranchial is laterally compressed and forms a weakly forked distal proximal  
299 margin, which likely aided in its suspension from the occipital region. An additional rod-like element  
300 associated with the third branchial arch is tentatively identified as an ossified third  
301 infrapharyngobranchial.

302 *Jaws:* The maxilla exhibits a robust horizontal process (Fig. 6J), which supports a single series of  
303 large, pointed teeth. The posterior plate of the maxilla is well developed, flat and tall, with its  
304 posterodorsal margin fitting in a notch on the preopercle. On the left side of the specimen (Fig. 2C),  
305 the maxilla is slightly disarticulated from the preopercle, which likely gave the impression of  
306 maxillary kinesis (hereby deemed absent) to previous authors (Hurley et al., 2007). Medially, the  
307 maxilla forms a well-developed horizontal lamina for attachment to the dermal palate (mxhl, Fig. 6C–  
308 E,J), similar to that of stem actinopterygians like †*Mimipiscis*, †*Pteronisculus*, or †*Australosomus*  
309 (Nielsen, 1942, 1949; Gardiner, 1984). The maxilla of MCZ VPF 6504 does not possess a posterior  
310 notch, contrasting a previous reconstruction of this feature (Hurley et al., 2007). We do not find  
311 evidence for a rod-like articular process with the ethmoid region of the skull like that of neopterygians  
312 (see e.g., *Amia* in Grande and Bemis, 1998). Instead, a short and thin, plate-like anterior process for  
313 firm articulation with the ethmoid and dermal snout ossifications of the skull is present (mxp, Fig. 6J).  
314 The dentary (dnt, Figs. 2–4, 7A,F–H) is the principal bone of the lateral surface of the jaw, and bears a

single row of teeth. The prearticular occupies most of the mesial surface of the lower jaw, but no teeth are apparent in the tomograms. Coronoids cannot be distinguished from the prearticular. Both the external and the  $\mu$ CT-aided examinations of the holotype suggest the presence of a surangular (sang, Fig. 7F) on the posterodorsal corner of the jaw and an angular on the posteroventral, but sutures between these bones could not be reliably determined. There is no well-developed coronoid process, but a faint one at best formed by the surangular alone. This process —if accepted as such— clearly differs from that of deeply diverging crown neopterygians, which receives contributions by the dentary and the prearticular (Olsen, 1984; Grande and Bemis, 1998; Fig. 8F). What was previously reconstructed as a pronounced coronoid process on the type specimen (Hurley et al., 2007) corresponds to a smooth, gentle shelf of the dentary for overlap by the maxilla (mxs, Fig. 7F). The deep adductor fossa is surrounded by the articular posteriorly, the prearticular medially, and the surangular and dentary laterally. In addition to the two depressions for the quadrate, the articular bears a posterior flat facet for the insertion of the condyle of the symplectic (syf, Fig. 7G,H).

*Postcranial skeleton:* The pectoral girdle (Fig. 10A–G) is largely preserved. The clavicles are broad triangular plates covering the anterior process of the massive cleithra, resembling the primitive (Nielsen, 1942; Gardiner, 1984) condition associated with non-neopterygians (Jollie, 1984; Hilton et al., 2011) but retained in †parasemionotids (Olsen, 1984) and some stem teleosts (Arratia, 2013). The cleithra lack the well-developed postbranchial lamina of many deeply diverging actinopterygians like †*Trawdenia* (Coates and Tietjen, 2018), but also extant chondrosteans (Hilton et al., 2011) and the parasemionotid †*Watsonulus* (Olsen, 1984). The cleithrum is rather tall and forms an acute dorsal tip. The posterior notch of the cleithrum faces posteroventrally. The scapulocoracoids of the type specimen could be largely reconstructed (scc, Fig. 10C–G), revealing a peculiar set of characters. The dorsal (scapular) portion of the scapulocoracoid is well-developed on both sides, whereas the ventral (coracoid) portion is not preserved and was conceivably cartilaginous. This is supported by the presence of a subhorizontal facet (fcpl, Fig. 10D) on the mesial surface of the middle region of the scapulocoracoid. The scapulocoracoid is attached to the cleithrum by means of a broad dorsal plate, and forms a dorsal, medially hooked, protrusion, which corresponds to the dorsal end of the

mesocoracoid arch (dmca, Fig.10D). The remainder of the mesocoracoid arch is not present and may have been cartilaginous. Sockets on the ventromedial side of the ‘scapular’ portion of the bone likely received either the ventral tip of a cartilaginous mesocoracoid arch and/or the putatively cartilaginous coracoid portion of the bone (vmca, Fig. 10D). A dorsal scapular process is not preserved. The supracoracoid foramen is oval and directed laterally–lateroventrally. It is preceded by a smaller round foramen. The middle posterior region for the articulation of the radials is medioventrally directed, as in most fossil and recent actinopterygians (Jessen, 1972). A single series of rod-like radials lie subparallel to each other. A short, stocky element is tentatively identified as a propterygium (ppt?, Fig. 10F), but we cannot confirm whether it is perforate or not.

The notochord is unconstricted, and only arcual elements are apparent (arc, bd, bv, Fig. 10H–J). Supraneurals are not observed in the anterior vertebral segments. Dorsally, the first abdominal vertebral segment comprises a stout, paired basidorsal bearing a short neural spine and a prezygapophysis. More posterior basidorsals exhibit thinner but longer neural spines and thinner prezygapophyses. A faint transverse canal extends along the medial surface of each neural hemispine. As in most crown actinopterygians, excluding teleosts (Arratia, 2013), epineural processes are not developed. A median hemi-cylindrical element in one of the anteriormost vertebral segments lacks parapophyses and might have resulted from the fusion of two basiventrals. However, all remaining basiventrals are paired and bear short, ventrolaterally expanding parapophyses, though no ossified ribs are present. The rhomboid scales (Fig. 10K) of †*Brachydegma* exhibit a dorsal articular peg and a small anterodorsal process. Their posterior scale margin forms acute serrations.

### Phylogenetic results.

*Equally weighted parsimony:* Our equally weighted parsimony analysis recovered 1412 most parsimonious trees of 1652 steps (Fig. 11). The crown neopterygian clade receives low Bremer support in our analysis (Bremer Decay Index [BDI]=2), and is diagnosed on the basis of eight synapomorphies, two of which are unique (marked here with \*): anterior expansion of lachrymal

(C.53); presence of multiple rami of infraorbital canal on jugal (C.56); mobile maxilla (C.73); presence of a peg-like anterior maxillary process (C.74\*); presence of an interopercle (C.119\*); internal carotid artery piercing the parasphenoid (C.180); presence of two ossifications of the ceratohyal (C.219); presence of ossified centra (C.287). These are all absent in †*Brachydegma*, which furthermore lacks any form of coronoid process, an essential component of the crown neopterygian hallmark. Therefore, †*Brachydegma* can be confidently excluded from the neopterygian crown, contrary to previous hypotheses (Hurley et al., 2007).

In our parsimony strict consensus tree (Fig. 11), †*Brachydegma* is resolved as sister to a clade containing †birgeriids and †scanilepiforms + polypterids. This topology is weakly supported (BDI=1) by three synapomorphies: extrascapular not reaching lateral margin of skull-roof (C.45); presence of three or more suborbitals (C.55); differentiation of braincase ossifications (C.159). †*Birgeria* is resolved as sister to †scanilepiforms + polypterids, receiving equally low support (BDI=1), on the basis of two ambiguous synapomorphies: imperforate hyomandibula (C.218); absence of a triradiate scapulocoracoid (C.243). We note ambiguities regarding this topology resulting from a poor understanding of the endoskeleton of †*Birgeria* (Nielsen, 1949).

Contrasting recent works (Giles et al., 2017; Argyriou et al., 2018; Latimer and Giles, 2018), †Saurichthyiformes are recovered as sister to Chondrostei (Gardiner and Schaeffer, 1989; Gardiner et al., 2005). Interestingly, a weakly supported (BDI=2) deep-bodied clade of durophagous taxa — comprising †pycnodonts and †dapediids — is recovered within the neopterygian crown (contra (Latimer and Giles, 2018) following the addition of †*Neoproscinetes penalvai*, the cranial endoskeleton of which (Nursall and Maisey, 1987; Machado, 2008) is better known than that of most other †pycnodonts (see also Hurley et al., 2007). This deep-bodied clade is resolved as sister to holosteans, but the interrelationships of most of its constituents are unclear. These topologies are also present in the agreement subtrees (Appendix Fig. 3).

*Constrained equally weighted parsimony analyses:* We ran additional unweighted parsimony experiments to investigate the number of steps needed to produce previously suggested topologies of

394 †*Brachydegma*. When †*Brachydegma* is constrained with halecomorphs and †*Watsonulus* (cf. Hurley  
395 et al., 2007), the resulting MPTs are 13 steps longer (1665 versus 1652 steps). When †*Brachydegma* is  
396 constrained in a monophyletic clade with actinopterygians (cf. Giles et al., 2017), the analyses resulted in  
397 MPTs that are three steps longer (1655 steps) than the unconstrained parsimony analyses.

398 *Equally weighted parsimony excluding †Brachydegma*: When reanalyzing our phylogenetic matrix  
399 after excluding †*Brachydegma*, but keeping newly added/modified characters, clades recovered in the  
400 previous rounds of analyses are not resolved (1646 steps; Appendix Fig. 4). Instead, the resolution of  
401 post-Devonian actinopterygian interrelationships is largely lost, and is replaced by a large polytomy  
402 containing major groups (e.g., †Scanilepiformes + Polypteridae, Chondrostei, and a poorly resolved  
403 neopterygian total group).

404 *Parsimony using implied weights*: A different phylogenetic picture of ‘early’ actinopterygian  
405 interrelationships emerges when analyzing our phylogenetic dataset with implied weights (Goloboff,  
406 1993; Goloboff et al., 2017) using a gentle concave (K=12; see Goloboff et al., 2017). We used 44  
407 best-fit trees (Fit Score=68.77) to produce a strict consensus tree (Appendix Fig. 5). In the strict  
408 consensus, †*Brachydegma* is resolved as a stem neopterygian, on the basis of three synapomorphies of  
409 varying fit scores (f): presence of a vertical preopercle (C.116; f:0.37); length of the median gular  
410 exceeding half the length of the lower jaw (C.124; f:0.14); and the presence of uncinat processes of  
411 the epibranchials (C.231; f:0.2). Still, †*Brachydegma* is clearly excluded from crown Neopterygii.  
412 Typically recognized neopterygian synapomorphies (see also equally weighted parsimony above)  
413 support a clade formed by †*Hulettia* (now excluded from crown Neopterygii) and crown  
414 neopterygians. These nine synapomorphies include: presence of multiple sensory rami on the jugal  
415 (C.56; f:0.45); mobile maxilla (C.73; f:0.2); presence of a peg-like anterior maxillary process (C.74\*;  
416 f:0); presence of an angular and a surangular in the lower jaw (C.90; f:0.57); presence of an  
417 anterodorsal process on the subopercle (C.113; f:0.52); presence of an interopercle (C.120\*; f:0.25);  
418 internal carotid artery piercing the parasphenoid (C.180; f:0.25); presence of two ossifications of the  
419 ceratohyal (C.219; f:0.2); presence of ossified centra (C.287; f:0.29). †*Brachydegma* shares with  
420 crown neopterygians + †*Hulettia* the same state for C.90, which is however widespread among

actinopterygians. Other notable departures in tree shape from the unweighted and unconstrained analysis include: i) the recovery of an ‘Ancient fish clade’ formed by Cladistia and Chondrostei and their fossil relatives; ii) recovery of a clade formed by †Saurichthyiformes and †Birgeriidae at the base of the neopterygian stem.

*Bayesian analysis:* The exclusion of †*Brachydegma* from the neopterygian crown group is ratified in our Bayesian analysis (Appendix Fig. 6), where the neopterygian crown is strongly supported (BPP=0.99). However, relationships outside of the neopterygian crown are volatile (compare e.g., Gardiner and Schaeffer, 1989; Gardiner et al., 2005; Hurley et al., 2007; Giles et al., 2017; Argyriou et al., 2018; Latimer and Giles, 2018; Figueroa et al., 2019) and poorly supported; for example, the actinopterygian crown node is not recovered. This picture does not change when †*Brachydegma* is removed from the matrix. We express caution in accepting hypotheses of relationships outside of the neopterygian crown.

## Discussion

### Comparative anatomy of †*Brachydegma*

†*Brachydegma* is thus far unique among described Permian actinopterygians in preserving the external dermal skeleton, braincase, hyoid arch, gill skeleton and shoulder girdle in three dimensions. It therefore represents an important addition between earlier Devonian-Carboniferous [e.g., †*Mimipiscis* (Gardiner, 1984); †*Raynerius* (Giles et al., 2015b); †*Lawrenciella* (Poplin, 1974; Pradel et al., 2016); †*Trawdenia* (Coates, 1999; Coates and Tietjen, 2018); †*Coccocephalichthys* (Poplin and Véran, 1996)] and later Triassic taxa (e.g., †*Watsonulus* (Olsen, 1984); †*Saurichthys* (Argyriou et al., 2018); †‘*Perleidus*’ and early teleosts (Patterson, 1975) for which similarly detailed anatomical information is available. †*Brachydegma* bears a novel combination of traits, but this is unsurprising given how little is known of the internal anatomy of any other Permian actinopterygian (but see Gill, 1923; Aldinger, 1937). The most notable new features of †*Brachydegma* revealed by our work relate to the braincase, palate, gill skeleton, and hyoid arch, as well as the pectoral endoskeleton and fin.

447 The braincase and parasphenoid of †*Brachydegma* display an unexpected combination of features.  
 448 Rather than having a single, co-ossified occipital arch, †*Brachydegma* exhibits differentiated  
 449 endochondral ossifications in the occipital region. This is the earliest example of a condition typically  
 450 associated with neopterygians (Patterson, 1975; Grande and Bemis, 1998; Grande, 2010). The  
 451 posterior parasphenoid stem extending behind the ventral otic fissure clearly differentiates  
 452 †*Brachydegma* from most anatomically generalized Paleozoic–early Mesozoic actinopterygians  
 453 (Nielsen, 1942, 1949; Schaeffer and Dalquest, 1978; Gardiner, 1984; Giles et al., 2015b; Figueroa et  
 454 al., 2019). The bifurcation of the dorsal aorta into lateral dorsal aortae occurs below the posterior stem  
 455 of the parasphenoid in †*Brachydegma*, resembling the condition seen in †saurchthyiforms (Argyriou  
 456 et al., 2018), conceivably †birgeriids (Nielsen, 1949) and most actinopterans (Patterson, 1975), but not  
 457 polypterids (Allis, 1922).

458 The presence of a dorsolateral metapterygoideal flange and groove in †*Brachydegma* is a possibly  
 459 derived feature, which is encountered in a rudimentary form in †*Australosomus* (Nielsen, 1949), but is  
 460 otherwise largely restricted to neopterygians (Olsen, 1984; Arratia and Schultze, 1991). In stem  
 461 actinopterygians, like e.g., †*Mimipiscis*, or †*Pteronisculus* the portion occupied by the metapterygoid  
 462 —or its co-ossified homolog— does not bear a clearly defined lateral flange (Nielsen, 1942; Gardiner,  
 463 1984; Arratia and Schultze, 1991). By contrast to the above, the intimate contact between the palate  
 464 and the maxilla, via overlapping flanges issuing from the ventral surfaces of both bones, is reminiscent  
 465 of the primitive configuration seen in most stem and early diverging actinopterygians, and to an extent  
 466 in *Polypterus* (Nielsen, 1942, 1949; Gardiner, 1984; Giles et al., 2017; Argyriou et al., 2018; Lemberg  
 467 et al., 2021).

468 The nearly complete branchial skeleton of †*Brachydegma* represents one of the best examples known  
 469 so far from a Paleozoic–early Mesozoic actinopterygian (Stensiö, 1921, 1932; Aldinger, 1937;  
 470 Nielsen, 1942, 1949; Giles et al., 2015b; Giles et al., 2017; Argyriou et al., 2018; Figueroa et al.,  
 471 2019). Unlike polypterids (Allis, 1922), †*Brachydegma* shares five gill arches —with the fifth  
 472 represented only by a pair of tiny ceratobranchials— and four independent hypobranchial ossifications  
 473 with most Permian–Triassic actinopterygians (Nielsen, 1942, 1949; Giles et al., 2017), chondrosteans



(Grande and Bemis, 1991; Hilton et al., 2011) and most teleosts (Nelson, 1969; Hilton, 2002). The dorsal gill skeleton of †*Brachydegma* lacks enlarged tooth patches and has a well-ossified series of suprapharyngobranchials; both contrast with derived conditions found in neopterygians (Nelson, 1969; Grande and Bemis, 1998; Hilton, 2002; Grande, 2010).

Shoulder girdles and their patterns of variation remain poorly characterized in early fossil actinopterygians. The dermal shoulder girdle of †*Brachydegma* is well-developed, comprising large supracleithra, presupracleithra, cleithra, postcleithra and clavicles, differing from the reduced complement of dermal bones in neopterygians. However, the endoskeletal girdle is only partially mineralised, in contrast to those of most Devonian–Carboniferous taxa (Gardiner 1984, Coates and Tietjen 2018), but bearing some possible resemblance to the much-modified girdles of living actinopterygians (Jessen, 1972; Grande and Bemis, 1998; Grande, 2010; Hilton et al., 2011). †*Brachydegma* lacks a mineralised coracoid plate or completely mineralised mesocoracoid arch, in contrast to most deeply diverging actinopterygians (Nielsen, 1942; Jessen, 1972; Gardiner, 1984; Coates and Tietjen, 2018) and the Triassic neopterygian †*Watsonulus* (Olsen 1984). We also found no evidence of a posterior mesocoracoid process, as that present in e.g., †*Mimipiscis* (Gardiner, 1984) or †*Trawdenia* (Coates and Tietjen, 2018). The lack of a dorsal scapular process resembles stem actinopterygians such as †*Trawdenia* (Coates and Tietjen, 2018), and clearly differs from the earliest neopterygian pectoral girdle known, that of †*Watsonulus* (Olsen, 1984). However, the endoskeleton of living actinopterygian taxa presents conflicting anatomical data, and the evolution of these features is difficult to resolve without additional information from fossils.

Perhaps most surprisingly, the hyoid arch of †*Brachydegma* shows the presence of two accessory hyoid elements between the dorsal and ventral components of the arch. These two ossifications exhibit a subparallel arrangement, with the anteriormost articulating with the lower jaw to form a double jaw joint.

#### **Phylogenetic position of †*Brachydegma***

The unanticipated combination of characters found in †*Brachydegma* is associated with ambiguity in its phylogenetic position, with equal weights parsimony, implied weights parsimony, and Bayesian analyses yielding conflicting placements. Although equal weights parsimony analyses suggested a close affinity with polypterids, †scanilepiforms and †*Birgeria* (Fig. 11), implied weights parsimony recovered †*Brachydegma* as a stem neopterygian (Appendix Fig. 5). Constrained analyses emulating previously proposed topologies for †*Brachydegma* as a stem actinopteran (Giles et al., 2017) or a halecomorph (Hurley et al., 2007) also resulted in longer trees. The volatility of early actinopterygian phylogeny between successive studies using similar character sets but different taxon samples suggests that these hypotheses should be viewed with caution, until more information of both the internal and external anatomy of additional late Paleozoic–early Mesozoic fossil groups becomes available (Giles et al., 2017; Argyriou et al., 2018; Latimer and Giles, 2018)).

Our reappraisal of the systematic affinities of †*Brachydegma* contrasts sharply with past hypotheses of crown neopterygian affinity (Hurley et al., 2007). Evidence previously advanced for a neopterygian (and specifically halecomorph) placement of †*Brachydegma* included the presence of: a supraorbital bone; a large median gular; a posteriorly indented and possibly free maxilla; an antorbital with a tube-like anterior process; and a neopterygian-like coronoid process (Hurley et al., 2007). The majority of these characters are either widely distributed across actinopterygians (supraorbitals, antorbital with a tube-like anterior process), or were misidentified in †*Brachydegma* (posteriorly indented maxilla, free maxilla, coronoid process, and the possible misidentification of the nasal as an antorbital). Our analyses recover †*Brachydegma* firmly outside the neopterygian crown (see also constrained analyses). This is despite the presence of features of the hyoid arch formerly thought to be restricted to crown neopterygians —halecomorphs in particular, the implications of which we discuss in greater detail below.

## **Evolution of accessory elements in the hyoid arch of actinopterygians**

The homology and evolution of hyoid elements is complex, and our new data on the hyoid arch of †*Brachydegma* add to this long-running debate (Patterson, 1973; Jollie, 1980; Patterson, 1982; Jollie,

1984; Véran, 1988; Gardiner and Schaeffer, 1989; Gardiner et al., 2005; Warth et al., 2017). Here we review past interpretations of accessory hyoid elements in living and fossil actinopterygians, and attempt to synthesise these data in light of new information from †*Brachydegma* (Fig. 12).

Polypterids possess a single accessory hyoid element that articulates with the full width of the hyomandibula dorsally and of the ceratohyal ventrally (Allis, 1922; Moy-Thomas, 1933; Jollie, 1984; Giles et al., 2017). This bone develops independently of the hyosymplectic cartilage and thus represents an interhyal (Moy-Thomas, 1933; Jollie, 1984). Neopterygians primitively have two accessory elements between the hyomandibula and ceratohyal. The more anterior of these—the symplectic—typically braces the mandibular arch (Patterson, 1973; Olsen, 1984; Véran, 1988; Gardiner and Schaeffer, 1989; Gardiner et al., 1996; Grande and Bemis, 1998; Grande, 2010; Arratia, 2013) and arises as an anteroventral outgrowth of the embryonic hyosymplectic cartilage that subsequently detaches in development (Holmgren, 1943; Bertmar, 1959; Konstantinidis et al., 2015; Mork and Crump, 2015; DeLaurier, 2019). The more posterior accessory element—the interhyal—articulates with the posteroventral portion of the hyomandibula and suspends the ventral hyoid elements (Patterson, 1982; Véran, 1988; Grande and Bemis, 1998; Grande, 2010; Konstantinidis et al., 2015; DeLaurier, 2019). The interhyal arises from an independent embryonic cartilage (Konstantinidis et al., 2015; Mork and Crump, 2015; DeLaurier, 2019). The interhyal remains cartilaginous in adult holosteans (Grande and Bemis, 1998; Grande, 2010), while the symplectic shows contrasting conditions in different members of that group. In halecomorphs, it is hatchet shaped and articulates with the articular forming a second jaw joint (Grande and Bemis, 1998). In ginglymodans, it is ‘L’ shaped and joins the back of the primary palate (Grande, 2010). In extant teleosts, the symplectic is wedge-shaped and typically inserts in a notch on the quadrate, while the interhyal is variably ossified and lies between the hyomandibula and posterior ceratohyal (Hilton, 2002; Arratia, 2013).

In contrast to the uncontroversial assessments for polypterids and neopterygians, both the number and identity of accessory hyoid elements in acipenseriforms has been the subject of considerable debate. Acipenseriform hyoid and mandibular arches are highly modified with respect to those of other actinopterygians. The anteroventral tip of the hyomandibula in acipenseriforms articulates with a large

552 cartilage or bone that in turn is linked with the palatoquadrate. This first bone or cartilage articulates  
553 ventrally with a second, often much smaller one, which articulates with a bone universally regarded as  
554 a ceratohyal. Two principal interpretations have been offered for the elements between the ceratohyal  
555 and hyomandibula. The first, initially proposed by Traquair (1877) and adopted by several subsequent  
556 authors (Sewertzoff, 1928; Marinelli and Strenger, 1973; Jollie, 1980; Véran, 1988), is that there are  
557 two accessory hyoid elements: the dorsal one representing a symplectic, and the ventral one  
558 representing an interhyal. The second, most forcefully argued by Patterson (1982), posits that the  
559 dorsal bone or cartilage is an interhyal. Under this interpretation, the smaller ventral cartilage is not an  
560 accessory element but rather a posterior ceratohyal, as indicated by a close association with a  
561 branchiostegal ray in *Polyodon* (Patterson, 1982). These competing models have contrasting  
562 implications for character distribution in actinopterygians: the first suggests a symplectic is a feature  
563 of actinopterans rather than neopterygians, while the second preserves the status of the symplectic as a  
564 neopterygian neomorph. Patterson's (1982) model is now dominant (e.g., Gardiner, 1984; Gardiner  
565 and Schaeffer, 1989; Gardiner et al., 1996; Coates, 1999; Gardiner et al., 2005; Grande, 2010; Xu et  
566 al., 2014; Warth et al., 2017; López-Arbarello and Sferco, 2018; Xu, 2019), but neither scheme is  
567 without its challenges. The interpretation of these elements as a symplectic and interhyal, respectively,  
568 requires a change in developmental pattern between the neopterygian (derived from common  
569 hyosymplectic cartilage: Konstantinidis et al., 2015; Mork and Crump, 2015) and chondrosteian  
570 symplectic (a separate cartilage throughout development: Warth et al., 2017) plus the neomorphic —  
571 but not unprecedented (see examples in teleosts: McAllister, 1968)— association between a  
572 branchiostegal and interhyal in paddlefishes (Patterson, 1982; Grande and Bemis, 1991). The  
573 alternative interpretation requires the origin of a symplectic-like association between the interhyal and  
574 palatoquadrate, and the migration of the ceratomandibular ligament from the posterior ceratohyal to  
575 the anterior, combined with the development of the posterior ceratohyal matching that of an interhyal  
576 (derived from an independent cartilage) rather than a neopterygian posterior ceratohyal (ossifies within  
577 the same cartilage as the anterior ceratohyal; Warth et al., 2017).

It is within this limited framework that previous authors have tried to interpret the accessory hyoid ossifications of fossil actinopterygians. †Parasemionotids (Stensiö, 1932; Patterson, 1973; Olsen, 1984, Fig. 8F–I) and †pycnodonts (Nursall and Maisey, 1987; Gardiner et al., 1996; Kriwet, 2005) have two accessory ossifications, which are unambiguously identified as an interhyal and symplectic. In both groups, these two elements are arranged in a sub-parallel manner and the symplectic articulates with the lower jaw forming a double jaw joint. Arratia (2013) argues that some stem teleosts (e.g., †*Pholidophorus gervasuttii*) likewise have a double jaw joint; the broad distribution of this character raises questions as to its reliability as a halecomorph synapomorphy. Interpretation of accessory elements in groups more remote from the neopterygian crown is less straightforward. This reflects a series of obstacles related to both fossils (distortion of spatial relationships, an inability to distinguish genuine absence of a structure from its failure to ossify, uncertain phylogenetic placements) and living taxa (unsettled interpretations of homologies). Most probable stem actinopterygians exhibit (or, more properly, preserve) a single ossified accessory hyoid element (Nielsen, 1942, 1949; Gardiner, 1984, Fig. 8J–M), conventionally identified as the interhyal following Patterson (1982). However, Véran (1988) reported a second ossification in some fossils, found in close association with the anteroventral tip of the hyomandibula and the palatoquadrate. Véran (1988) argued this second bone is a symplectic, and that both it and an interhyal were primitively present in actinopterygians (see also Olsen, 1984). In some probable stem actinopterygians of Triassic–Jurassic age (e.g., †*Boreosomus reuterskioldi*, †*Pteronisculus gyrolepidoides*, †*Ptycholepis bollensis*), these two intermediate elements appear to be arranged in a dorsoventral series, rather than in a sub-parallel manner (Véran, 1988). This hypothesis gained little traction, however, and subsequent authors reinterpreted putative symplectics in extinct non-neopterygians as interhyals, with the bones reported by Véran as interhyals reclassified as posterior ceratohyals or articulars (Gardiner and Schaeffer, 1989; Patterson, 1994; Gardiner et al., 1996; Gardiner et al., 2005). A key argument for the dismissal of putative non-neopterygian symplectics was the apparent absence of a break in the perichondral lining of the so-called symplectic, which would imply the articulation of the symplectic with the lower jaw in a neopterygian manner (Patterson, 1994; Gardiner et al., 1996).

†*Brachydegma* provides a new perspective on this debate (Fig. 5) for two reasons. First, it preserves two accessory hyoid elements in three dimensions and life position. Second, its phylogenetic position, although ambiguous, clearly lies far outside halecomorphs, or the neopterygian crown. In this context, it is significant that the more anterior element matches structural criteria used to identify the symplectic in crown neopterygians: it lies immediately posterior to the quadrate, between the hyomandibula and lower jaw, and it forms a clear articulation with the latter via a condyle (Patterson, 1973, 1982; Gardiner et al., 1996; Grande and Bemis, 1998). A further similarity between this anterior element of †*Brachydegma* and the undisputed symplectic of †parasemionotids is the presence of an aortic groove (sensu Véran, 1988) on the dorsal anterolateral and lateral surface of the bone (Fig. 8). Under this interpretation, the slender, rod-shaped posterior element of †*Brachydegma* would represent an interhyal.

Our µCT-aided examination of the hyoid arch of the putative stem actinopterygian †*Pteronisculus gunnari* revealed a single accessory element (Fig. 8J–M), which presents many similarities with the symplectic of †*Brachydegma* and also satisfies most criteria for establishing its homology with the neopterygian symplectic. Specifically, it: i) forms an anterior thickening—but not a condyle—for attachment to the lower jaw; ii) bears an arterial groove (sensu Véran, 1988); and iii) displays a topology identical to that of the neopterygian symplectic, as well as the now-recognized symplectic of †*Brachydegma*. We note that there is no concave socket in the articular of †*Pteronisculus* for the insertion of the anterior thickening of the ‘symplectic’, but rather a flat surface. Similar features and geometries to those of †*Pteronisculus* were also recognized in the ‘symplectics’ of putative stem actinopterygians, such as †*Boreosomus*, †*Ptycholepis*, †*Acrorhabdus* and †*Pteronisculus* (Véran, 1988). These similarities provide support to previous hypotheses for a widespread distribution of the presence of a symplectic in actinopterygian fishes (Olsen, 1984; Véran, 1988). Finally, direct observations (T.A.) on mechanically prepared specimens of †*Boreosomus reuterskioldi* (MNHN.F SVT 14a; MNHN.F SVT 15b; Appendix Fig. 7E,F), previously studied by Véran (1988, 1996), confirmed the presence of two accessory hyoid elements: a symplectic-like bone and an interhyal. Both accessory elements lie in series, as depicted by Véran (1998:pl. 1; Appendix Fig. 7E,F).

Direct homology between the arrangement in †*Brachydegma*, crown neopterygians and stem actinopterygians would also bolster arguments that the large accessory hyoidean cartilage of chondrosteans is a symplectic (Fig. 8N–Q; Fig. 12). Establishing these homologies faces outstanding challenges, including the scarcity of reliable accessory hyoid data for extinct actinopterygians, lack of developmental information in fossils, and the difficulty in identifying true absence from taphonomic loss or persistence as a cartilage. Only the first of these issues can be addressed, the path toward its resolution is clear: systematic re-examination of hyoid-arch structure in fossil taxa. The resolution of key issues concerning hyoid arch evolution in actinopterygians—including the homology of accessory elements across living lineages—will only be possible when high-quality anatomical data are available for a range of fossil taxa with well-supported phylogenetic placements. Despite uncertainties regarding the precise evolutionary affinities of †*Brachydegma* with regards to crown actinopterygian groups, the discovery of a double jaw joint in the former taxon suggests, at minimum, that this feature can no longer be treated as unique synapomorphy for halecomorphs. The possibility of a symplectic, or a double jaw joint evolving convergently (Xu, 2019) in halecomorphs and other fossil groups, including †*Brachydegma*, †pycnodonts and possibly early teleosts, becomes very remote when accounting for the likely presence of these features in stem actinopterygians.

## Materials and Methods

**Institutional abbreviations:** MCZ: Museum of Comparative Zoology, Harvard University, Cambridge, Massachusetts, USA; MNHN: Muséum National d'Histoire Naturelle, Paris, France; NHMD: Natural History Museum of Denmark, University of Copenhagen, Copenhagen, Denmark; UMMZ: University of Michigan Museum of Zoology, Ann Arbor, Michigan, USA.

**Comparative material:** NHMD 73588 A, †*Pteronisculus gunnari*, holotype preserving cranial skeleton, Early Triassic, East Greenland; NHMD 74424 A (Appendix Fig. 7A,B), †Parasemionotidae indet. Early Triassic, East Greenland; MNHN.F SVT 14a and MNHN.F SVT 15b, †*Boreosomus reuterskioldi*, mechanically prepared crania with mandibular, hyoidean and gill arches preserved in

situ, Early Triassic, Spitsbergen (Appendix Fig. 7C,D). The latter specimens were studied by V  ran (1988, 1996); UMMZ 64250, *Acipenser brevirostrum*, scan of PTA-stained head.

**X-ray computed microtomography:**  $\mu$ CT of the two specimens of †*Brachydegma* was performed with a Nikon XT H 225 ST scanner at the CTEES lab in the Department of Earth and Environmental Sciences, University of Michigan. The parameters are as follows: MCZ VPF 6503: 200Kv, 200uA, 1.25 mm copper filter, giving a voxel size of 48.4um; MCZ VPF 6504: 215Kv, 265uA, 3.5mm copper filter, giving a voxel size of 61.2um. The head of *Acipenser brevirostrum* (UMMZ 64250) was also scanned using the same facilities, and the parameters are: 75Kv, 290uA, no filtering, giving a voxel size of 60.2um.  $\mu$ CTs of †*Pteronisculus gunnari* (NHMD 73588 A) and the †parasemionotid (NHMD 74424 A) were performed at the University of Bristol using a Nikon XT H 225 ST scanner. The parameters are as follows: NHMD 73588: 224Kv, 191uA, 1mm copper filter giving a voxel size of 22.5um; NHMD 74424a: 223Kv, 155uA, 0.5mm copper filter, giving a voxel size of 20.3um. The resulting tomograms were processed in Mimics (biomedical.materialise.com/mimics; Materialise, Leuven, Belgium) for the creation of three-dimensional, digital anatomical models. The reconstruction process of the two †*Brachydegma* specimens was challenging, since the accommodating matrix is particularly rich in radiodense content. In the case of MCZ VPF 6503, the external surfaces of endoskeletal elements are lined with a dense mineral layer, hampering beam penetration and voxel size of smaller structures, such as nerve foramina. However, we were able to reconstruct the gross morphology of the endoskeleton. The completed models were exported in .ply format, and processed in Blender (blender.org) for imaging.

**Phylogenetic analysis:** For analyzing the interrelationships of †*Brachydegma* in a broader osteichthyan context, we modified an already existing, large-scale phylogenetic matrix (Giles et al., 2017; Argyriou et al., 2018; Latimer and Giles, 2018; Figueroa et al., 2019; see Appendix 2 for details). The matrix was edited in Mesquite (Maddison and Maddison, 2017), and the parsimony analyses were performed with ‘New Technology Search’ implemented in TNT (Goloboff et al., 2008; Goloboff and Catalano, 2016). We used the windows-based version of TNT. We enforced an outgroup constraint to ensure the monophyly of Osteichthyes. Relative fit difference was set to 0.1 and



suboptimal trees up to 10 steps longer were retained. Initial trees were created by 1000 random addition sequences using 100 iterations or rounds of the four ‘New Technology search’ algorithms (Sectorial Search, Ratchet, Drift, Tree Fusing). For Sectorial Search algorithms, minimum sector size was set to five and maximum sector size was set to 58, which corresponds to ~50% taxa in our matrix. All other parameters remained unchanged. To ensure an exhaustive search of the dataset, two separate analyses of three rounds each were conducted using an alternation of 1000 iterations of ‘Ratchet’ and ‘Sectorial Search’ algorithms. The first analysis comprised a round of Sectorial Search, followed by two rounds using Ratchet. The second analysis started with a Ratchet round, followed by a round of Sectorial Search and then another round of Ratchet. All trees including suboptimals were saved at the end of each round, but only optimal trees (MPTs) were kept in memory for running the following round. Each round in both analyses was always complemented by the 1000 iterations of ‘Tree Fusing’. Suboptimal trees from all rounds of analyses were used at the end to calculate Bremer supports (BDI) in TNT. Bootstrap values were calculated by reanalyzing the matrix with 10,000 iterations of the ‘Traditional Search’ algorithm. Agreement subtrees were also produced using the relevant function in TNT. Consistency (C.I.) and Retention (R.I.) indices were calculated using Mesquite. Additional analyses following the same methodology were run with constraints to investigate previous hypotheses for the placement of †*Brachydegma*. The same analysis procedure was replicated for producing the implied weights analyses, after selecting the relevant function in TNT and setting the constant K to K=12 (Goloboff et al., 2017). The latter analysis was conducted in order to visualize the interrelationships of actinopterygians —†*Brachydegma* in particular— in a scenario that softly penalizes homoplasy (homoplastic character downweighting), which is otherwise widespread in our unweighted parsimony generated trees. Characters are assigned fit values (f) between 0 and 1, with a value of 0 indicating that the character is not homoplastic (see e.g., C.74).

We also conducted a Bayesian analysis of our dataset in MrBayes (Ronquist et al., 2012), employing the same outgroup constraint as applied in parsimony analyses. The datatype was set to ‘standard’ (=morphological). We specified a gamma distribution for rates of character evolution, and indicated that invariant characters were not included in the matrix. We conducted two runs using the default of

four chains, one cold and three heated. We assessed convergence by examining: the standard deviations of split frequencies; ESS values; and visual inspection of the trace of log likelihoods. We discarded the first 50% of sampled trees as burnin.

**Acknowledgments:** S. Pierce and J. Cundiff (MCZ), D. Nelson, (UMMZ), B. E. K. Lindow and K. M. Gregersen (both NHMD) are thanked for kindly providing access to fossil and/or recent material. M. R. Sánchez-Villagra, C. Romano (both PIMUZ), M. Coates (University of Chicago) and T. Miyashita (Canadian Museum of Nature), T. Simões (Harvard University), O. Vernygora (University of Kentucky), A. López-Arbarello (LMU) and M. Véran (MNHN) are thanked for useful discussions. M. R. Sánchez-Villagra is also thanked for additional administrative support to T.A. A. Pradel and G. Clément (both MNHN) are thanked for facilitating access to the collections of the MNHN. D. Germain and P. Vincent (both MNHN) and the FOSFO team of the CR2P are acknowledged for further facilitating the research activities of TA at the MNHN. C. Abraczinskas (UMMP) created the weighted line drawings of the holotype (Figs. 2–4). Christina Byrd (MCZ) provided guidance in archiving data in Morphosource. We thank the reviewing editor, Zhu Min (Institute of Vertebrate Paleontology and Paleoanthropology, Chinese Academy of Sciences), P. Ahlberg (Uppsala University) and an anonymous referee for their constructive feedback that improved earlier versions of this contribution. The Willi Hennig Society is acknowledged for making TNT available free of charge. This study includes data produced in the CTEES facility at University of Michigan, supported by the Department of Earth and Environmental Sciences and the College of Literature, Science, and the Arts.

**Funding:** This research was supported by P1ZHP3\_168253 and P2ZHP3\_184216 Swiss National Science Foundation grants to T.A. Support during the late stages of this work was provided by an Alexander von Humboldt fellowship to T.A.

**Competing interests:** There are no competing interests.

**Data and materials availability:**  $\mu$ CT raw and/or derived data are available on Morphosource. Links to parent directories for each studied specimen are given below.

738 †*Brachydegma caelatum* (MCZ VPF 6503): [www.morphosource.org/concern/media/000440974](http://www.morphosource.org/concern/media/000440974)

739 †*Brachydegma caelatum* (MCZ VPF 6504): [www.morphosource.org/concern/media/000441020](http://www.morphosource.org/concern/media/000441020)

740 †*Pteronisculus gunnari* (NHMD VP 73588A): [www.morphosource.org/concern/media/000441157](http://www.morphosource.org/concern/media/000441157)

741 †Parasemionotidae indet. (NHMD VP 74424A): [www.morphosource.org/concern/media/000441197](http://www.morphosource.org/concern/media/000441197)

742 *Acipenser brevirostrum* (UMMZ 64250): [www.morphosource.org/concern/media/000441184](http://www.morphosource.org/concern/media/000441184)

743 Phylogenetic matrix and trees available through Dryad at: [doi.org/10.5061/dryad.jsxksn0bz](https://doi.org/10.5061/dryad.jsxksn0bz)

744

## 745 References

746 Aldinger, H. 1937. Permische Ganoidfische aus Östgrönland. Meddelelser om Grønland 102:1–392 +  
 747 44 tabs.

748 Allis, E. P. 1922. The Cranial Anatomy of *Polypterus*, with Special Reference to *Polypterus bichir*.  
 749 Journal of Anatomy 56:189–294.43.

750 Argyriou, T., S. Giles, M. Friedman, C. Romano, I. Kogan, and M. R. Sánchez-Villagra. 2018.  
 751 Internal cranial anatomy of Early Triassic species of †*Saurichthys* (Actinopterygii:  
 752 †*Saurichthyiformes*): implications for the phylogenetic placement of †saurichthyiforms. BMC  
 753 evolutionary biology 18:161.

754 Arratia, G. 2013. Morphology, taxonomy, and phylogeny of Triassic pholidophorid fishes  
 755 (Actinopterygii, Teleostei). Journal of Vertebrate Paleontology 33:1–138.

756 Arratia, G., and H.-P. Schultze. 1991. Palatoquadrate and its ossifications: Development and  
 757 homology within osteichthyans. Journal of Morphology 208:1–81.

758 Bertmar, G. 1959. On the ontogeny of the chondral skull in Characidae, with a discussion on the  
 759 chondrocranial base and the visceral chondrocranium in fishes. Acta Zoologica 40:204–364.

760 Broughton, R. E., R. Betancur-R, C. Li, G. Arratia, and G. Ortí. 2013. Multi-locus phylogenetic  
 761 analysis reveals the pattern and tempo of bony fish evolution. PLoS Currents  
 762 5:ecurrents.tol.2ca8041495ffafd0c92756e75247483e.

763 Campbell, K. S. W., and L. D. Phuoc. 1983. A Late Permian actinopterygian fish from Australia.  
764 Palaeontology 26:33–70.

765 Choo, B., J. A. Long, and K. Trinajstić. 2009. A new genus and species of basal actinopterygian fish  
766 from the Upper Devonian Gogo Formation of Western Australia. Acta Zoologica 90:194–210.

767 Claeson, K. M., W. E. Bemis, and J. W. Hagadorn. 2007. New interpretations of the skull of a  
768 primitive bony fish *Erpetoichthys calabaricus* (Actinopterygii: Cladistia). Journal of  
769 Morphology 268:1021–1039.

770 Cloutier, R., and G. Arratia. 2004. Early diversification of actinopterygians; pp. 217–270 in G. Arratia,  
771 M. V. H. Wilson, and R. Cloutier (eds.), Recent advances in the origin and early radiation of  
772 vertebrates. Dr. Friedrich Pfeil, München, Germany.

773 Coates, M. I. 1999. Endocranial preservation of a Carboniferous actinopterygian from Lancashire, UK,  
774 and the interrelationships of primitive actinopterygians. Philosophical Transactions of the  
775 Royal Society B: Biological Sciences 354:435–462.

776 Coates, M. I., and K. Tietjen. 2018. ‘This strange little palaeoniscid’: a new early actinopterygian  
777 genus, and commentary on pectoral fin conditions and function. Earth and Environmental  
778 Science Transactions of the Royal Society of Edinburgh 109:15–31.

779 DeLaurier, A. 2019. Evolution and development of the fish jaw skeleton. WIREs Developmental  
780 Biology 8:e337.

781 Dunkle, D. H. 1939. A new paleoniscid fish from the Texas Permian. American Journal of Science  
782 237:262–274.

783 Dunkle, D. H. 1946. A new palaeoniscoid fish from the Lower Permian of Texas. Journal of the  
784 Washington Academy of Sciences 36.

785 Figueroa, R. T., M. Friedman, and V. Gallo. 2019. Cranial anatomy of the predatory actinopterygian  
786 *Brazilichthys macrognathus* from the Permian (Cisuralian) Pedra de Fogo Formation,  
787 Parnaíba Basin, Brazil. Journal of Vertebrate Paleontology:1–17.

788 Friedman, M., S. E. Pierce, M. Coates, and S. Giles. 2018. Feeding structures in the ray-finned fish  
789 *Eurynotus crenatus* (Actinopterygii: Eurynotiformes): implications for trophic diversification

790 among Carboniferous actinopterygians. Earth and Environmental Science Transactions of the  
 791 Royal Society of Edinburgh 109:33–47.

792 Friedman, M., and L. C. Sallan. 2012. Five hundred million years of extinction and recovery: a  
 793 phanerozoic survey of large-scale diversity patterns in fishes. Palaeontology 55:707–742.

794 Gardiner, B., B. Schaeffer, and J. Masserie. 2005. A review of the lower actinopterygian phylogeny.  
 795 Zoological Journal of the Linnean Society 144:511–525.

796 Gardiner, B. G. 1960. A revision of certain actinopterygian and coelacanth fishes, chiefly from the  
 797 Lower Lias. Bulletin of the British Museum (Natural History), Geology 4:241–384.

798 Gardiner, B. G. 1984. The relationships of the palaeoniscid fishes, a review based on new specimens  
 799 of *Mimia* and *Moythomasia* from the Upper Devonian of Western Australia. Bulletin of the  
 800 British Museum (Natural History), Geology series 37:173–428.

801 Gardiner, B. G., J. G. Maisey, and D. T. J. Littlewood. 1996. Interrelationships of basal neopterygians;  
 802 pp. 117–146 in M. Stiassny, L. Parenti, and G. D. Johnson (eds.), Interrelationships of fishes.  
 803 Academic Press, London.

804 Gardiner, B. G., and B. Schaeffer. 1989. Interrelationships of lower actinopterygian fishes. Zoological  
 805 Journal of the Linnean Society 97:135–187.

806 Giles, S., M. I. Coates, R. J. Garwood, M. D. Brazeau, R. Atwood, Z. Johanson, and M. Friedman.  
 807 2015a. Endoskeletal structure in *Cheirolepis* (Osteichthyes, Actinopterygii), An early ray-  
 808 finned fish. Palaeontology 58:849–870.

809 Giles, S., L. Darras, G. Clément, A. Blieck, and M. Friedman. 2015b. An exceptionally preserved Late  
 810 Devonian actinopterygian provides a new model for primitive cranial anatomy in ray-finned  
 811 fishes. Proceedings of the Royal Society of London B: Biological Sciences 282.

812 Giles, S., G.-H. Xu, T. J. Near, and M. Friedman. 2017. Early members of ‘living fossil’ lineage imply  
 813 later origin of modern ray-finned fishes. Nature 549:265–268.

814 Gill, E. L. 1923. The Permian fishes of the genus *Acentrophorus*. Proceedings of the Zoological  
 815 Society of London 93:19–40.

816 Goloboff, P. A. 1993. Estimating character weights during tree search. Cladistics 9:83–91.

817 Goloboff, P. A., and S. A. Catalano. 2016. TNT version 1.5, including a full implementation of  
818 phylogenetic morphometrics. *Cladistics* 32:221–238.

819 Goloboff, P. A., J. S. Farris, and K. C. Nixon. 2008. TNT, a free program for phylogenetic analysis.  
820 *Cladistics* 24:774–786.

821 Goloboff, P. A., A. Torres, and J. S. Arias. 2017. Weighted parsimony outperforms other methods of  
822 phylogenetic inference under models appropriate for morphology. *Cladistics* 34:407–437.

823 Goodrich, E. S. 1930. *Studies on the Structure & Development of Vertebrates*. Macmillan and Co.,  
824 London.

825 Grande, L. 2010. An empirical synthetic pattern study of gars (*Lepisosteiformes*) and closely related  
826 species, based mostly on skeletal anatomy: the resurrection of *Holostei*. *American Society of*  
827 *Ichthyologists and Herpetologists Special Publication 6 Copeia Suppl* 10:871.

828 Grande, L., and W. Bemis. 1991. Osteology and phylogenetic relationships of fossil and recent  
829 paddlefishes (*Polyodontidae*) with comments on the interrelationships of *Acipenseriformes*.  
830 *Society of Vertebrate Paleontology Memoir* 11:1–121.

831 Grande, L., and W. E. Bemis. 1998. A Comprehensive Phylogenetic Study of Amiid Fishes (*Amiidae*)  
832 Based on Comparative Skeletal Anatomy. an Empirical Search for Interconnected Patterns of  
833 Natural History. *Journal of Vertebrate Paleontology* 18:1–696.

834 Hamel, M.-H., and C. Poplin. 2008. The braincase anatomy of *Lawrenciella schaefferi*,  
835 actinopterygian from the Upper Carboniferous of Kansas (USA). *Journal of Vertebrate*  
836 *Paleontology* 28:989–1006.

837 Hilton, E., L. Grande, and W. Bemis. 2011. Skeletal anatomy of the shortnose sturgeon *Acipenser*  
838 *brevirostrum* Lesueur, 1818, and the systematics of sturgeons (*Acipenseriformes*,  
839 *Acipenseridae*). *Fieldiana: Life and Earth Sciences* 3:1–168.

840 Hilton, E. J. 2002. Osteology of the extant North American fishes of the genus *Hiodon* Lesueur, 1818  
841 (*Teleostei*: *Osteoglossomorpha*: *Hiodontiformes*). *Feldiana Zoology* 100:1–142.

842 Holmgren, N. 1943. Studies on the head of fishes. An embryological, morphological and  
843 phyogenetical study. Part IV. General morphology of the head in fish. *Acta Zoologica* 24:1–  
844 188.

845 Hurley, I. A., R. L. Mueller, K. A. Dunn, E. J. Schmidt, M. Friedman, R. K. Ho, V. E. Prince, Z.  
 846 Yang, M. G. Thomas, and M. I. Coates. 2007. A new time-scale for ray-finned fish evolution.  
 847 Proceedings of the Royal Society of London B: Biological Sciences 274:489–498.  
 848 Jessen, H. 1972. Schultergürtel und Pectoralflosse bei Actinopterygiern. Fossils and Strata 1:1–101 +  
 849 25 pl.  
 850 Jollie, M. 1980. Development of Head and Pectoral Girdle Skeleton and Scales in Acipenser. Copeia  
 851 1980:226–249.  
 852 Jollie, M. 1984. Development of the head and pectoral skeleton of *Polypterus* with a note on scales  
 853 (Pisces: Actinopterygii). Journal of Zoology 204:469–507.  
 854 Konstantinidis, P., P. Warth, B. Naumann, B. Metscher, E. J. Hilton, and L. Olsson. 2015. The  
 855 Developmental Pattern of the Musculature Associated with the Mandibular and Hyoid Arches  
 856 in the Longnose Gar, *Lepisosteus osseus* (Actinopterygii, Ginglymodi, Lepisosteiformes).  
 857 Copeia 103:920–932.  
 858 Kriwet, J. 2005. A comprehensive study of the skull and dentition of pycnodont fishes. Zitteliana A45.  
 859 Latimer, A. E., and S. Giles. 2018. A giant dapediid from the Late Triassic of Switzerland and insights  
 860 into neopterygian phylogeny. Royal Society Open Science 5.  
 861 Lemberg, J. B., E. B. Daeschler, and N. H. Shubin. 2021. The feeding system of *Tiktaalik roseae*: an  
 862 intermediate between suction feeding and biting. Proceedings of the National Academy of  
 863 Sciences 118:e2016421118.  
 864 Long, J. 1988. New palaeoniscoid fishes from the Late Devonian and Early Carboniferous of Victoria.  
 865 Memoirs of the Association of Australasian Palaeontologists 7:1–64.  
 866 López-Arbarello, A., and E. Sferco. 2018. Neopterygian phylogeny: the merger assay. Royal Society  
 867 Open Science 5.  
 868 Lund, R. 2000. The new actinopterygian order Guildayichthyiformes from the Lower Carboniferous of  
 869 Montana (USA). Geodiversitas 22:171–206.  
 870 Machado, L. P. 2008. The braincase of *Neoprosclinetes penalvai* (Pycnodontiformes, Pycnodontidae);  
 871 pp. 167–180 in G. Arratia, H. P. Schultze, and M. V. H. Wilson (eds.), Mesozoic Fishes 4 –  
 872 Homology and Phylogeny. Dr. Friedrich Pfeil, München.

873 Maddison, W., and D. Maddison. 2017. Mesquite: a modular system for evolutionary analysis.

874 Marinelli, W., and A. Strenger. 1973. Vergleichende Anatomie und Morphologie der Wirbeltiere. IV.

875 Lieferung. Franz Deuticke, Wien.

876 McAllister, D. A. 1968. The evolution of branchiostegals and associated opercular, gular, and hyoid

877 bones, and the classification of teleostome fishes, living and fossil. National Museum of

878 Canada Bulletin 221:1–239.

879 Mickle, K. E., R. Lund, and E. D. Grogan. 2009. Three new palaeoniscoid fishes from the Bear Gulch

880 Limestone (Serpukhovian, Mississippian) of Montana (USA) and the relationships of lower

881 actinopterygians. *Geodiversitas* 31:623–668.

882 Mork, L., and G. Crump. 2015. Chapter Ten - Zebrafish Craniofacial Development: A Window into

883 Early Patterning; pp. 235–269 in Y. Chai (ed.), *Current Topics in Developmental Biology*.

884 Academic Press.

885 Moy-Thomas, J. A. 1933. Memoirs: Notes on the Development of the Chondrocranium of *Polypterus*

886 *senegalus*. *Quarterly Journal of Microscopical Science* s2–76:209–229.

887 Moy-Thomas, J. A., and M. B. Dyne. 1938. XVII.—The Actinopterygian Fishes from the Lower

888 Carboniferous of Glencartholm, Eskdale, Dumfriesshire. *Transactions of the Royal Society of*

889 *Edinburgh* 59:437–480.

890 Near, T. J., A. Dornburg, R. I. Eytan, B. P. Keck, W. L. Smith, K. L. Kuhn, J. A. Moore, S. A. Price,

891 F. T. Burbrink, M. Friedman, and P. C. Wainwright. 2013. Phylogeny and tempo of

892 diversification in the superradiation of spiny-rayed fishes. *Proceedings of the National*

893 *Academy of Sciences* 110:12738–12743.

894 Near, T. J., R. I. Eytan, A. Dornburg, K. L. Kuhn, J. A. Moore, M. P. Davis, P. C. Wainwright, M.

895 Friedman, and W. L. Smith. 2012. Resolution of ray-finned fish phylogeny and timing of

896 diversification. *Proceedings of the National Academy of Sciences* 109:13698–13703.

897 Nelson, G. J. 1969. Gill arches and the phylogeny of fishes, with notes on the classification of

898 vertebrates. *Bulletin of the American Museum of Natural History* 141:475–552 + 79–92pl.

899 Nelson, J. S., T. C. Grande, and M. V. H. Wilson. 2016. *Fishes of the world*. i–xli + 707 pp. John

900 Wiley & Sons, Inc., Hoboken, New Jersey, USA.



901 Nelson, W. J., R. W. Hook, and D. S. Chaney. 2013. Lithostratigraphy of the lower Permian  
 902 (Leonardian) Clear Fork Formation of north-central Texas; pp. 286–311 in S. G. Lucas, W. A.  
 903 DiMichele, J. E. Barrick, J. W. Schneider, and J. A. Spielmann (eds.), The Carboniferous-  
 904 Permian transition. New Mexico Museum of Natural History & Science, Albuquerque.  
 905 Nielsen, E. 1942. Studies on the Triassic fishes from East Greenland I. *Glaucolepis* and *Boreosomus*.  
 906 Palaeozoologica Groenlandica 138. 394 + 30pl.  
 907 Nielsen, E. 1949. Studies on Triassic fishes II. *Australosomus* and *Birgeria*. Palaeozoologica  
 908 Groenlandica 146. 1–309 + 20pl.  
 909 Nursall, J. R., and J. G. Maisey. 1987. *Neoproscinetes* Figueiredo and Silva Santos, 1987; pp. 125–137  
 910 in J. G. Maisey (ed.), Santana Fossils: an Illustrated Atlas. TFH Publications, Neptune, NJ.  
 911 Olsen, P. E. 1984. The skull and pectoral girdle of the parasemionotid fish *Watsonulus eugnathoides*  
 912 from the Early Triassic Sakamena Group of Madagascar, with comments on the relationships  
 913 of the holostean fishes. Journal of Vertebrate Paleontology 4:481–499.  
 914 Olson, E. C. 1989. The Arroyo Formation (Leonardian: Lower Permian) and its vertebrate fossils.  
 915 Texas Memorial Museum bulletin 35:1–25.  
 916 Patterson, C. 1973. Interrelationships of holosteans; pp. 233–305 in P. H. Greenwood, R. S. Miles, and  
 917 C. Patterson (eds.), Interrelationships of fishes. Academic Press, London.  
 918 Patterson, C. 1975. The braincase of pholidophorid and leptolepid fishes, with a review of the  
 919 actinopterygian braincase. Philosophical Transactions of the Royal Society of London. B,  
 920 Biological Sciences 269:275–579.  
 921 Patterson, C. 1982. Morphology and Interrelationships of Primitive Actinopterygian Fishes. American  
 922 Zoologist 22:241–259.  
 923 Patterson, C. 1994. Bony Fishes. Short Courses in Paleontology 7:57–84.  
 924 Poplin, C. 1974. Étude de quelques paléoniscidés pennsylvaniens du Kansas. Cahiers de  
 925 paléontology:1–148+I–XL pl.  
 926 Poplin, C., and M. Véran. 1996. A revision of the actinopterygian fish *Coccocephalus wildi* from the  
 927 Upper Carboniferous of Lancashire. Special Papers in Palaeontology 52:7–30.

928 Pradel, A., J. G. Maisey, R. H. Mapes, and I. Kruta. 2016. First evidence of an intercalary bone in the  
929 braincase of “palaeonisciform” actinopterygians, with a virtual reconstruction of a new  
930 braincase of *Lawrenciella* Poplin, 1984 from the Carboniferous of Oklahoma. *Geodiversitas*  
931 38:489–504.

932 Ronquist, F., M. Teslenko, P. van der Mark, D. L. Ayres, A. Darling, S. Höhna, B. Larget, L. Liu, M.  
933 A. Suchard, and J. P. Huelsenbeck. 2012. MrBayes 3.2: Efficient Bayesian Phylogenetic  
934 Inference and Model Choice Across a Large Model Space. *Systematic Biology* 61:539–542.

935 Sallan, L. C. 2014. Major issues in the origins of ray-finned fish (Actinopterygii) biodiversity.  
936 *Biological Reviews* 89:950–971.

937 Sallan, L. C., and M. I. Coates. 2013. Styracopterid (Actinopterygii) ontogeny and the multiple origins  
938 of post-Hangenberg deep-bodied fishes. *Zoological Journal of the Linnean Society* 169:156–  
939 199.

940 Schaeffer, B. 1973. Interrelationships of chondrosteans; pp. 207–226 in P. H. Greenwood, R. H. Miles,  
941 and C. Patterson (eds.), *Interrelationships of fishes*. Academic Press Inc, London.

942 Schaeffer, B., and W. W. Dalquest. 1978. A palaeonisciform braincase from the Permian of Texas,  
943 with comments on cranial fissures and the posterior myodome. *American Museum Novitates*  
944 2658:1–15.

945 Sewertzoff, A. N. 1928. The head skeleton and muscles of *Acipenser ruthenus*. *Acta Zoologica* 9:1–  
946 127 + I–IX pl.

947 Stamberger, S. 1991. Actinopterygians of the central bohemian Carboniferous basins. *Acta Musei*  
948 *Nationalis Pragae. B, Hist. naturalis* 47:25–104 + I–XXIV pl.

949 Stensiö, E. A. 1921. Triassic fishes from Spitzbergen (Part 1). 307+35 plates pp. Adolf Holzhausen,  
950 Vienna.

951 Stensiö, E. A. 1932. Triassic fishes from East Greenland. 305 + XXXIX pl. pp. Bianco Lunos  
952 Bogtrykkeri A/S, Copenhagen.

953 Traquair, R. H. 1877. The Ganoid Fishes of the British Carboniferous Formations. Part 1.  
954 *Palaeoniscidae*. Pages 1–60; Plates I–VII. *Monographs of the Palaeontographical Society* 31:1–  
955 60.

- 956 Véran, M. 1988. Les éléments accessoires de l'arc hyoïdien des poissons téléostomes (Acanthodiens et  
957 Osteichthyens) fossiles et actuels. Mémoires du museum national d'histoire naturelle 54:1–98  
958 + I–VII pl.
- 959 Véran, M. 1996. Le labial des poissons actinoptérygiens fossiles et actuels. Bulletin du Muséum  
960 National d'Histoire Naturelle, Paris 18:1–55.
- 961 Warth, P., E. J. Hilton, B. Naumann, L. Olsson, and P. Konstantinidis. 2017. Development of the skull  
962 and pectoral girdle in Siberian sturgeon, *Acipenser baerii*, and Russian sturgeon, *Acipenser*  
963 *gueldenstaedtii* (Acipenseriformes: Acipenseridae). Journal of Morphology 278:418–442.
- 964 Xu, G.-H. 2019. Osteology and phylogeny of *Robustichthys luopingensis*, the largest holostean fish in  
965 the Middle Triassic. PeerJ 7:e7184.
- 966 Xu, G.-H., K.-Q. Gao, and J. A. Finarelli. 2014. A revision of the Middle Triassic scanilepiform fish  
967 *Fukangichthys longidorsalis* from Xinjiang, China, with comments on the phylogeny of the  
968 Actinopteri. Journal of Vertebrate Paleontology 34:747–759.
- 969

971 **Fig. 1. Previously hypothesized phylogenetic placements of †*Brachydegma caelatum*.** Simplified  
 972 trees given contain an indicative subset of taxa common to all published phylogenetic hypotheses.

973

974 **Fig. 2. External anatomy of †*Brachydegma caelatum* holotype (MCZ VPF 6503), right lateral**  
 975 **view.** Specimen photograph (A) and weighted-line drawing (B). Abbreviations: ?, uncertain; ?ao,  
 976 possible antorbital; ang, angular; aop, accessory opercles; cl, cleithrum; dhy, dermohyal; dnt,  
 977 dentary; dpt, dermopterotic; dsp, dermosphenotic; fr, frontal; hm, hyomandibula; io, infraorbital; ju,  
 978 jugal; la, lachrymal; lexsc, lateral extrascapular; lg, lateral gular; mg, median gular; mx, maxilla; o  
 979 supo, overlap areas on frontal for supraorbitals; op, opercle; pa, parietal; pcl, postcleithrum; pop,  
 980 preopercle; pscl, presupracleithrum; ptmp, posttemporal; qj, quadratojugal; rbr, branchiostegal rays;  
 981 scl, supracleithrum; sop, suboperculum; subo, suborbitals; supo, supraorbital. Abbreviations preceded  
 982 by l or r indicate left or right structure, respectively. +, dermohyal overlying hyomandibula. Dashed  
 983 lines indicate a missing margin; hatching indicates a broken surface; gray tone indicates matrix. Scale  
 984 bar equals 20 mm. Specimen photograph copyright President and Fellows of Harvard College.

985

986 **Fig. 3. External anatomy of †*Brachydegma caelatum* holotype (MCZ VPF 6503), left lateral view.**  
 987 Specimen photograph (A) and weighted-line drawing (B). Abbreviations: ?, uncertain; ang, angular;  
 988 aop, accessory opercle; dnt, dentary; dpt, dermopterotic; dsp, dermosphenotic; fr, frontal; ju, jugal;  
 989 lexsc, lateral extrascapular; mx, maxilla; na, nasal; pa, parietal; pal, palate; pmx, premaxilla; pop,  
 990 preopercle; o dnt, overlap area for the dentary on the preopercle; op, opercle; qj, quadratojugal; rbr,  
 991 branchiostegal ray; sop, subopercle. Dashed lines indicate a missing margin; hatching indicates a  
 992 broken surface; gray tone indicates matrix. Scale bar equals 20 mm. Specimen photograph copyright  
 993 President and Fellows of Harvard College.

994

995 **Fig. 4. External anatomy of †*Brachydegma caelatum* holotype (MCZ VPF 6503), dorsal and**  
 996 **ventral views.** Specimen photograph (A) and weighted-line drawing (B) in dorsal view. Specimen  
 997 photograph (C) and weighted-line drawing (D) in ventral view. Abbreviations: ?, uncertain; ?ao,  
 998 antorbital; ang, angular; aop, accessory opercle; cl, cleithrum; dnt, dentary; dpt, dermopterotic; dsp,  
 999 dermosphenotic; fr, frontal; ju, jugal; la, lachrymal; lexsc, lateral extrascapular; lg, lateral gular; mg,  
 1000 median gular; mx, maxilla; na, nasal; o supo, overlap areas on frontal for supraorbitals; op, opercle;  
 1001 pa, parietal; pmx, premaxilla; pop, preopercle; pscl, presupracleithrum; ptmp, posttemporal; qj,  
 1002 quadratojugal; rbr, branchiostegal rays; scl, supracleithrum; sop, subopercle. Abbreviations preceded  
 1003 by l or r indicate left or right structure, respectively. Dashed lines indicate a missing margin; hatching  
 1004 indicates a broken surface; gray tone indicates matrix. Scale bar equals 20 mm. Specimen photographs  
 1005 copyright President and Fellows of Harvard College.

1006

1007 **Fig. 5. Braincase and parasphenoid of †*Brachydegma caelatum*.** Type specimen (MCZ VPF 6503)  
 1008 in (A) right lateral, (B) dorsal, (C) ventral, (D) posterior views; (E) line drawing of D with separate  
 1009 ossifications color coded. Paratype (MCZ VPF 3504) in (F) right lateral, (G) dorsal, (H) ventral, (I)  
 1010 posterolateral view with separate ossifications color coded; (J) line drawing of H with separate

ossifications color coded, **(L)** composite reconstruction of preserved aspects of the braincase in lateral view with separate ossifications color coded. Abbreviations: **II**, orbital opening; **aoca**, anterior opening or aortic canal; **aocp**, posterior opening of aortic canal; **apal**, furrows for suspension of palate or parabasal canals; **asp**, ascending process of parasphenoid; **boc**, basioccipital; **exo**, exoccipitals; **fm**, foramen magnum; **not**, notochordal opening; **osph**, orbitosphenoid; **pmy**, posterior myodome; **pspf**, median furrow of parasphenoid; **pspk**, ventral keel of parasphenoid; **spig**, spiracular groove. Scale bars equal 10 mm. Specimen renderings copyright President and Fellows of Harvard College.

**Fig. 6. Palatal complex and maxilla of †*Brachydegma caelatum*.** Type specimen (MCZ VPF 6503): **(A)** Palatal complex and ‘labial cartilage’ in lateral view; palatal complex and maxilla in medial **(B)** and **(C)** ventral views; cross sections demarcated by arrows in A, B, C showing the relationship of palatal complex and maxilla at **(D)** the level of lateral process and **(E)** the level of the orbital notch. **(F)** lateral view of the ossified labial element; **(G)** anterior view of the same element. Paratype (MCZ VPF 6504): **(H)** palatal complex and maxilla in medial view; **(I)** palatal complex in lateral view; **(J)** maxilla in ventromedial view. **(L)** Schematic reconstruction of palatal complex in lateral view; **(M)** Schematic reconstruction of maxilla in ventromedial view. Abbreviations: **avm**, accessory vomer; **calg**, canal for the passage of ligaments; **lbe**, ossified ‘labial element’; **ltp**, lateral process of the ectopterygoid; **mptf**, metapterygoideal flange; **mx**, maxilla; **mxhl**, horizontal lamina of maxilla; **mxxp**, ethmoid articulation of maxilla; **qd**, quadrate; **vpl**, ventrolateral palatal lamina. Scale bars equal 10 mm. Specimen renderings copyright President and Fellows of Harvard College.

**Fig. 7. Suspensorium and lower jaw of †*Brachydegma caelatum*.** Right palatal complex and suspensorium of type specimen (MCZ VPF 6503) shown as preserved in **(A)** lateral and **(B)** medial views. Paratype (MCZ VPF 6504): right hyomandibula in **(C)** lateral and **(D)** medial views; **(E)** left ceratohyal in lateral view; Right lower jaw of type specimen in **(F)** lateral, **(G)** dorsal, and **(H)** medial views. Abbreviations: **VIIhm**, hyomandibular trunk of facial nerve; **adf**, adductor fossa; **art**, articular; **chy**, ceratohyal; **chyg**, arterial groove; **dhy**, dermohyal; **dnt**, dentary; **hh**, hypohyal; **hm**, hyomandibula; **mxxs**, maxillary shelf on dentary; **opp**, opercular process; **pal**, palatal complex; **qf**, quadrate facets; **qj?**, putative quadratojugal; **sang**, surangular; **sy**, symplectic; **syf**, symplectic fossa. Scale bars equal 10 mm. Specimen renderings copyright President and Fellows of Harvard College.

**Fig. 8. Accessory hyoidean ossifications in †*Brachydegma caelatum* and other actinopterygians.** †*Brachydegma caelatum* type specimen (MCZ VPF 6503): **(A)** left suspensorium shown as preserved in lateral view; **(B)** posterior view of quadrate and articular; **(C)** anterior and **(D)** anterolateral detail of symplectic; **(E)** line drawing of D. †*Parasemionotidae* indet. (NHMD 74424 A): **(F)** left suspensorium shown as preserved in lateral view; in **(G)** anterior and **(H)** lateral detail of symplectic; **(I)** posterior view of quadrate and articular; †*Pteronisculus gunnari* (NHMD 73588 A): **(J)** right suspensorium in mirrored lateral view; **(K)** anterior and **(L)** lateral detail of symplectic; **(M)** posterior view of quadrate and articular; *Acipenser brevirostrum* (UMMZ 64250): **(N)** left suspensorium in lateral view; **(O)** anterior and **(P)** lateral detail of ‘symplectic’; **(Q)** posterior view of palatoquadrate and meckel’s cartilage. Abbreviations: **afmd**, groove for afferent mandibular artery; **art**, articular; **chy**, ceratohyal; **cnd**, anterior condyle of symplectic; **ih**, interhyal; **mk**, meckel’s cartilage; **pq**, palatoquadrate; **qd**, quadrate; **qdgr**, posterior groove on quadrate; **sy**, symplectic; **syf**, symplectic fossa; **vpsy**, ventral process of symplectic. Scale bars for A, B, F, I, J, M–Q equal 10 mm; scale bars for C–E, G, H, K, L

equal 5 mm. Specimen renderings of †*Brachydegma* copyright President and Fellows of Harvard College.

**Fig. 9. Branchial anatomy of †*Brachydegma caelatum*.** Type specimen (MCZ VPF 6503): (A) right and (B) left lateral views of complete branchial and ventral hyoid skeleton shown as preserved; (C) branchial arches of left side in medial view; (D) ventral view of preserved branchial elements of paratype (MCZ VPF 6504); (E) composite reconstruction of gill skeleton with branchial arches spaced and splayed ventrally. Abbreviations: **bb**, basibranchial; **bb/bh**, basibranchial or basihyal; **cb1–5**, ceratobranchial 1–5; **chy**, ceratohyal; **ep1–4**, epibranchial 1–4; **gr**, gill rakers; **hb1–4**, hypobranchial 1–4; **hh**, hypohyal; **ipb1–3**, infrapharyngobranchial 1–3; **spb1,2**, suprapharyngobranchial 1,2. Scale bars equal 10 mm. Specimen renderings copyright President and Fellows of Harvard College.

**Fig. 10. Pectoral fin and axial anatomy of †*Brachydegma caelatum*.** Type specimen (MCZ VPF 6503): (A) Right pectoral girdle in lateral view; (B) anterior view of right cleithrum; (C) right pectoral girdle in medial view; (D) right scapulocoracoid and reconstructed fin ossifications in medial view; (E) line drawing of D with dotted line indicating the conceived course of the mesocoracoid arch; (F) right scapulocoracoid and reconstructed fin ossifications in medial view; (G) scapulocoracoid and cleithrum in posterior view; (H) anterior axial skeleton; (I) anterodorsal view of fused arcual element; (J) medial view of left basidorsal; (K) medial view of lateral line scale. Abbreviations: **adp**, anterodorsal process of scale; **bd**, basidorsal; **bdf**, medial furrow on basidorsal; **bds**, hemi-neural spine; **bv**, basiventral; **cl**, cleithrum; **clv**, clavicle; **dmca**, dorsal limit of the mesocoracoid arch; **fcpl**, facet for the coracoid plate; **ll**, lateral line pore; **pap**, parapophysis; **pbl**, post-branchial lamina; **pcl**, postcleithrum; **pg**, articular peg of scale; **ppt?**, putative propterygium; **pzg**, prezygapophysis; **rd**, radials; **scc**, scapulocoracoid; **sccm**, middle (articular) region of scapulocoracoid; **scf**, supracoracoid foramen; **scl**, supracleithrum; **vmca**, ventral limit of the mesocoracoid arch. Scale bars for A–H equal 10 mm; scale bars for I–K equal 5 mm. Specimen renderings copyright President and Fellows of Harvard College.

**Fig 11. Strict consensus of the 1412 most parsimonious trees of 1652 steps for 117 taxa and 300 equally weighted characters.** Consistency index=0.203, Retention index=0.66. Numbers above nodes indicate Bremer values above 1. Numbers below nodes indicate bootstrap percentages above 50%. Selected node optimizations are as follows: **a** (Actinopterygii total group): C.6(1→0); C.29(0→1,2); C.43(0→1); C.45(1→0); C.46(0→1); C.54(0→1); C.57(0→1); C.63(1→0); C.64(0→1); C.69(0→1); 70(0→1); C.77(0→1); C.79(0→1); C.90(0→1); C.109(0→1); C.139(0→1); C.152(0→1); C.199(0→1); C.215(0→1); C.257(0→1); C.258(0→1); C.264(0→1); **b** (Actinopterygii crown group): C.67(1→0); C.101(0→1); C.103(0→1); C.107(0→1); C.157(0→2); C.174(0→2); **c** (†*Brachydegma*+†*Birgeriidae*+†*Scanilepiformes*+†*Polypteridae*): C.45(1→0); C.55(0→3); C.158(0→1); **d** (Chondrostei+†*Saurichthiiformes*): C.14(1→0); C.111(1→2); C.123(1→0); C.210(1→0); **e** (Neopterygii crown group): C.53(0→1); C.56(0→1); C.73(0→1); C.74(0→1); C.119(0→1); C.180(0→1); C.219(0→1); C.287(0→1); **f** (Teleostei total group): C.9(0→1); C.47(1→0); C.55(3→1); C.168(0→1); C.169(0→1); C.225(0→1); C.270(0→1); **g** (*Halecomorphi*+†*Watsonulus*): C.75(0→1); C.76(0→1); C.97(0→1); C.135(0→1); C.220(1→0); C.280(1→0); **h** (†*Dapediidae*+†*Pycnodontiformes*+†*Tetragonolepis*): C.59(2→1); C.223(0→1); C.255(0→2); C.266(0→1); C.278(0→1); C.284(0→1); C.285(0→1); C.289(0→1).

1099

1100 **Fig. 12. Evolutionary morphology of accessory hyoidean elements of actinopterygians.** Simplified  
1101 evolutionary hypothesis from Fig. 11. Nodes are as follows: **A** stem Actinopterygii; **B** †*Brachydegma*  
1102 + Polypteridae; **C** Actinopteri; **D** Neopterygii; **E** Teleostei; **F** †Pycnodontiformes; **G** Holostei. Sources  
1103 of anatomical information: †*Pteronisculus*, †*Brachydegma*, *Acipenser*, †Parasemionotidae indet. this  
1104 work; *Polypterus* (Allis, 1922; Jollie, 1984); †*Pholidophorus gervasuttii* (Arratia, 2013); *Hiodon*, with  
1105 cartilaginous interhyal omitted as it does not articulate with the hyomandibula (Hilton, 2002);  
1106 †*Neoproscinetes* (Nursall and Maisey, 1987; Gardiner et al., 1996); *Lepisosteus* (Grande, 2010); *Amia*  
1107 (Grande and Bemis, 1998). Drawings not to scale.

1108

1 **A Permian fish reveals widespread distribution of neopterygian-like jaw suspension**

2

3 Thodoris Argyriou\*, Sam Giles, Matt Friedman

4

5 **Appendix 1. Additional figures and phylogenetic trees**

6



A



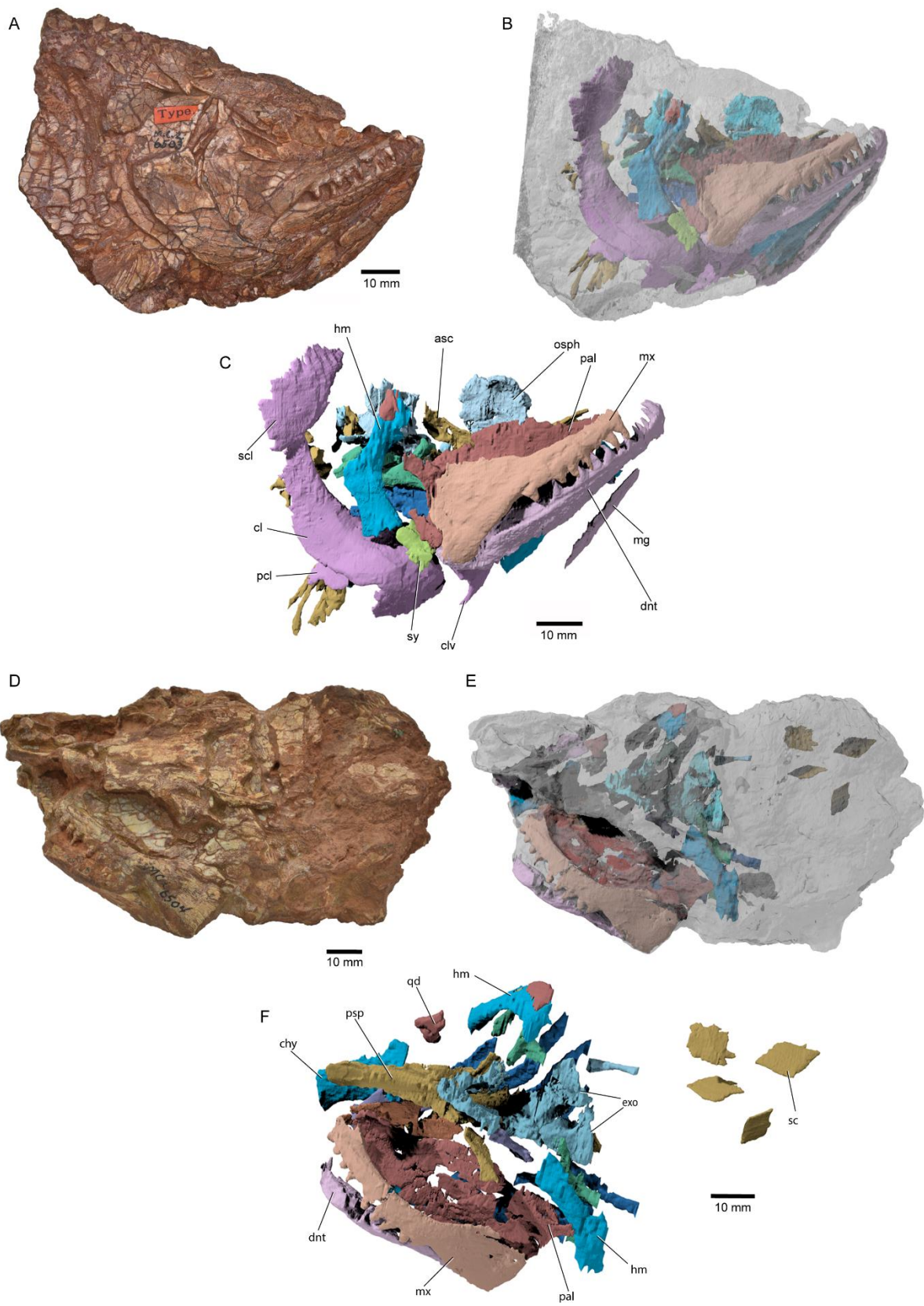
B



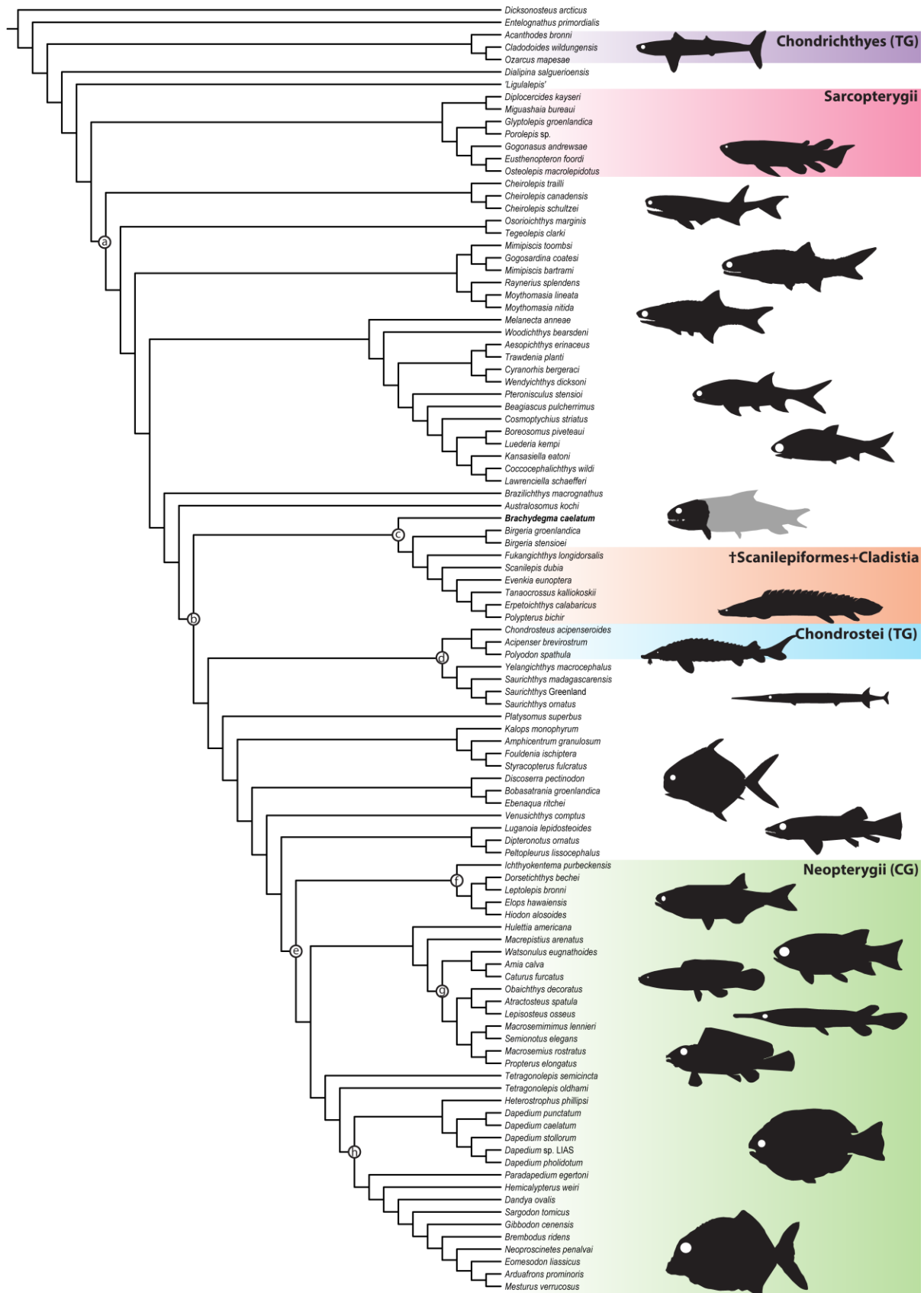
10 mm

8 **Appendix Fig. 1.** †*Brachydegma caelatum* paratype specimen (MCZ\_VPF\_6504). Compressed  
9 specimen in (A) dorsolateral and (B) ventrolateral (bottom) views. Images copyright President and  
10 Fellows of Harvard College.

11

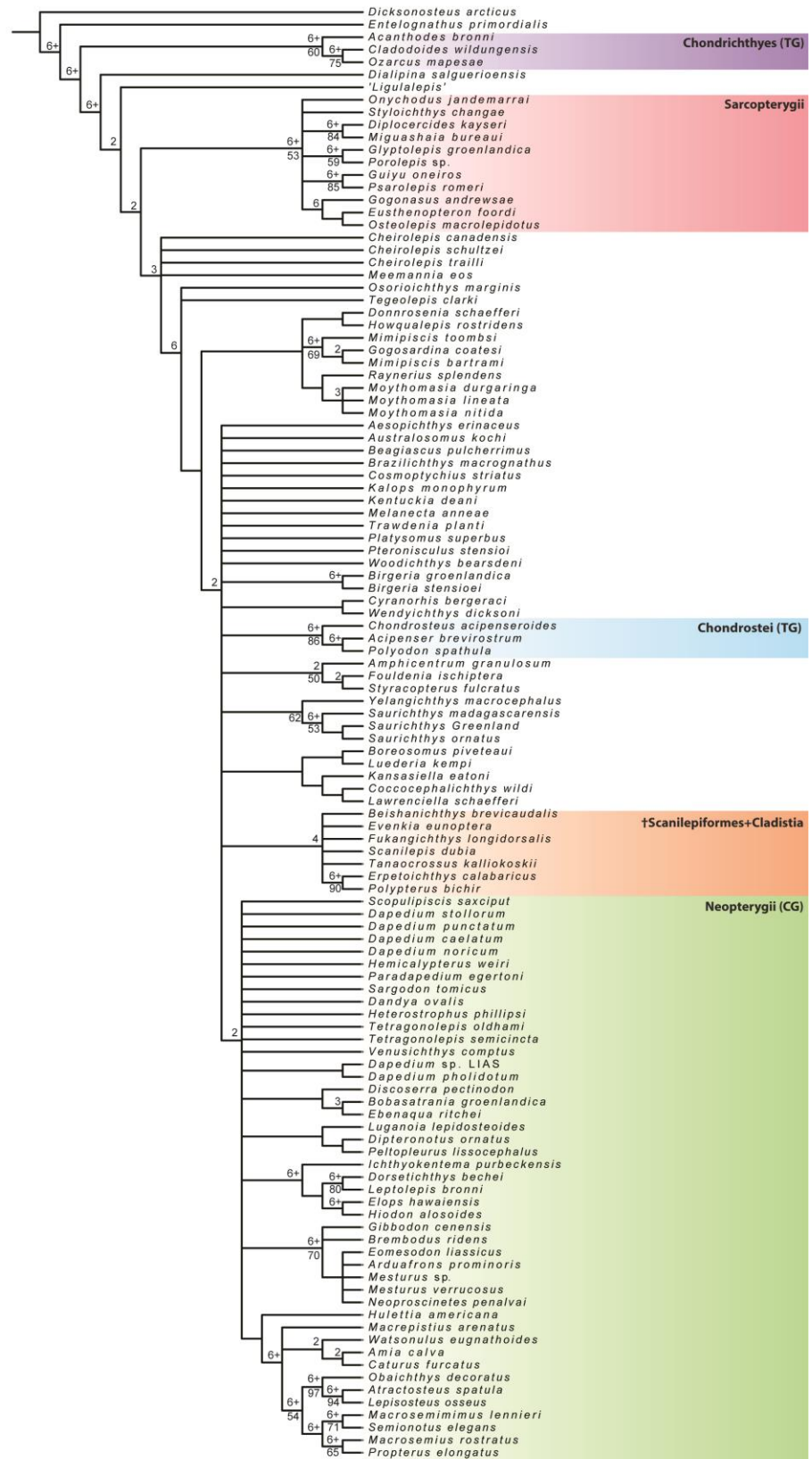


**Appendix Fig. 2. 3D-reconstructed portions of †*Brachydegma caelatum*.** Type specimen (MCZ\_VPF\_6503): **(A)** right lateral view of actual specimen; **(B)** geometry of reconstructed endoskeletal elements; **(C)** complete reconstruction of right side of the specimen (slightly enlarged); Paratype specimen (MCZ\_VPF\_6504): **(D)** left dorsolateral view of the specimen; **(E)** geometry of reconstructed endoskeletal elements; **(F)** complete reconstruction in left laterodorsal view. Abbreviations: **asc**, ascending process of parasphenoid; **chy**, ceratohyal; **cl**, cleithrum; **clv**, clavicle; **dnt**, dentary; **exo**, exoccipitals; **hm**, hyomandibula; **mg**, median gular; **mx**, maxilla; **osph**, orbitosphenoid portion of braincase; **pal**, palatal complex; **pcl**, postcleithrum; **psp**, parasphenoid; **qd**, quadrate; **sc**, scales; **scl**, supracleithrum; **sy**, symplectic. Images copyright President and Fellows of Harvard College.



**Appendix Fig. 3. Agreement subtree (one of 23) resulting from parsimony analysis using equal weights and without constraining the topology of †*Brachydegma*.** It contains 104 out of 117 taxa. Pruned taxa: †*Onychodus jandermarrai*; †*Styloichthys change*; †*Guiyu oneiros*; †*Psarolepis romeri*; †*Meemania eos*; †*Donnrosenia schaefferi*; †*Howqualepis rostridens*; †*Moythomasia durgaringa*; †*Melanecta anneae*; †*Beishanichthys brevicaudalis*; †*Scopulipiscis saxciput*; †*Dapedium noricum*; †*Mesturus* sp. Lettered nodes as in text Fig. 11.

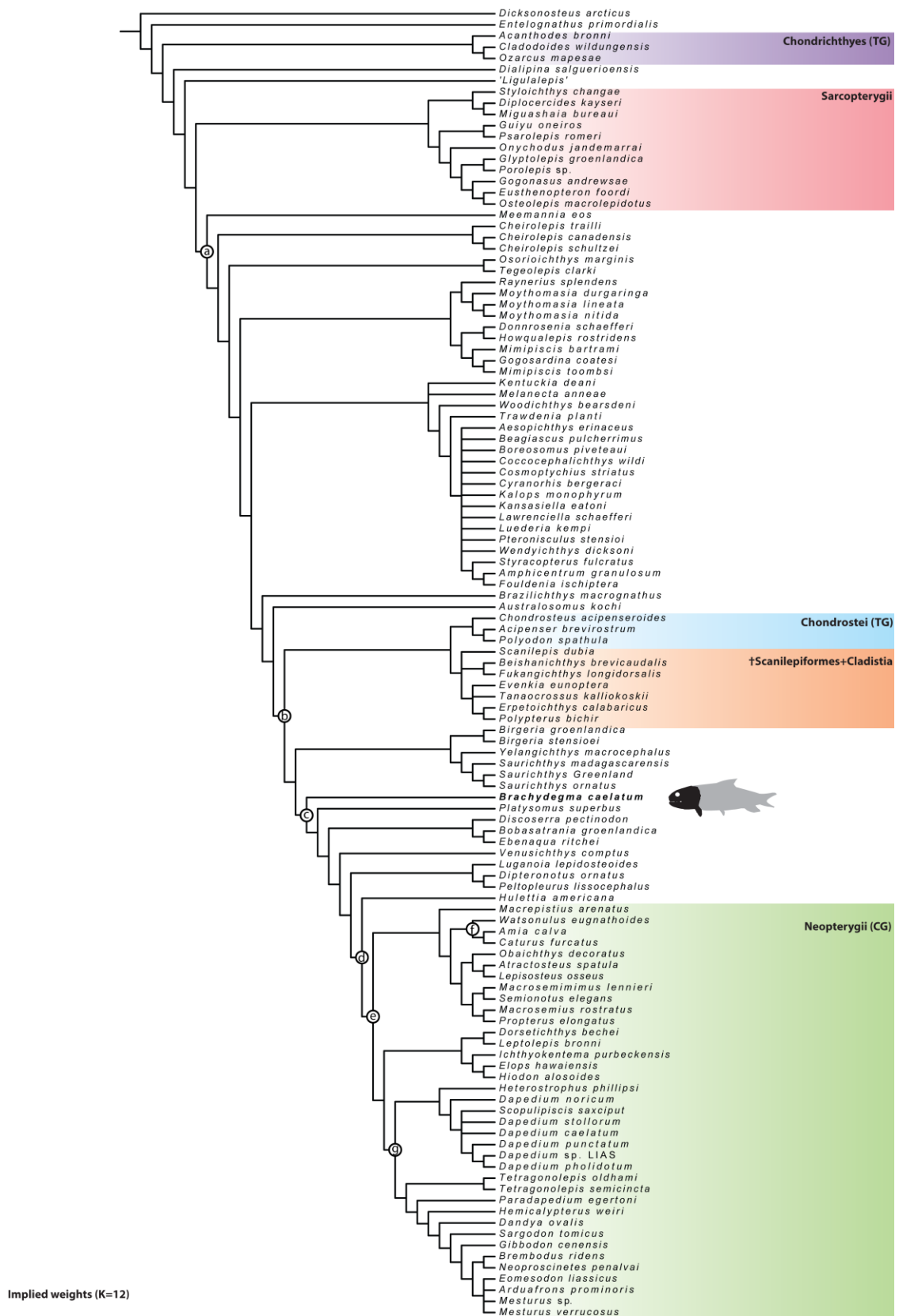




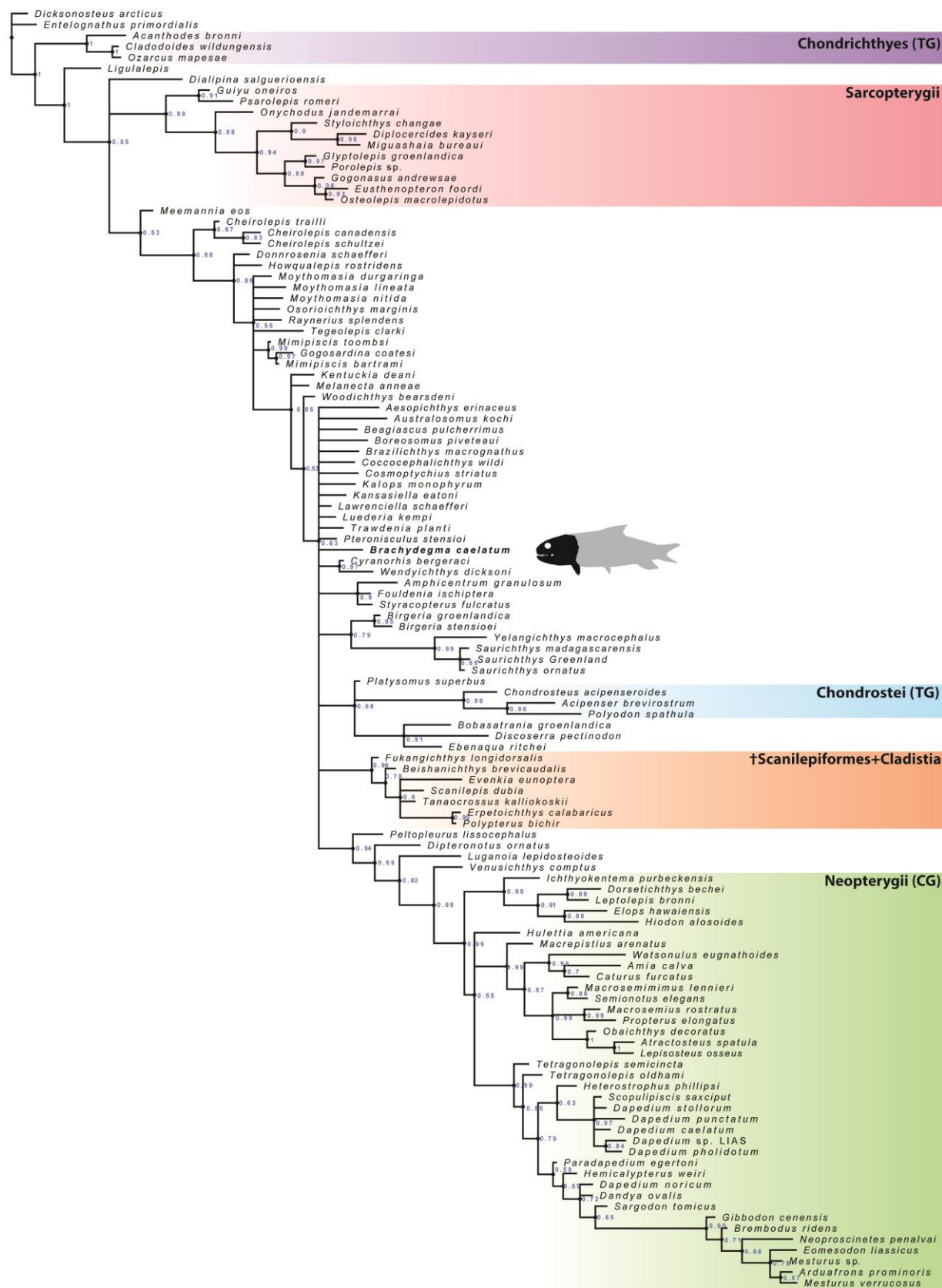
32 **Appendix Fig. 4. Strict consensus of the 1740 most parsimonious trees of 1646 steps for 116 taxa**  
33 **and 300 equally weighted characters. †*Brachydegma* was excluded.** Consistency index=0.204,  
34 Retention index=0.661. Numbers above nodes indicate Bremer values above 1. Numbers below nodes  
35 indicate bootstrap percentages above 50%.

36



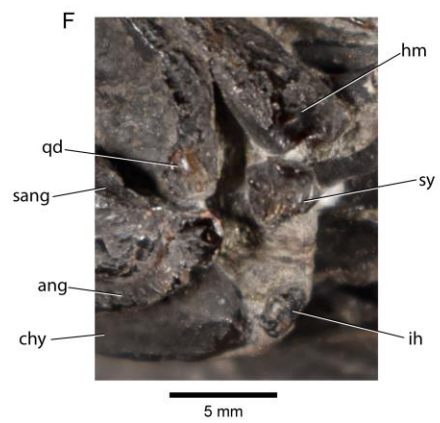
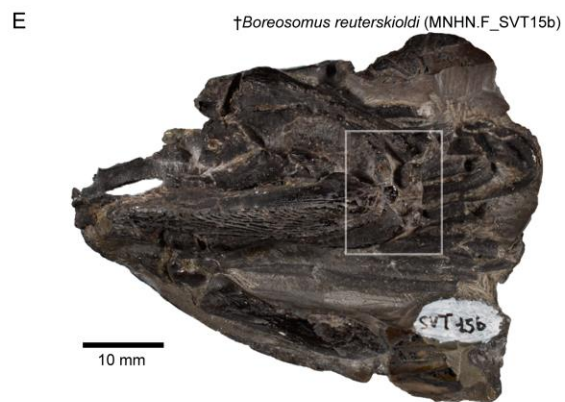


**Appendix Fig. 5. Strict consensus of the 44 best fit trees (Fit Score=68.77) resulting from analyses using implied weights with a K=12.** Selected node optimizations are as follows: **a** (Actinopterygii total group): C.43(0→1); C.45(1→0); C.139(0→1); C.199(0→1); **b** (Actinopterygii crown group): C.67(1→0); C.101(0→1); C.107(0→1); C.157(0→2); C.158(0→1); C.174(0→2); C.262(0→1); **c** (†*Brachydegma*+Neopterygii total group): C.116(0→1); C.124(0→1); C.231(0→1); **d** (†*Hulettia*+Neopterygii crown group): C.56(0→1); C.73(0→1); C.74(0→1); C.90(2→1); C.113(0→1); C.119(0→1); C.180(0→1); C.219(0→1); C.287(0→1); **e** (Neopterygii crown group): C.18(0→1); C.34(0→1); C.149(1→0); C.160(0→1); C.171(0→1); **f** (Halecomorphi+†*Watsonulus*): C.75(0→1); C.76(0→1); C.97(0→1); C.135(0→1); C.220(1→0); C.280(1→0); **g** (†Dapediidae+(†Pycnodontiformes)+†*Tetragonolepis*): C.28(1→0); C.255(0→2); C.257(0→1); C.266(0→1); C.278(0→1); C.281(0→1); C.284(0→1); C.285(0→1); C.293(1→0).



51 **Appendix Fig. 6. Phylogenetic tree from Bayesian analysis of morphological phylogenetic dataset.**  
52 Values below nodes represent posterior probability support (BPP).

53



54

55

56

57 **Appendix Fig. 7. Triassic actinopterygians used for comparison with †*Brachydegma*. (A), (B)**  
58 †*Pteronisculus gunnari* (NHMD\_73588\_A), Early Triassic, East Greenland; (C), (D) †Parasemionotidae  
59 indet. (NHMD\_74424\_A), Early Triassic, East Greenland; (E) †*Boreosomus reuterskioldi*  
60 (MNHN.F\_SVT15b), Early Triassic, Spitsbergen, Svalbard, prepared and figured by M. Véran  
61 (1988;1996); (F) magnification of jaw joint area, contained within a white box in (E). Abbreviations: **ang**,  
62 angular; **chy**, ceratohyal; **hm**, hyomandibula; **ih**, interhyal; **qd**, quadrate; **sang**, surangular; **sy**, symplectic.  
63 Scale bars equal 10 mm.

# **A Permian fish reveals widespread distribution of neopterygian feeding innovations**

Thodoris Argyriou\*, Sam Giles, Matt Friedman

## **Appendix 2. Modifications and additions to morphological phylogenetic dataset**

### **1. General notes.**

We expanded the morphological character matrix of Latimer and Giles (Latimer and Giles, 2018), by adding all taxa and most new characters, character states and amendments presented in Argyriou et al. (Argyriou et al., 2018), as well as adding and modifying existing characters (see detailed list of changes below regarding (Argyriou et al., 2018; Latimer and Giles, 2018). We removed a character regarding the presence of an ectopterygoid process on the palate (Giles et al. 2017), as the distribution of this feature needs to be reevaluated (see e.g., V  ran, 1996). The external anatomy of †*Brachydegma*, which was included in a previous version of this matrix (Giles et al., 2017), was coded anew, while †*Saurichthys madagascariensis* was extensively recoded in Argyriou et al., 2018; these changes are not repeated here. We modified the scores for †*Trawdenia* (=†*Mesopoma*) *planti* sensu Coates and Tietjen, 2018. We expanded our taxonomic coverage of stem ray-fins by adding †*Brazilichthys macrognathus* (Figueroa et al., 2019). Furthermore, to provide a better-informed picture of the distribution of accessory hyoidean elements in ray-fins, and also of neopterygian interrelationships, we scored the pycnodont †*Neoproscinetes penalvai*, for which both external (Nursall and Maisey, 1987) and braincase (Machado, 2008) anatomical information is available.

### **2. List of added, removed and modified characters**

#### **A) Characters and character states added:**

23 **C.21:** Both nostrils accommodated within single ossification: 0=absent, 1=present (from Argyriou et al.,  
24 2018).

25 **C.97:** Accessory hyoid element involvement in jaw joint: 0=absent, 1=present (modified from Latimer  
26 and Giles, 2018 and references therein). We modified the name of this character as well as the scores to  
27 reflect the uncertainty regarding the involvement of these rarely preserved elements in fossils. This  
28 character is coded only in taxa where accessory hyoid elements are present, or where there is adequate  
29 data regarding their presence, absence. For example, †*Pteronisculus stensioi* is coded as 1, following our  
30 investigations and interpretations (see also Nielsen, 1942).

31 **C.110:** Operculum: 0=absent, 1=present (from Argyriou et al., 2018).

32 **C.152:** Craniospinal process: 0=absent, 1=present (from Gardiner et al., 2005; Argyriou et al., 2018).

33 **C.159:** Bifurcation of dorsal aorta into lateral dorsal aortae: 0=open in endoskeletal groove, 1=enclosed  
34 in canal, 2=below parasphenoid (state 2 added, sensu Argyriou et al., 2018)

35 **C.167:** Occipital region ossification pattern: 0=basioccipital and exoccipitals as separate ossifications,  
36 1=comineralized (from Argyriou et al., 2018).

37 **C.179:** Parasphenoid pierced by ascending common carotids: 0=absent, 1=present (from Argyriou et al.,  
38 2018).

39 **C.187:** Arrangement of olfactory nerve in orbital region: 0=completely enclosed in endoskeletal olfactory  
40 canal, 1=traversing the orbit lateral to the interorbital septum, at times leaving a groove on the latter (from  
41 Argyriou et al., 2018).

42 **C.201:** Lateral cranial canal connects to lateral wall of braincase: 0=absent, 1=present (from Argyriou et  
43 al., 2018).

44 **C.202:** Intramural diverticula opening in fossa bridgei: 0=absent, 1=present (from Argyriou et al., 2018).



**C.222:** Ossified accessory hyoid elements: 0=absent; 1=present (new character). In most primitive gnathostomes and chondrichthyans elements situated between the epihyal or hyomandibula and the ceratohyal are completely absent.

**C.223:** If present, number of accessory hyoid elements: 0=one; 1=two (new character). The homology of some of the constituents of the hyoid arch—the so-called intermediate or accessory hyoid elements—in modern ray-fins remains controversial. The history attached to naming these elements is very complex (Sewertzoff, 1928; Patterson, 1973, 1982; Jollie, 1984; Véran, 1988; Gardiner and Schaeffer, 1989; Grande and Bemis, 1991; Gardiner et al., 1996; Grande and Bemis, 1998; Grande, 2010; Hilton et al., 2011), and we have tried here to apply a simple, consistent approach and code for the number of ossified accessory hyoidean elements alone. Polypterids exhibit a single ossified element connecting the hyomandibula with the ceratohyal, which has been identified as the primitively present interhyal (Allis, 1922; Patterson, 1982; Jollie, 1984). A second independently ossified element (a ‘symplectic’) does not develop (Jollie, 1984). Neopterygians (e.g. *Amia*, *Lepisosteus*, *Hiodon*, †*Dorsetichthys*, †*Macrosemionotus*, †*Watsonulus* etc.) exhibit two intermediate hyoidean elements, a symplectic and an interhyal. The interhyal connects the hyomandibula with the ceratohyal. This may be very reduced (e.g. †*Watsonulus*, *Elops*), or entirely cartilaginous (e.g. *Amia*, *Lepisosteus*) in many actinopts. The ossification that contacts the hyomandibula (and typically the quadrate and the articular), but does not articulate with the ceratohyal, is termed the symplectic. This element may brace the quadrate, and in †*Watsonulus*, †*Caturus*, *Amia* and possibly pycnodonts (Patterson, 1973; Olsen, 1984; Véran, 1988; Gardiner et al., 1996; Grande and Bemis, 1998) additionally forms an articulation with the lower jaw. Although the presence of a true symplectic in stem actinopterygians (‘paleoniscoids’) has been rejected by many authors (Patterson, 1973, 1982; Gardiner and Schaeffer, 1989; Gardiner et al., 1996), Véran (Véran, 1988) identified a second, symplectic-like, intermediate ossification in the hyoid arch in a number of ‘paleoniscoids’. Our reexamination of part of her material (†*Boreosomus reuteskioldi*) confirmed her observations of two ossified accessory hyoidean elements. These include a symplectic-like element

associated with the anteroventral portion of the hyomandibula and in close association with the palatoquadrate and lower jaw; and a small interhyal articulating with the posterodorsal tip of the ceratohyal. †*Brachydegma*, which is not a crown neopterygian, also exhibits both a symplectic and an interhyal. The condition in modern Chondrostei is extremely complicated. Two intermediate hyoidean elements are present, but unlike in other extant ray-fins these are serially arranged. Dorsally, a hypertrophied element connects the hyomandibula with the quadrate and lower jaw, and might partially ossify in very large sturgeons (Hilton et al., 2011). This element has been variably homologized with the symplectic or the interhyal. A second, smaller, element suspends the ventral portion of the hyoid arch from the former hypertrophied element, but does not ossify. This element has been identified as either an interhyal, or a posterior ceratohyal. Given the fact that only one of the two elements ossify, we code *Acipenser* as 0.

**C.225:** Position of symplectic: 0=posterior to the posterior margin of quadrate, 1=medial to the posterior margin of quadrate (modified from Arratia, 2013).

**C.267:** Epineural processes: 0=absent, 1=present (from Arratia, 2013; Argyriou et al., 2018).

## **B. Character scores updated from Latimer and Giles (2018), unless stated otherwise**

†*Acantodes bronni*

C.110: ? → -

C.111: ? → -

C.112: ? → -

C.113: ? → -

C.114: ? → -

92

93 *Acipenser brevirostrum*

94 C.111:  $2 \rightarrow -$

95 C.128:  $1 \rightarrow 0$

96 C.140:  $0 \rightarrow 1$

97 C.157:  $- \rightarrow 1/2$

98 C.196:  $? \rightarrow 1$

99 C.197:  $? \rightarrow 0$

100 C.198:  $? \rightarrow 1$

101 C.199:  $? \rightarrow 0$

102 C.200:  $0 \rightarrow -$

103 C.207:  $- \rightarrow 0$

104 C.208:  $- \rightarrow 1$

105 C.209:  $- \rightarrow 0$

106 C.211:  $- \rightarrow 0$

107 C.212:  $- \rightarrow 0$

108 C.215:  $0 \rightarrow 1$

109 C.219:  $1 \rightarrow 0$

110 C.224:  $- \rightarrow ?$

111 C.230:  $0 \rightarrow 0/1$

112

113 *Amia calva*

114 C.157:  $0 \rightarrow 2$

115

116 †*Amphicentrum granulosum*

117 C.72:  $1 \rightarrow 0$

118

119 †*Arduafrons prominoris*

120 C.273:  $0 \rightarrow -$

121

122 *Atractosteus spatula*

123 C.157:  $0 \rightarrow 2$

124 C.186:  $0 \rightarrow 1$

125

126 †*Australosomus kochi*

127 C.202:  $- \rightarrow 0$

128 C.224:  $- \rightarrow ?$

129

130 †*Beishanichthys brevicaudalis*

131 C.224:  $- \rightarrow ?$

132

133 †*Birgeria groenlandica*

134 C.3:  $0 \rightarrow 1$

135 C.4:  $0 \rightarrow -$

136 C.5:  $1 \rightarrow -$

137 C.7:  $0 \rightarrow -$

138 C.9:  $0 \rightarrow -$

139 C.10:  $0 \rightarrow -$

140 C.11:  $1 \rightarrow -$

141 C.12:  $0 \rightarrow -$

142 C.47:  $0 \rightarrow 1$

143 C.64:  $0 \rightarrow 1$

144 C.65:  $- \rightarrow ?$

145 C.66:  $- \rightarrow 1$

146 C.70:  $0 \rightarrow 1$

147 C.97:  $- \rightarrow ?$

148 C.100:  $2 \rightarrow 0$

149 C.111:  $1 \rightarrow ?$

150 C.157:  $? \rightarrow 2$

151 C.183:  $1 \rightarrow ?$

152 C.207:  $1 \rightarrow 0$

153 C.209:  $? \rightarrow 0$

154 C.211:  $? \rightarrow 0$

155 C.219:  $0 \rightarrow ?$

156 C.224:  $- \rightarrow ?$

157 C.244:  $- \rightarrow ?$

158 C.245:  $- \rightarrow ?$

159 C.249:  $3 \rightarrow 1$

160 C.273:  $0 \rightarrow -$

161

162 †*Birgeria stensioei* (changes regarding Argyriou et al., 2018)

163 C.270:  $? \rightarrow 0$

164 C.271:  $? \rightarrow 0$

165 C.272:  $? \rightarrow 0$

166 C.273:  $? \rightarrow 0$

167

168 †*Bobasatrania groenlandica*

169 C.224:  $- 1 \rightarrow ?$

170

171 †*Boreosomus piveteaui*

172 C.188:  $1 \rightarrow ?$

173 C.224:  $- \rightarrow ?$

174 C.273:  $0 \rightarrow -$

175

176 †*Brembodus ridens*

177 C.273:  $0 \rightarrow -$

178

179 †*Caturus furcatus*

180 C.273:  $0 \rightarrow -$

181

182 †*Cheirolepis trailli*

183 C.224: -  $\rightarrow$  ?

184

185 †*Chondrosteus acipenseroides*

186 C.28: 1  $\rightarrow$  0

187 C.52: 1  $\rightarrow$  0

188 C.140: 0  $\rightarrow$  ?

189 C.141: 0  $\rightarrow$  ?

190

191 †*Dapedium* sp. (Lias)

192 C.201: -  $\rightarrow$  0

193 C.202: -  $\rightarrow$  ?

194

195 *Elops hawaiiensis*

196 C.157: 0  $\rightarrow$  2

197

198 †*Eomesodon liassicus*

199 C.273: 0  $\rightarrow$  -



200

201 †*Eusthenopteron foordi*

202 C.273: 0 → -

203

204 †*Fouldenia ischiptera*

205 C.43: ? → 1

206

207 †*Fukangichthys longidorsalis*

208 C.221: 0 → 1

209 C.224: - → ?

210

211 †*Gogonasus andrewsae*

212 C.152: 1 → 0

213

214 †*Hulettia americana*

215 C.157: 0 → 2

216 C.176: 1 → 2

217

218 †*Ichthyokentema purbeckensis*

219 C.157:  $0 \rightarrow 2$

220

221 *Lepisosteus osseus*

222 C.157:  $0 \rightarrow 2$

223

224 †*Leptolepis bronni*

225 C.154:  $1 \rightarrow 0$

226 C.157:  $0 \rightarrow 2$

227 C.273:  $0 \rightarrow -$

228

229 †*Luederia kemp*i

230 C.186:  $? \rightarrow 0$

231

232 †*Luganoia lepidosteoides*

233 C.52:  $0 \rightarrow 1$

234 C.53:  $- \rightarrow 0$

235

236 †*Meemania eos*

237 C.224: -  $\rightarrow$  ?

238

239 †*Melanecta annae*

240 C.37: 1  $\rightarrow$  ?

241

242 †*Mesturus verrucosus*

243 C.273: 0  $\rightarrow$  -

244

245 †*Mimipiscis bartrami*

246 C.273: 0  $\rightarrow$  -

247

248 †*Mimipiscis toombsi*

249 C.273: 0  $\rightarrow$  -

250

251 †*Moythomasia durgaringa*

252 C.273: 0  $\rightarrow$  -

253

254 †*Obaichthys decoratus*

255 C.157:  $0 \rightarrow 2$

256

257 †*Ozarcus mapesae*

258 C.111:  $? \rightarrow -$

259 C.113:  $? \rightarrow -$

260 C.141:  $0 \rightarrow -$

261 C.142:  $0 \rightarrow -$

262

263 †*Peltopleurus lissocephalus*

264 C.69:  $0 \rightarrow 1$

265 C.239:  $1 \rightarrow ?$

266 C.265:  $0 \rightarrow 1$

267

268 *Polyodon spathula*

269 C.142:  $- \rightarrow 0$  (modified regarding Argyriou et al., 2018)

270 C.147:  $? \rightarrow -$  (modified regarding Argyriou et al., 2018)

271 C.273:  $0 \rightarrow -$

272

273 *Polypterus bichir*

274 C.153:  $? \rightarrow 1$

275 C.154:  $? \rightarrow 0$

276 C.155:  $? \rightarrow 0$

277 C.156:  $? \rightarrow 1$

278 C.157:  $? \rightarrow 1$

279

280 †*Pteronisculus stensioi*

281 C.224:  $- \rightarrow ?$

282

283 †*Raynerius splendens*

284 C.201:  $1 \rightarrow ?$

285 C.224:  $- \rightarrow ?$

286

287 †*Saurichthys madagascariensis*

288 C.7: maintained as 0 as in Latimer and Giles, 2018 and not Argyriou et al., 2018

289 C.14:  $1 \rightarrow ?$

290 C.20:  $1 \rightarrow -$

291 C.22:  $0 \rightarrow -$

292 C.62: maintained as 0 as in Latimer and Giles, 2018 and not Argyriou et al., 2018

293 C.64: maintained as 1 as in Latimer and Giles, 2018 and not Argyriou et al., 2018

294 C.65: maintained as 1 as in Latimer and Giles, 2018 and not Argyriou et al., 2018

295 C.66:  $1 \rightarrow ?$

296 C.101:  $0 \rightarrow ?$

297 C.111:  $- \rightarrow 2$

298 C.112:  $1 \rightarrow 0$

299 C.113:  $- \rightarrow 0$

300 C.114:  $- \rightarrow 0$

301 C.131:  $0 \rightarrow ?$

302 C.136:  $? \rightarrow 1$

303 C.143: maintained as 0 as in Latimer and Giles, 2018 and not Argyriou et al., 2018

304 C.191:  $1 \rightarrow ?$

305 C.241: maintained as 0 as in Latimer and Giles, 2018 and not Argyriou et al., 2018

306 C.243: maintained as 1 as in Latimer and Giles, 2018 and not Argyriou et al., 2018

307 C.294:  $0 \rightarrow 1$

308

309 †*Saurichthys* sp. Greenland (NHMD\_157546\_A)

310 C.119:  $0 \rightarrow ?$  (modified regarding Argyriou et al., 2018)

311 C.142:  $- \rightarrow 0$  (modified regarding Argyriou et al., 2018)

312 C.198:  $? \rightarrow 0$  (modified regarding Argyriou et al., 2018)

313

314 †*Saurichthys ornatus*

315 C.142:  $- \rightarrow 0$

316 C.242:  $0 \rightarrow ?$

317 C.250:  $? \rightarrow 1$

318

319 †*Semionotus elegans*

320 C.174:  $1 \rightarrow ?$

321

322 †*Trawdenia* (=†*Mesopoma*) *planti*

323 C.33:  $? \rightarrow 0$

324 C.52:  $? \rightarrow 1$

325 C.54:  $? \rightarrow 1$

326 C.65:  $? \rightarrow 0$

327 C.71:  $? \rightarrow 0$

328 C.72:  $? \rightarrow 0$

329 C.76:  $? \rightarrow 0$

330 C.85:  $? \rightarrow 2$

331 C.90:  $? \rightarrow 1$

332 C.94:  $? \rightarrow 1$

333 C.95:  $? \rightarrow 1$

334 C.122:  $? \rightarrow 1$

335 C.186:  $? \rightarrow 0$

336 C.234:  $? \rightarrow 1$

337 C.235:  $? \rightarrow 0$

338 C.237:  $? \rightarrow 0$

339 C.240:  $? \rightarrow 0$

340 C.242:  $? \rightarrow 1$

341 C.243:  $? \rightarrow 0$

342 C.244:  $? \rightarrow 1$

343 C.245:  $? \rightarrow 0$



344 C.246:  $? \rightarrow 0$

345 C.247:  $? \rightarrow 0$

346 C.248:  $? \rightarrow 1$

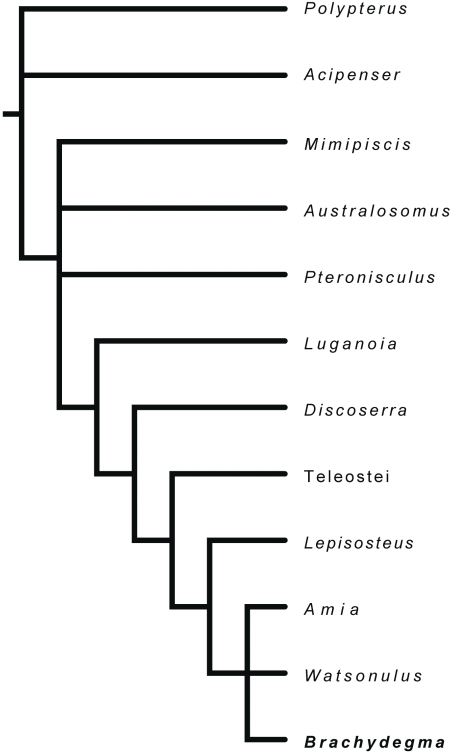
347

348 †*Watsonulus eugnathoides*

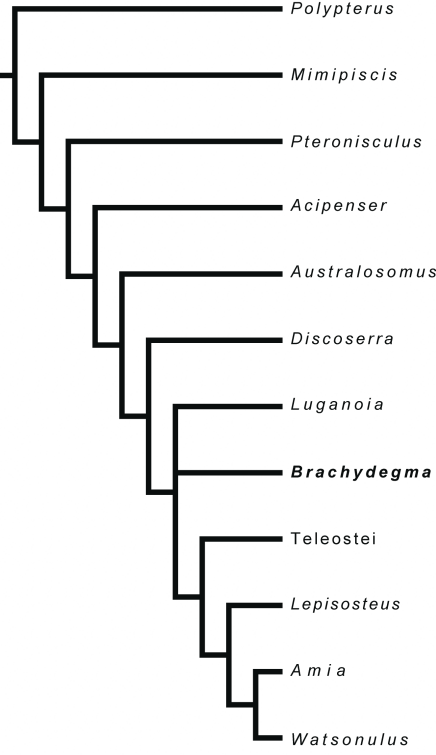
349 C.112:  $1 \rightarrow 0$

350 C.157:  $0 \rightarrow 2$

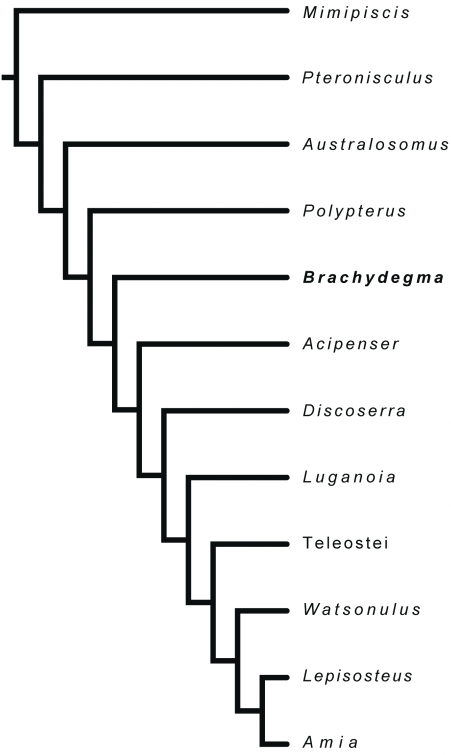
Hurley et al. 2007



Xu et al. 2014



Giles et al. 2017

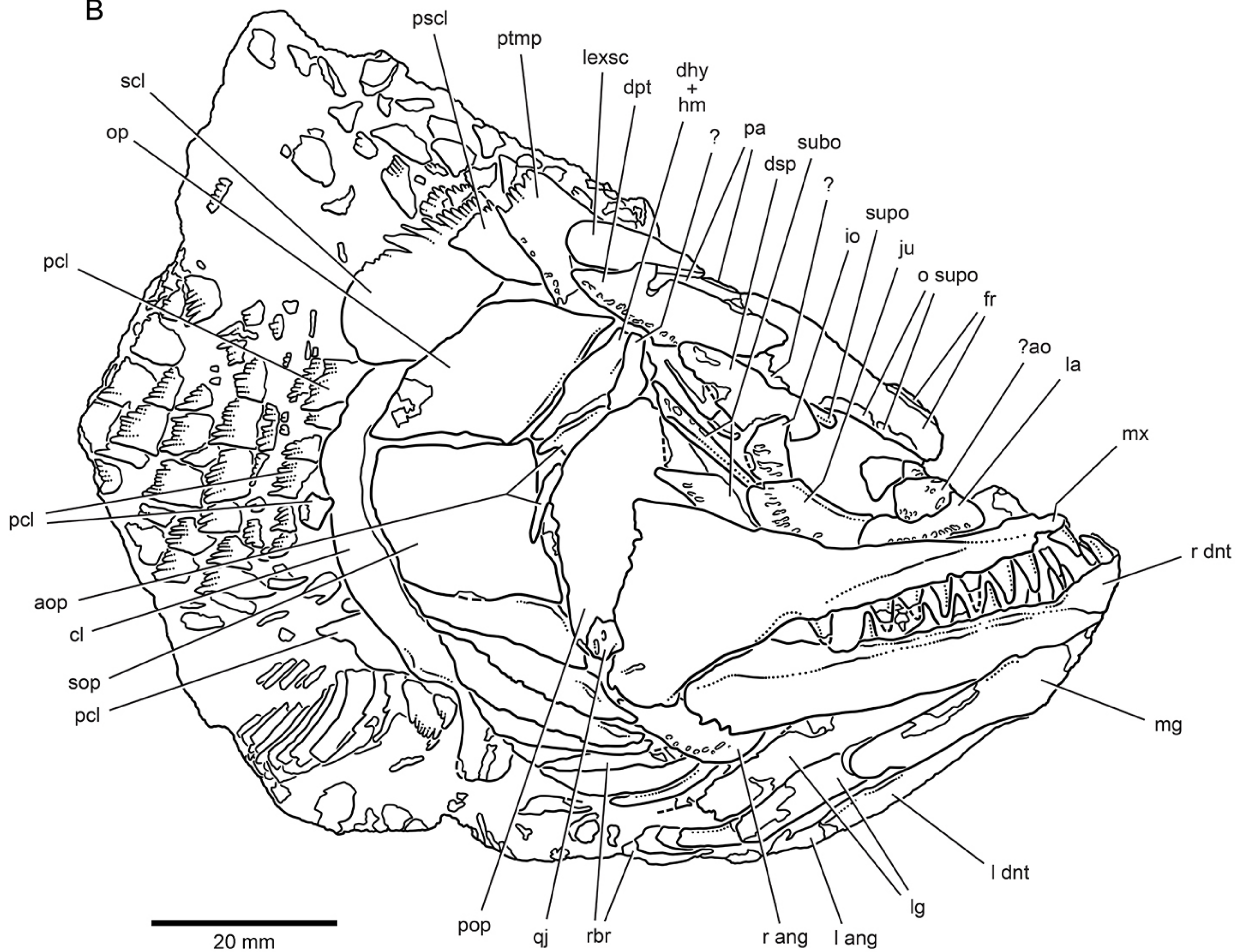




A



B

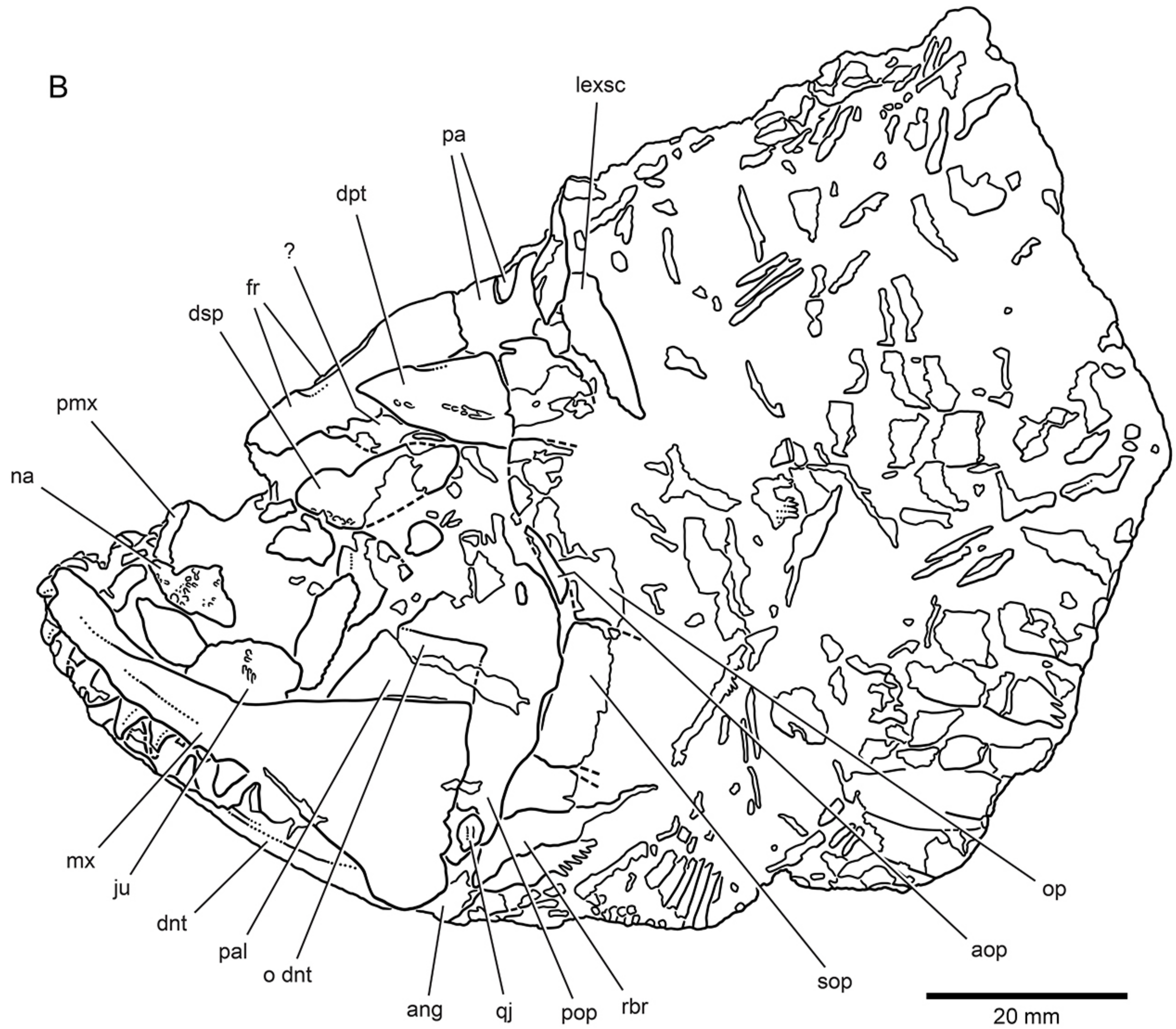




A



B

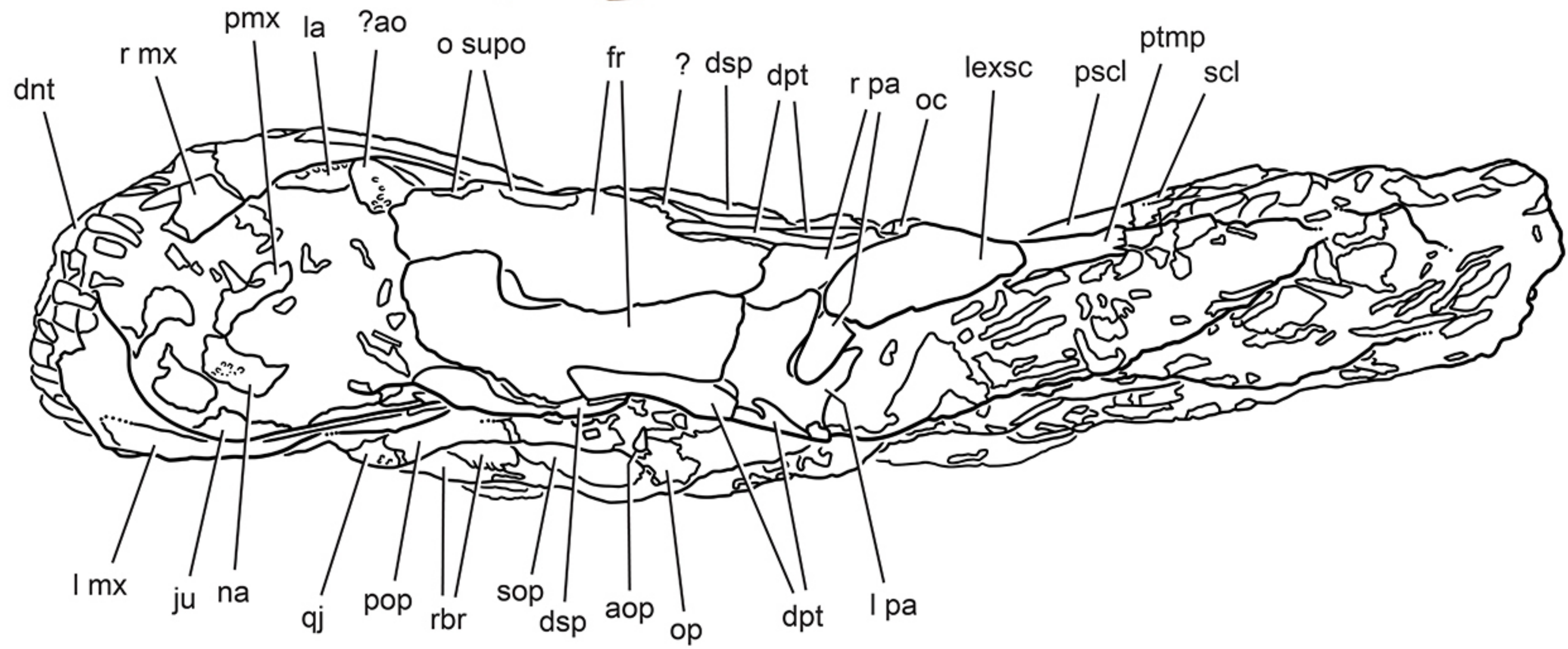




A



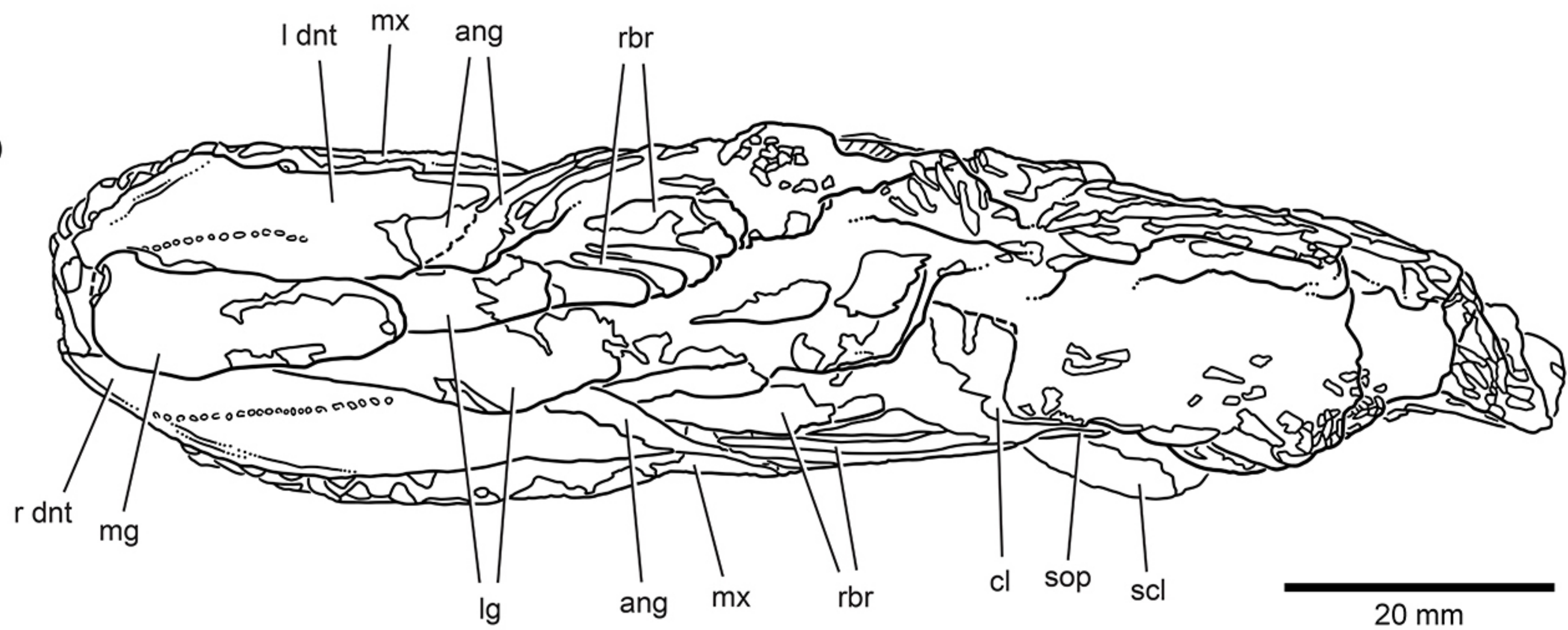
B



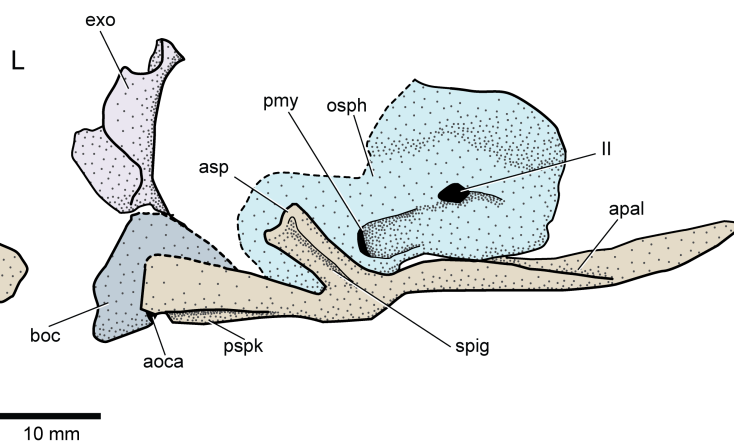
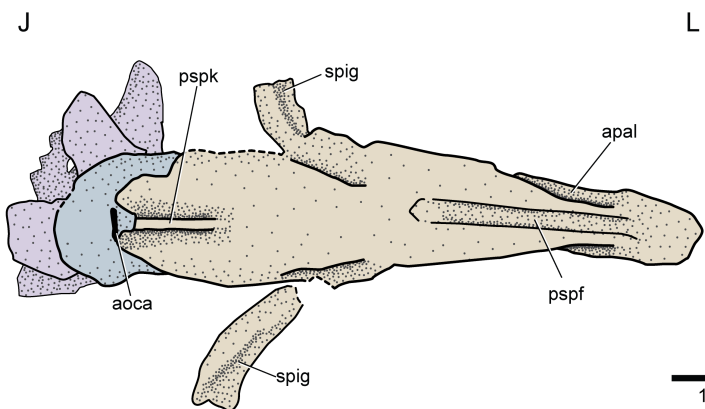
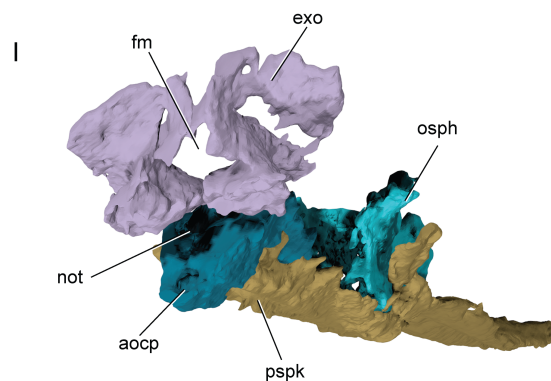
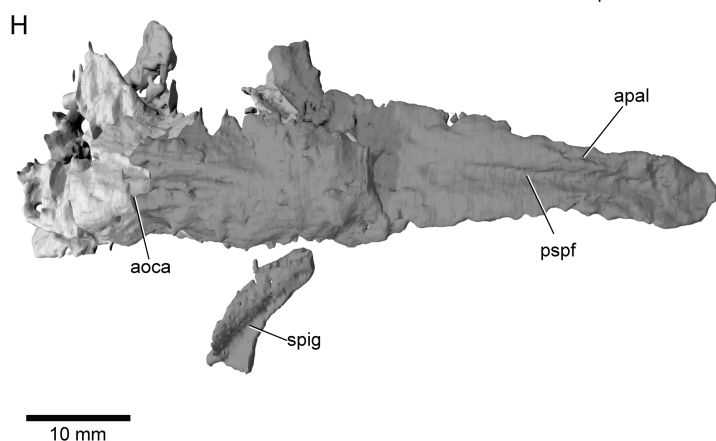
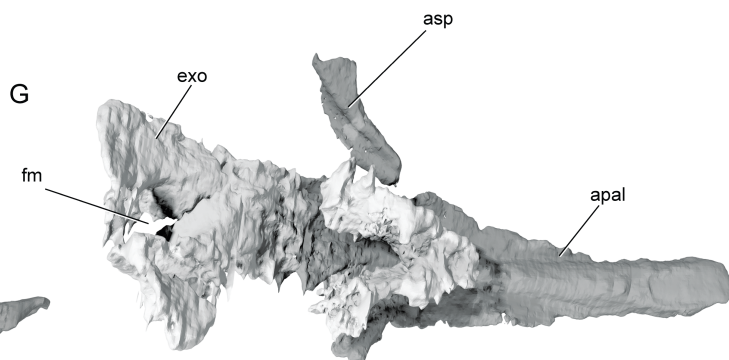
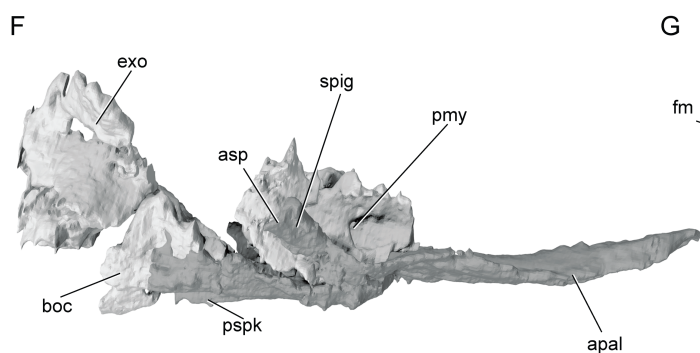
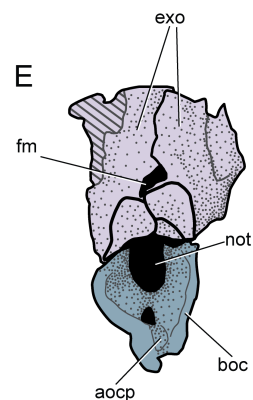
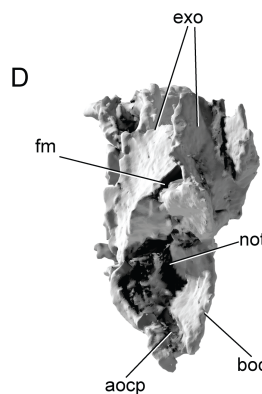
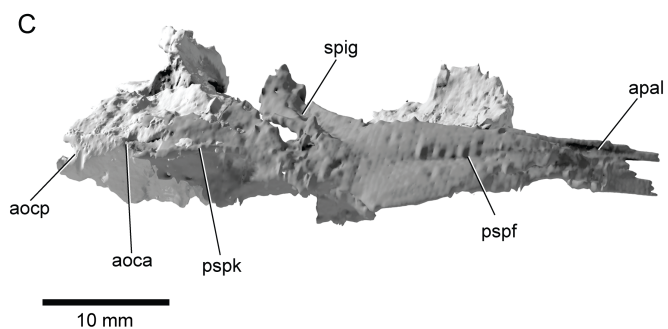
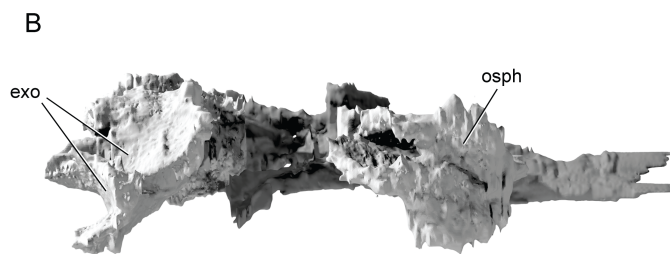
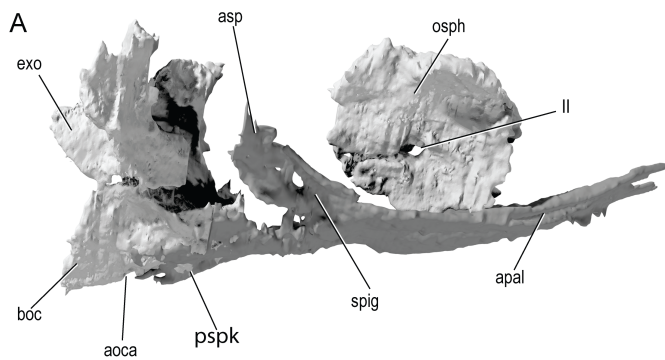
C



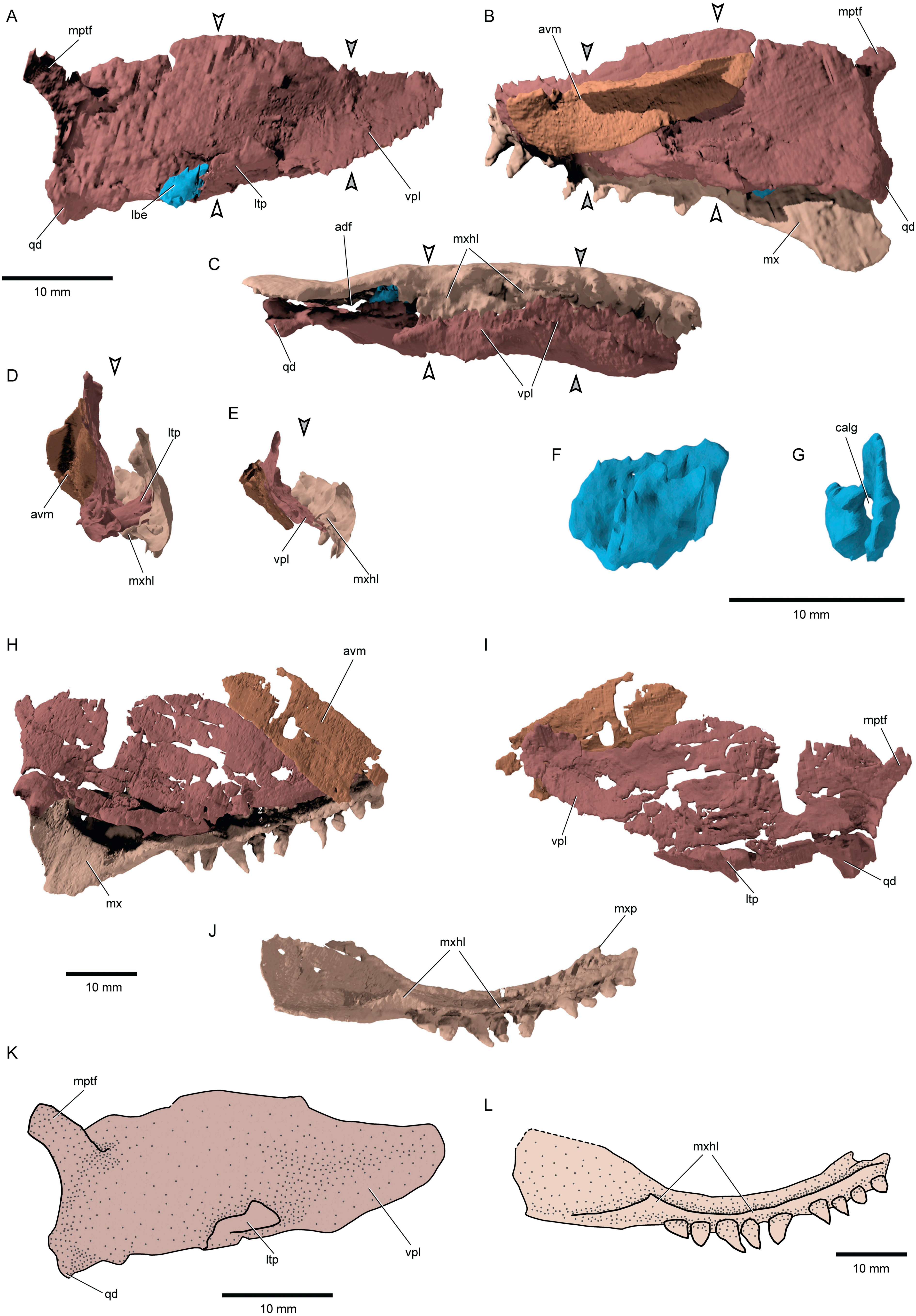
D



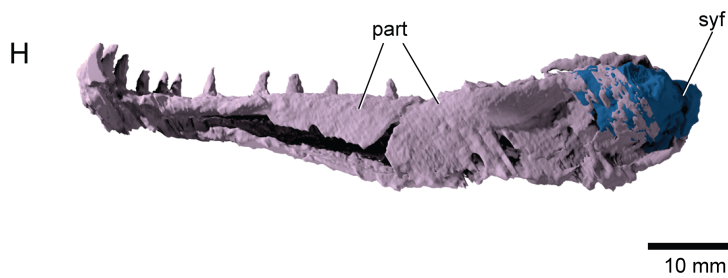
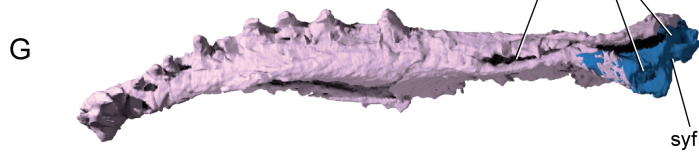
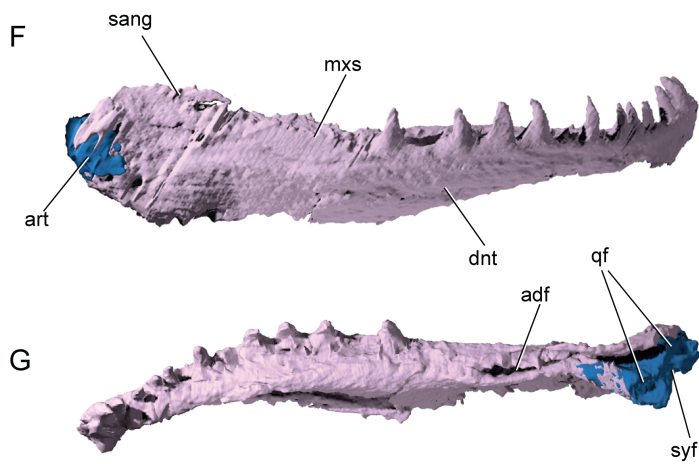
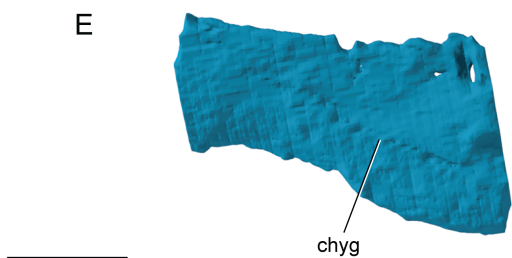
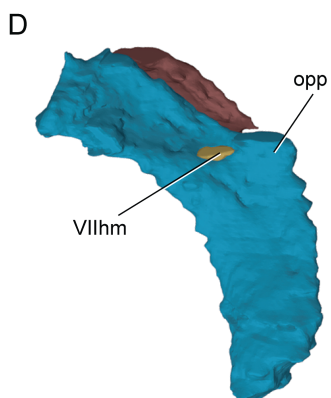
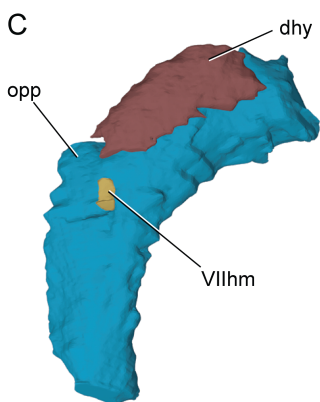
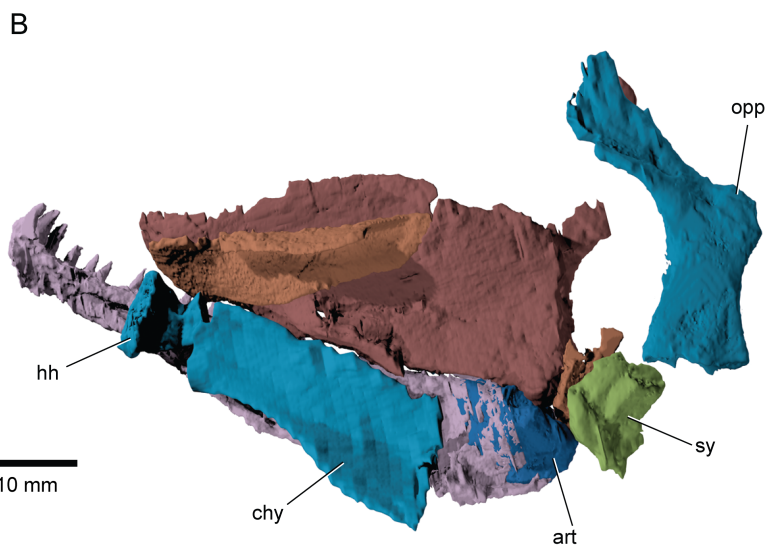
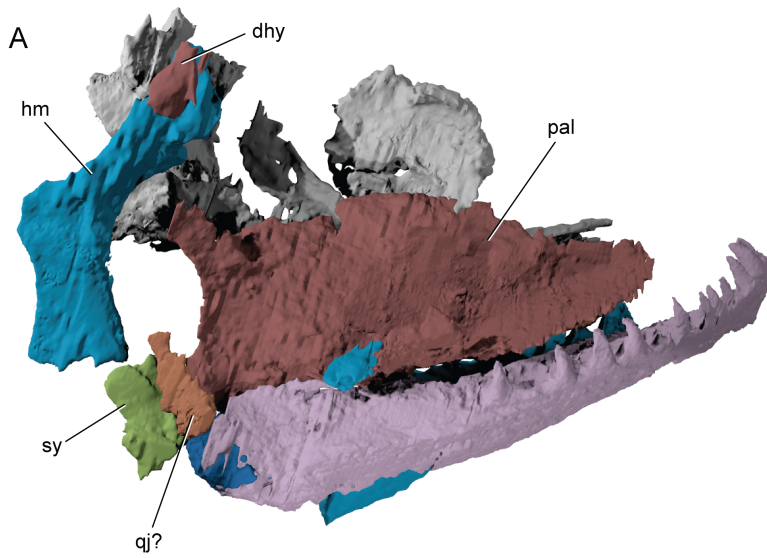




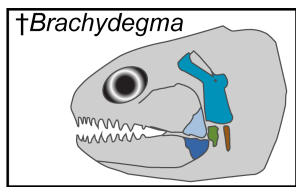




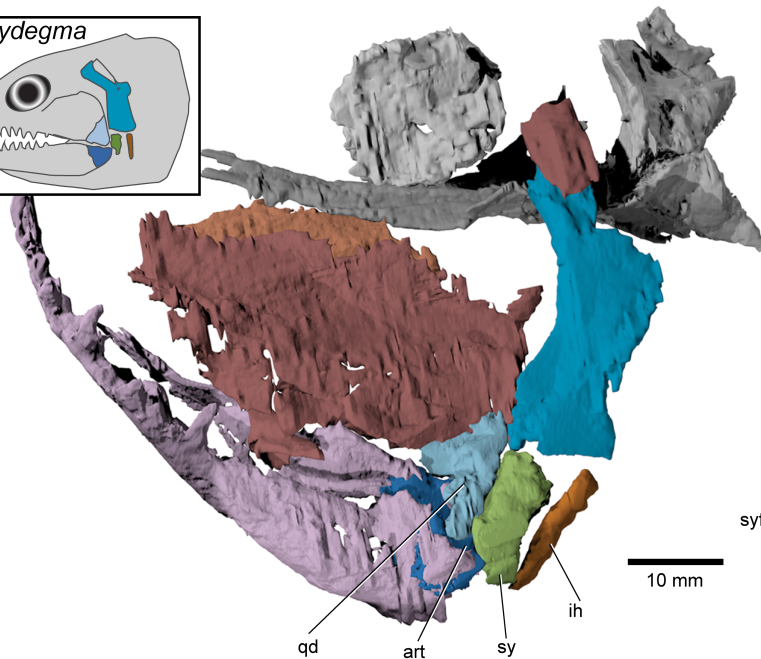




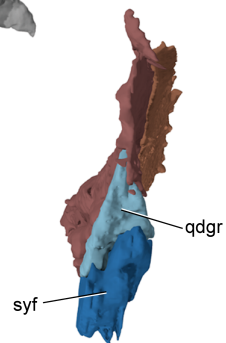




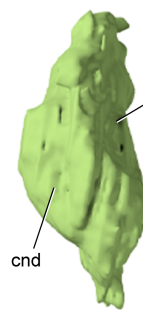
A



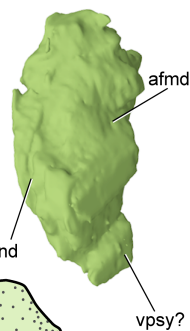
B



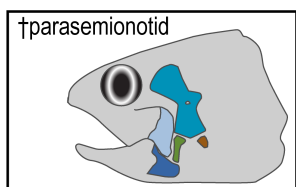
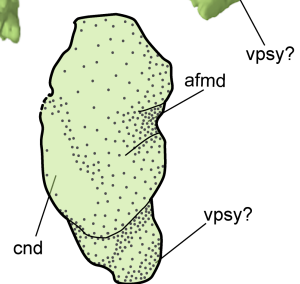
C



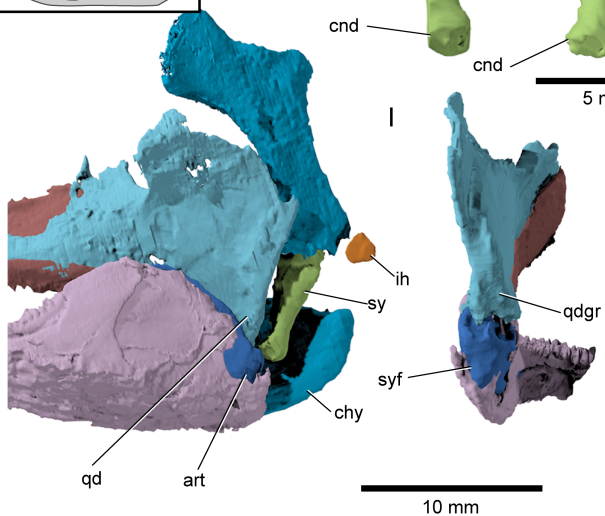
D



E



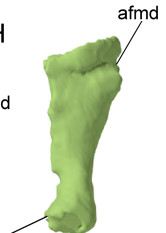
F



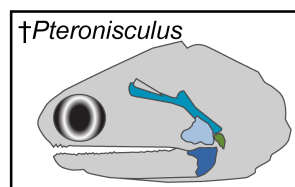
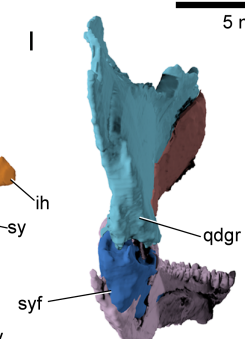
G



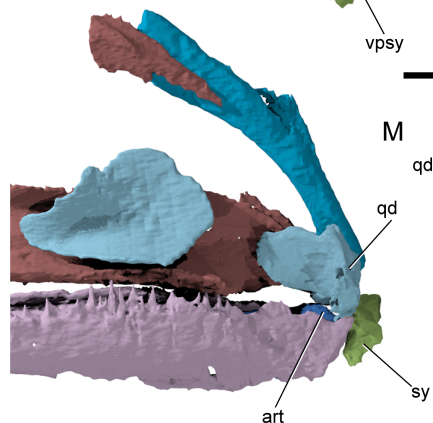
H



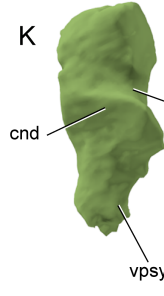
I



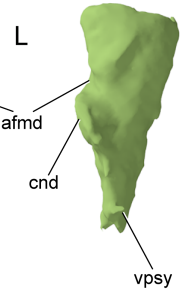
J



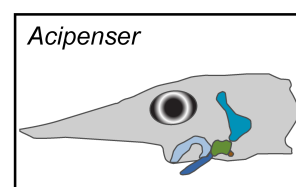
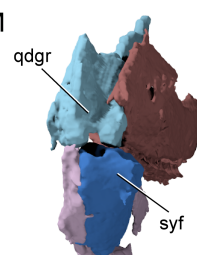
K



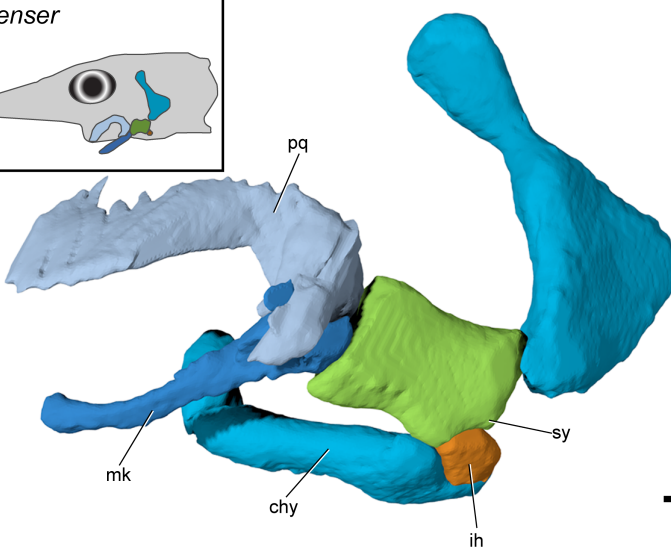
L



M



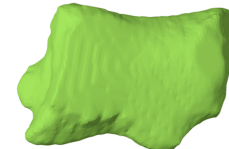
N



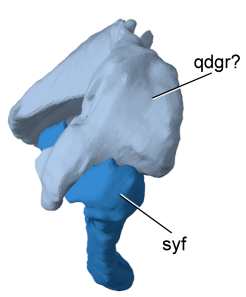
O

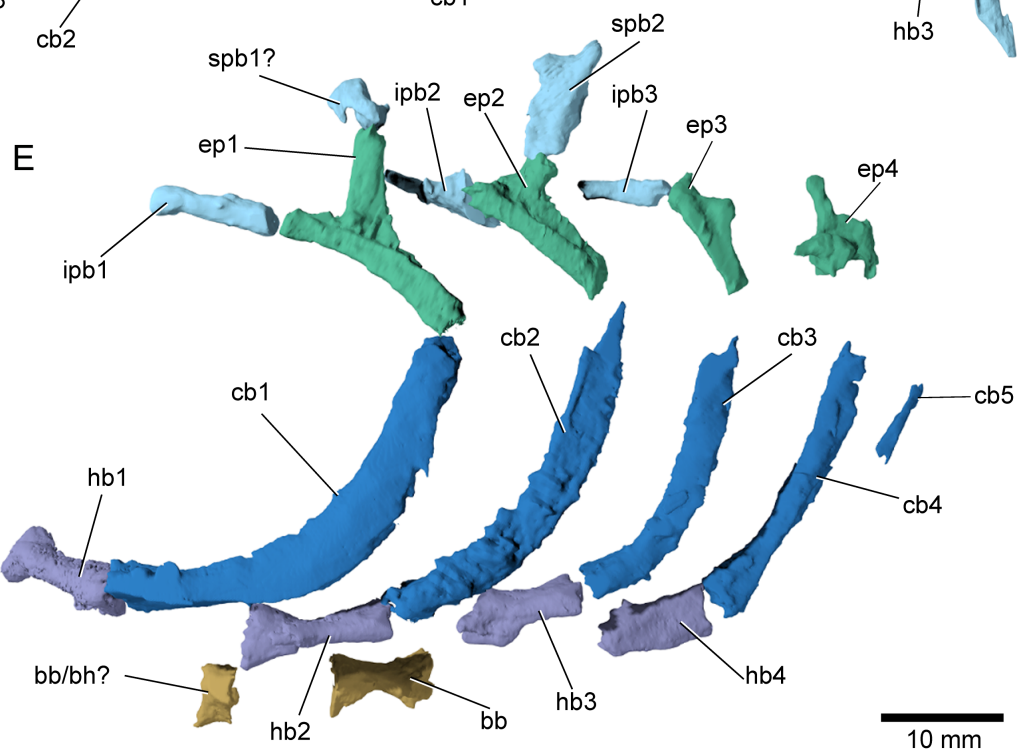
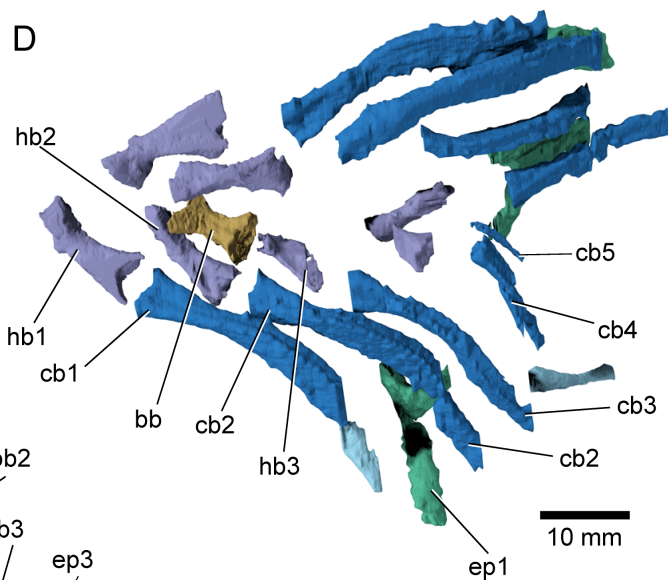
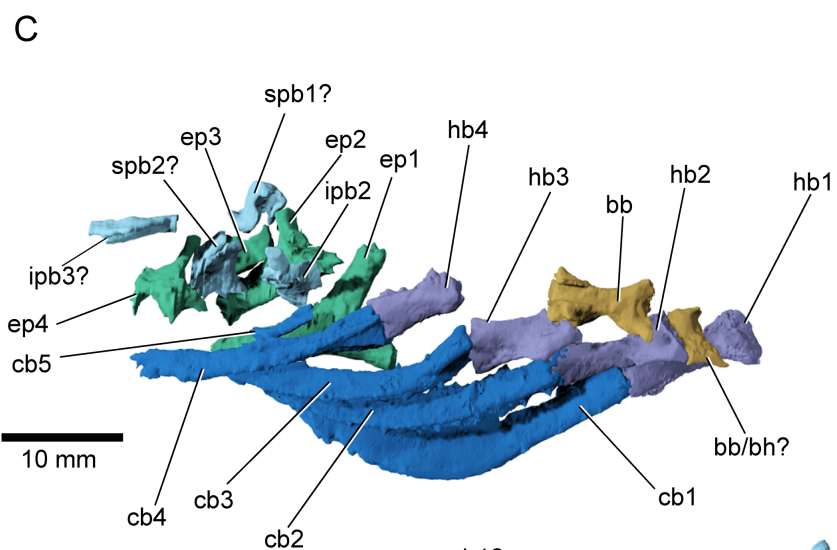
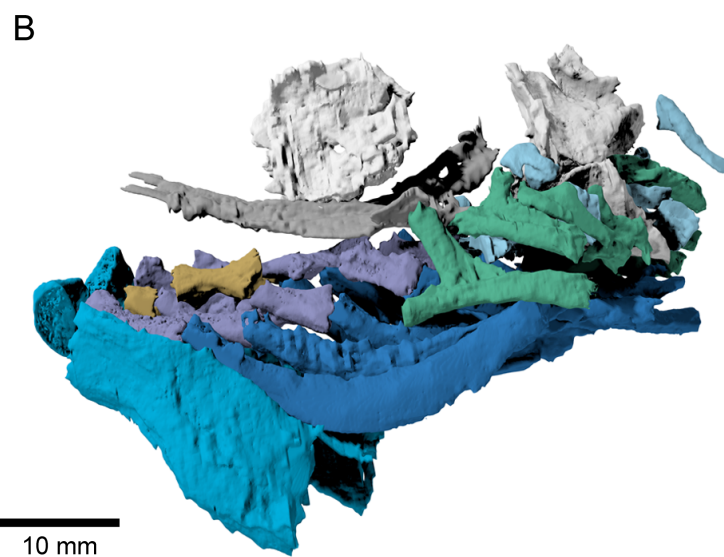
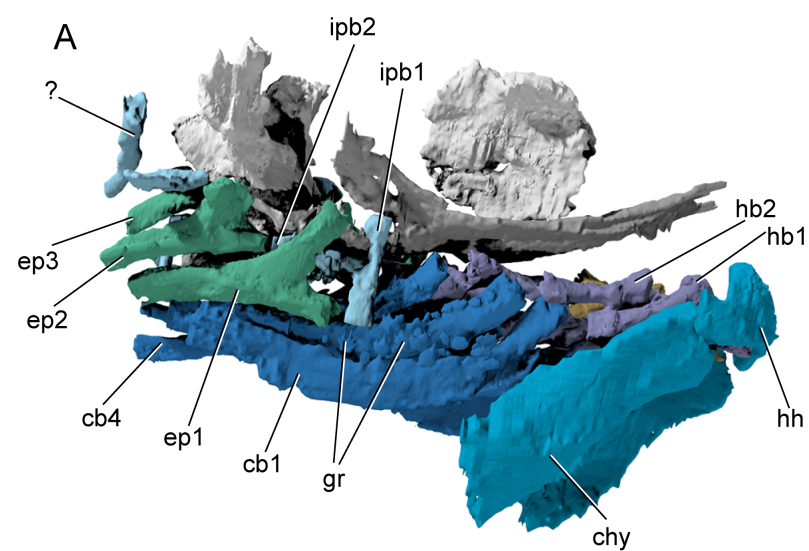


P



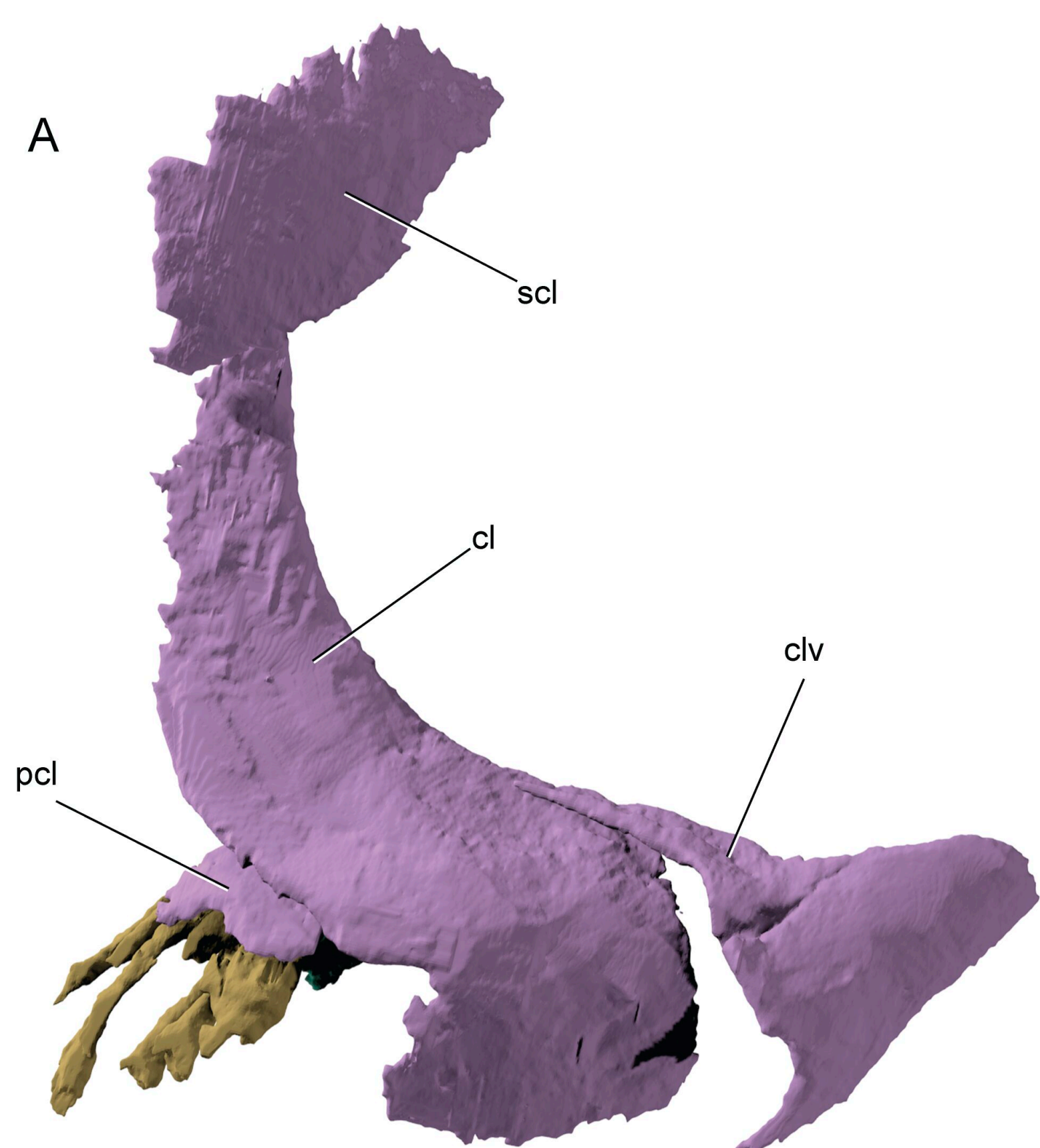
Q



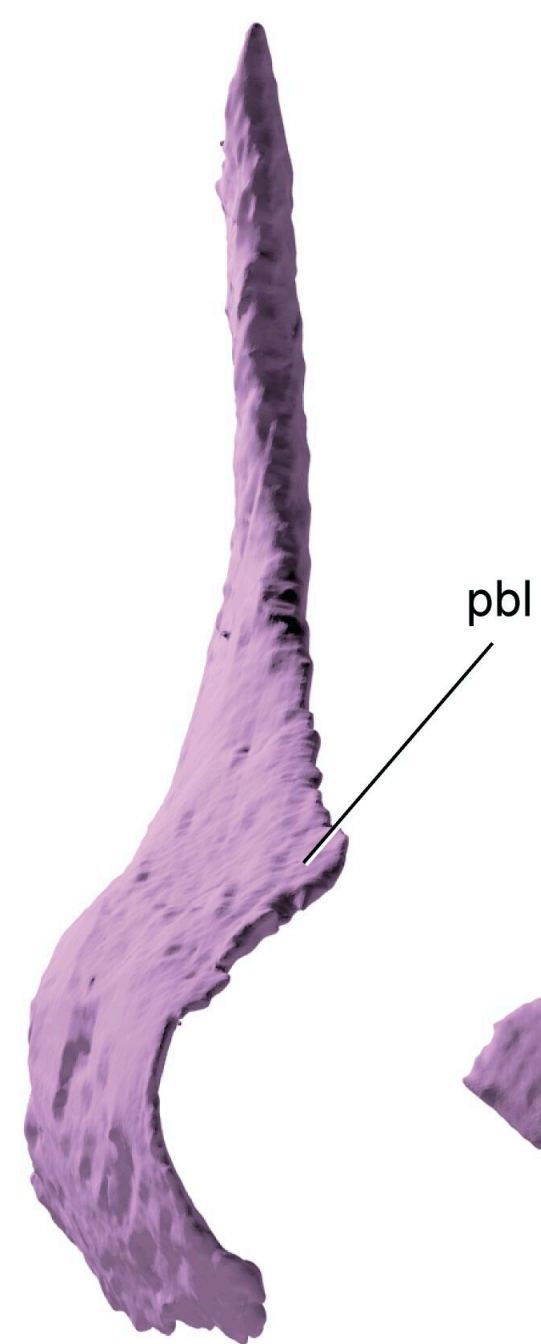




A

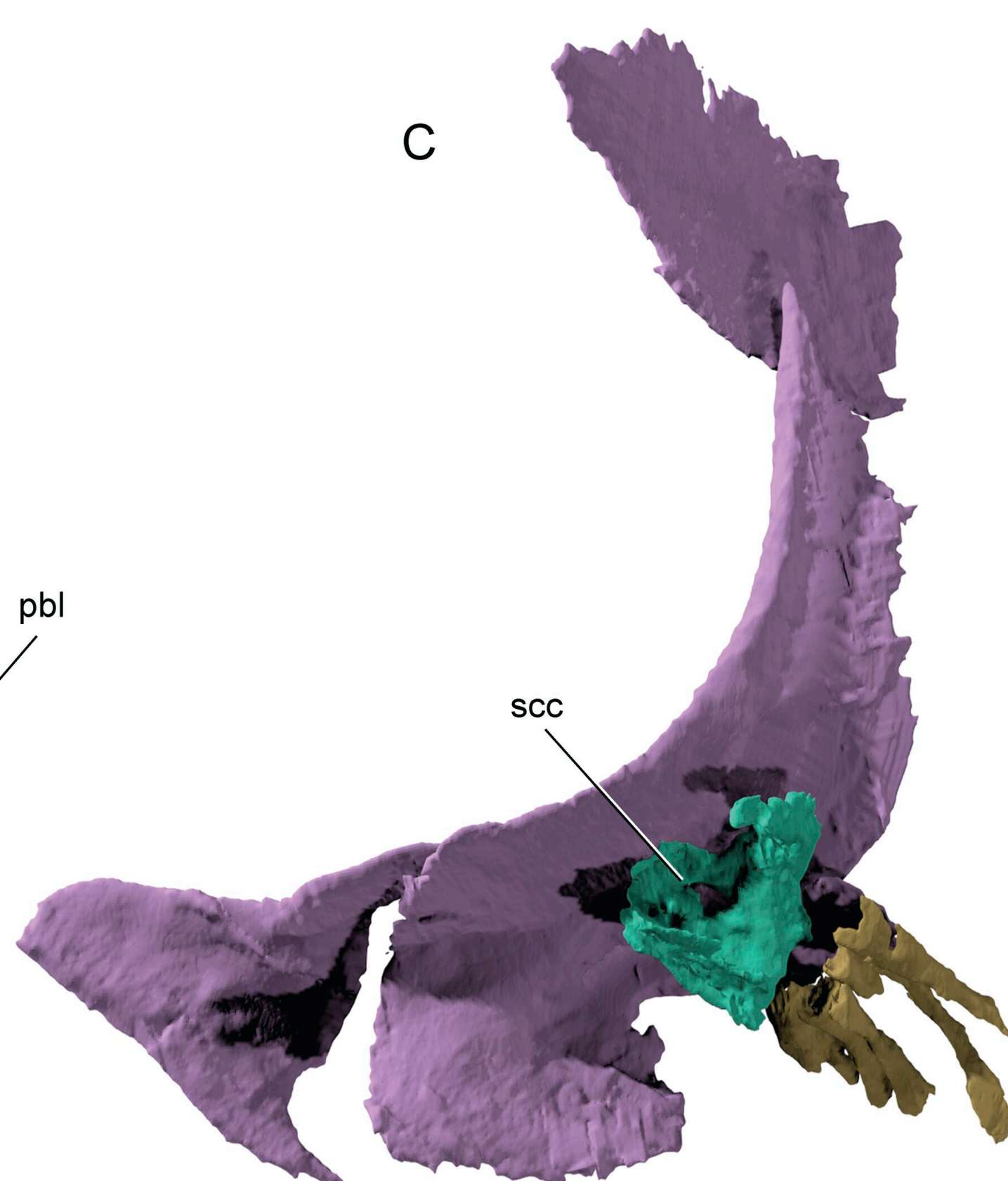


B

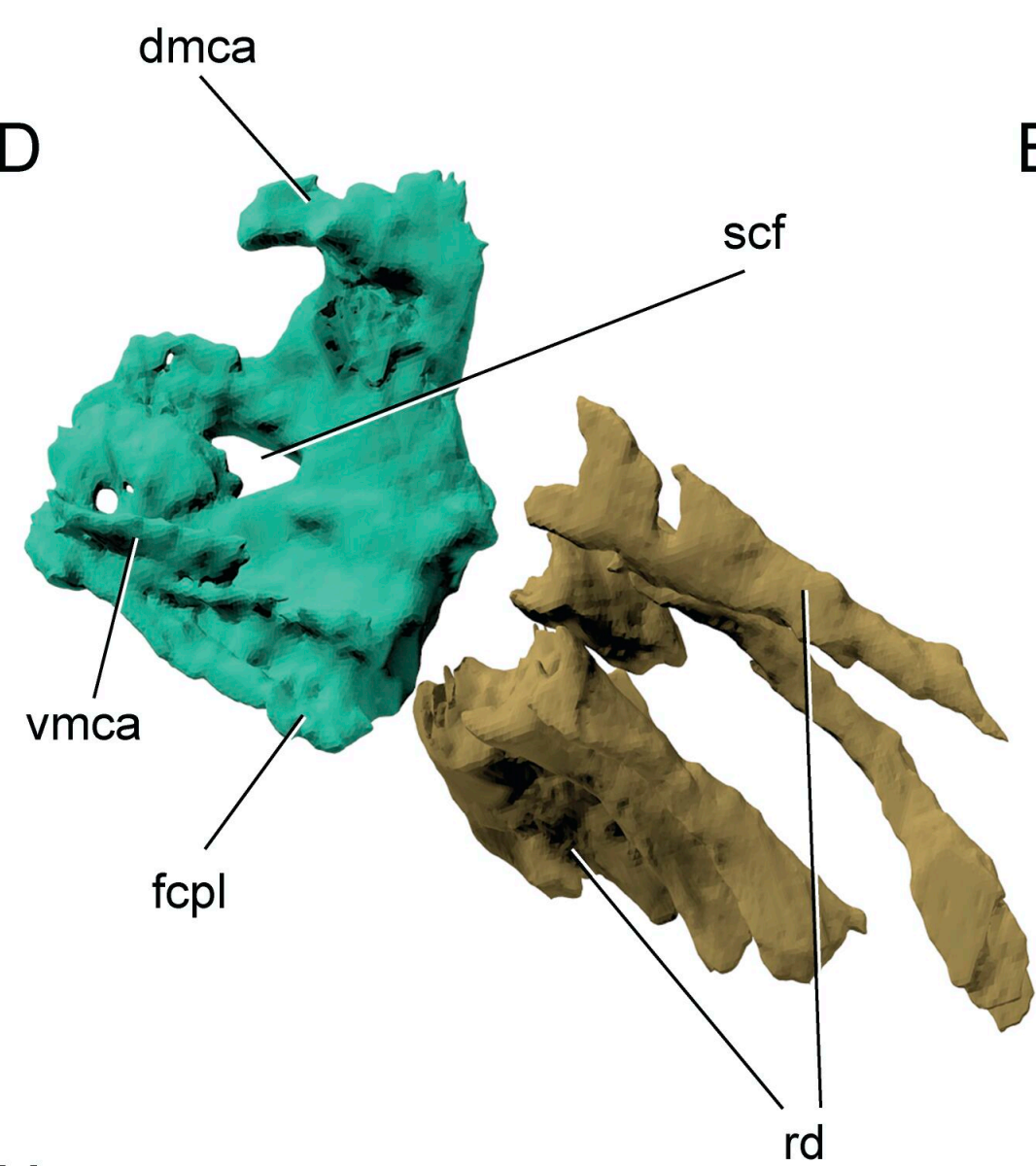


10 mm

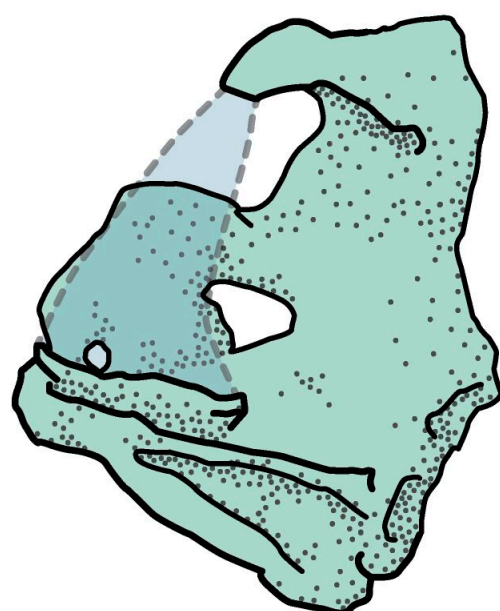
C



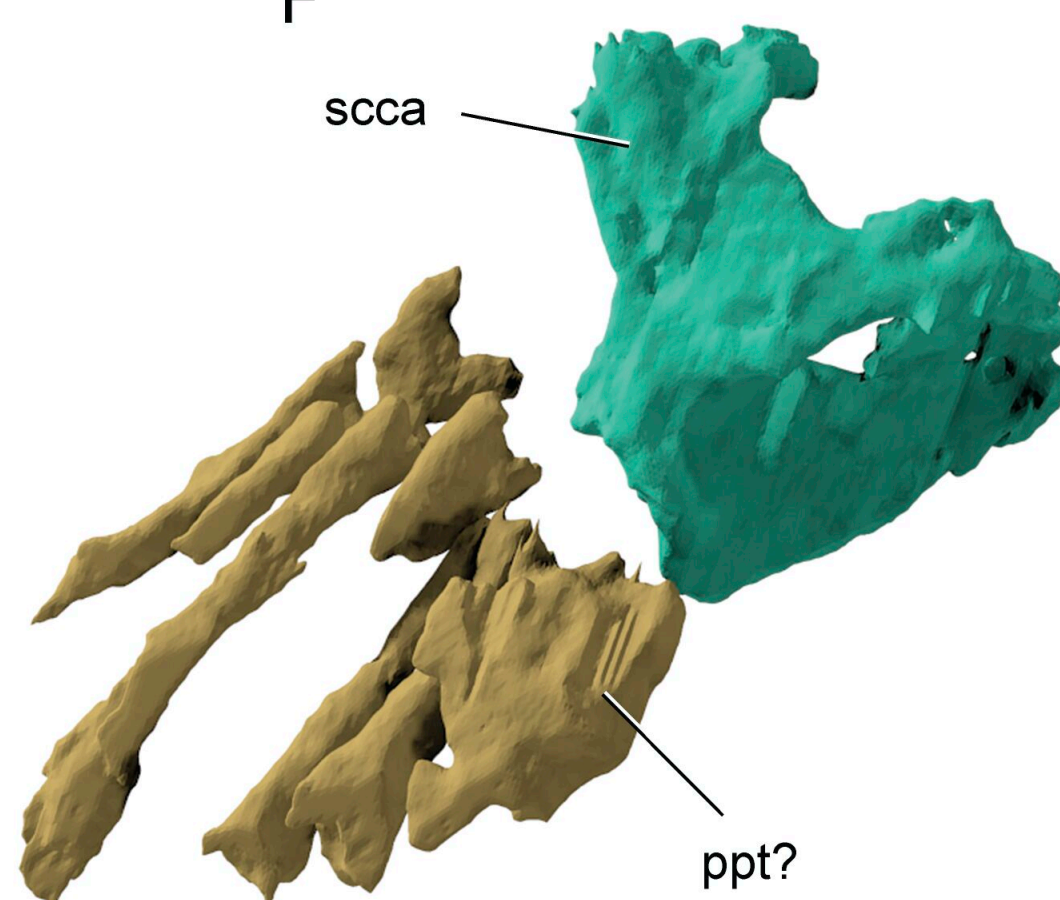
D



E

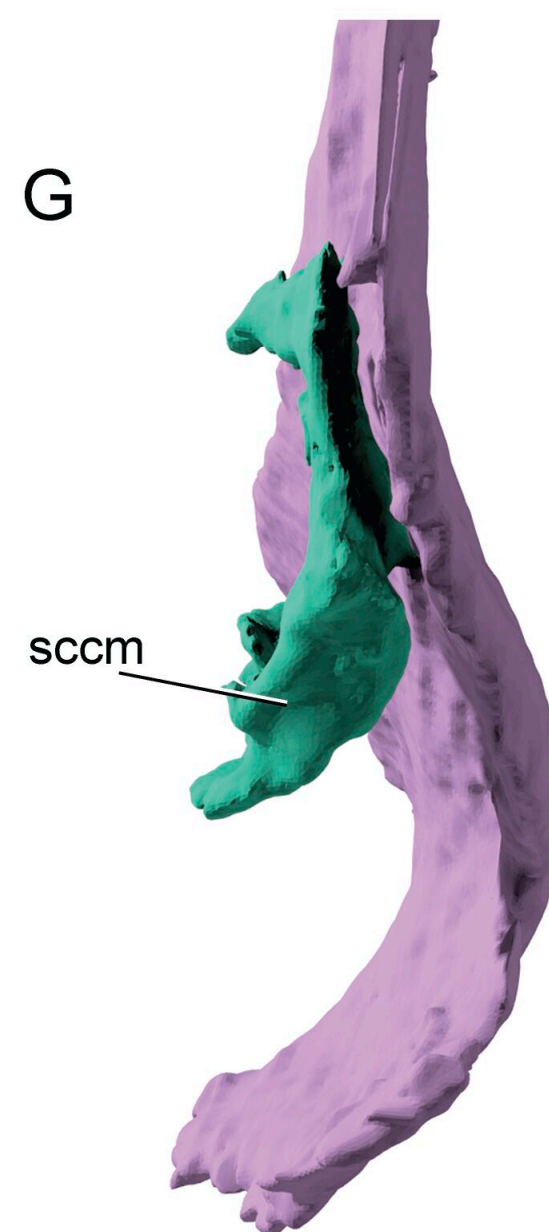


F

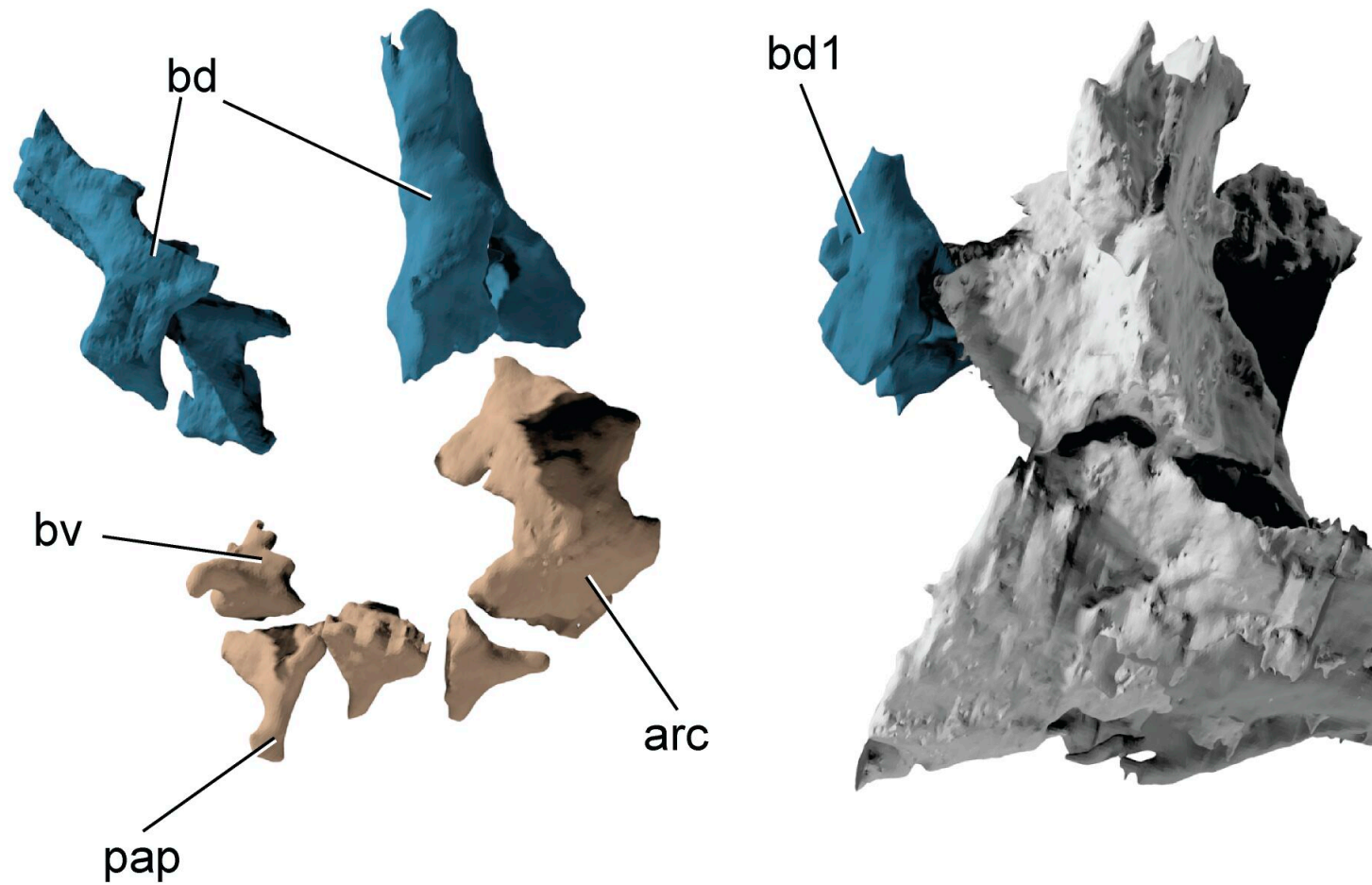


10 mm

G

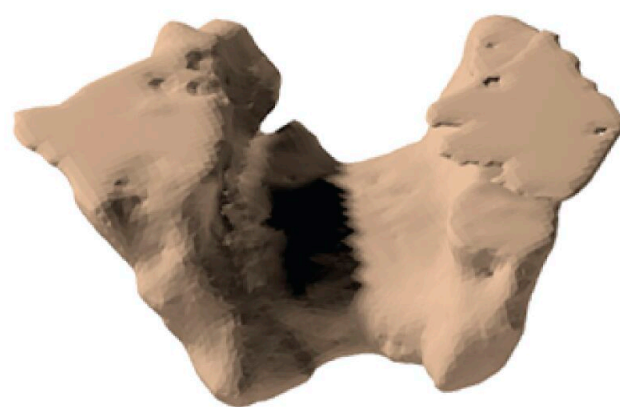


H

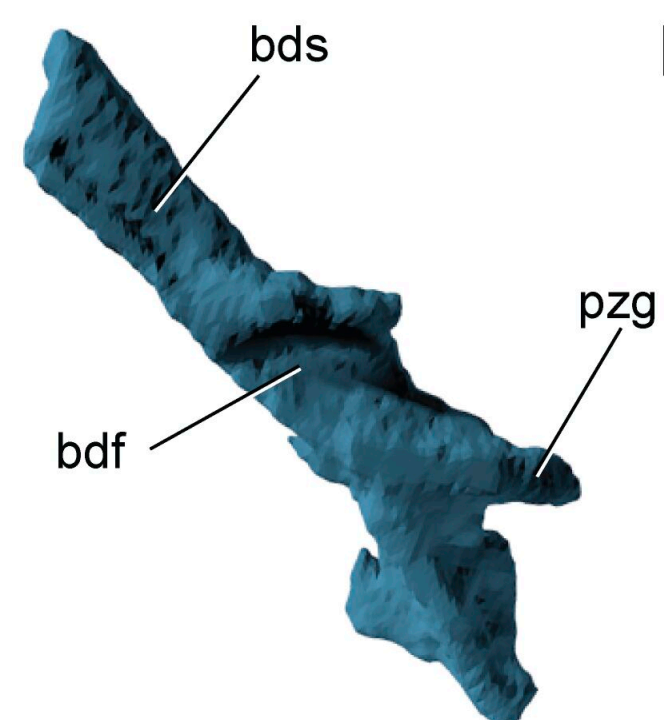


10 mm

I

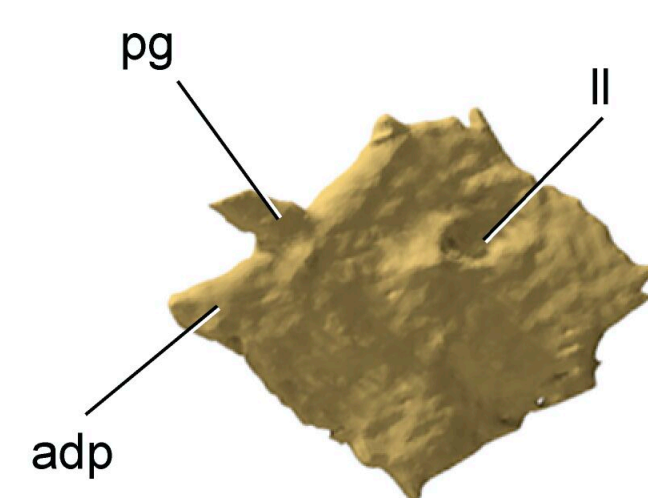


J



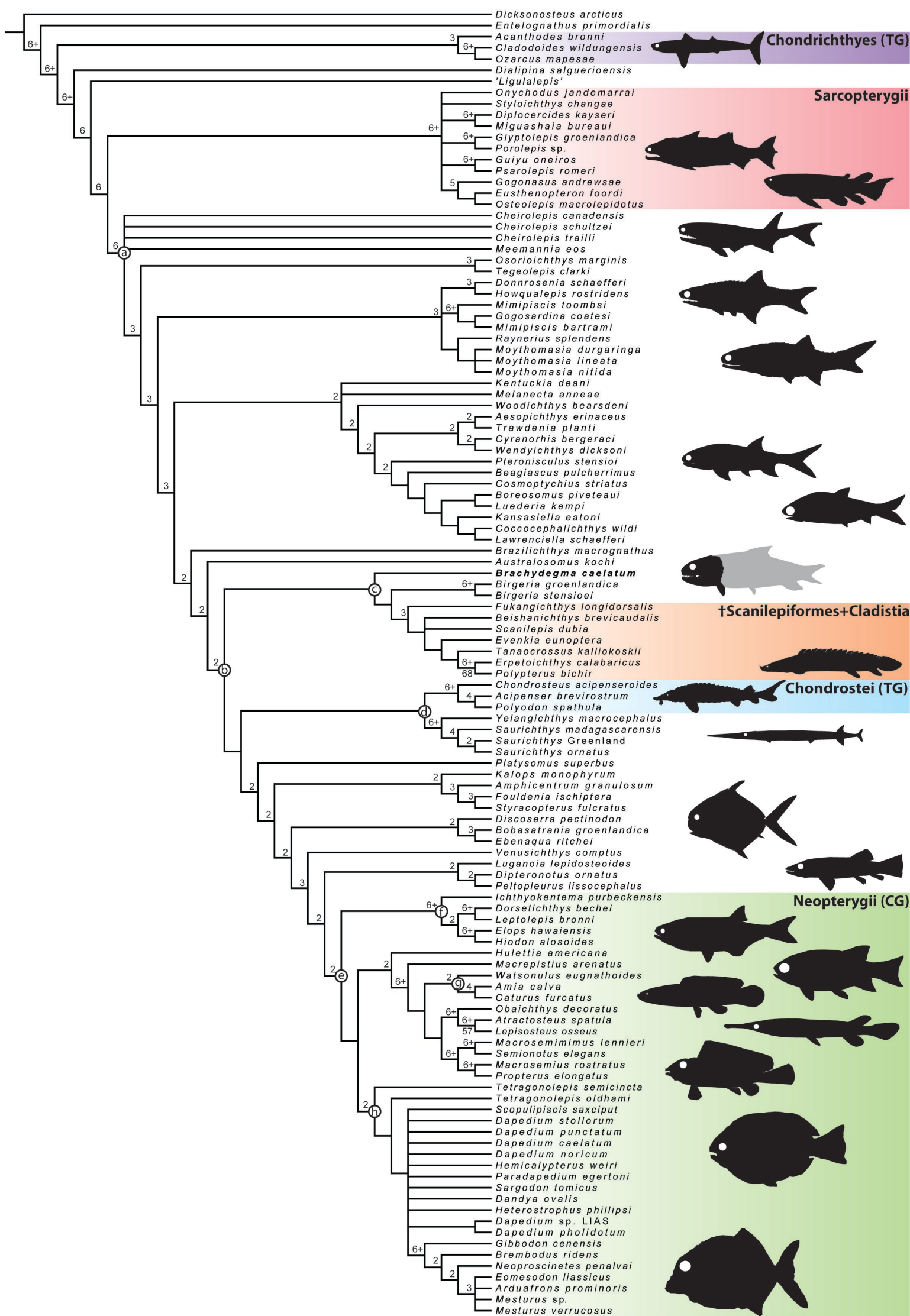
5 mm

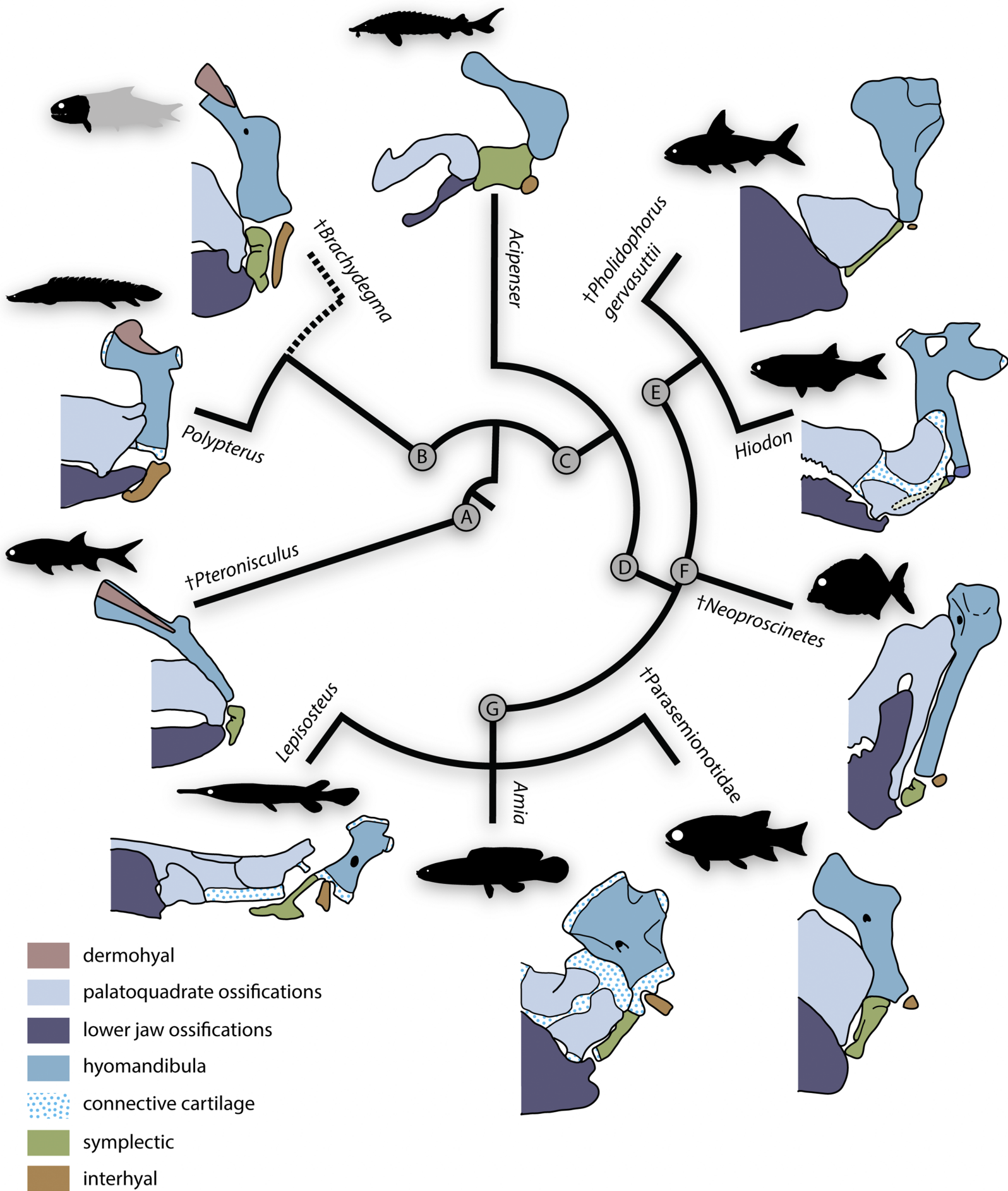
K



5 mm









A

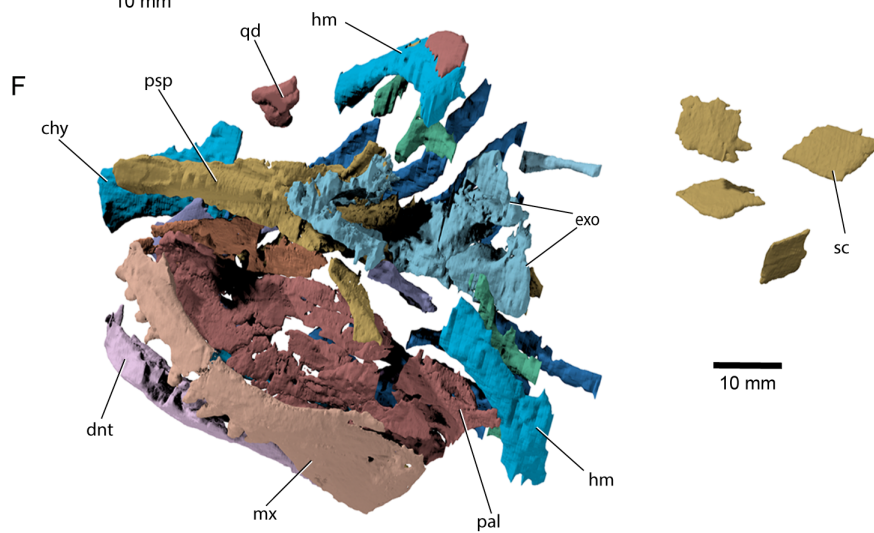
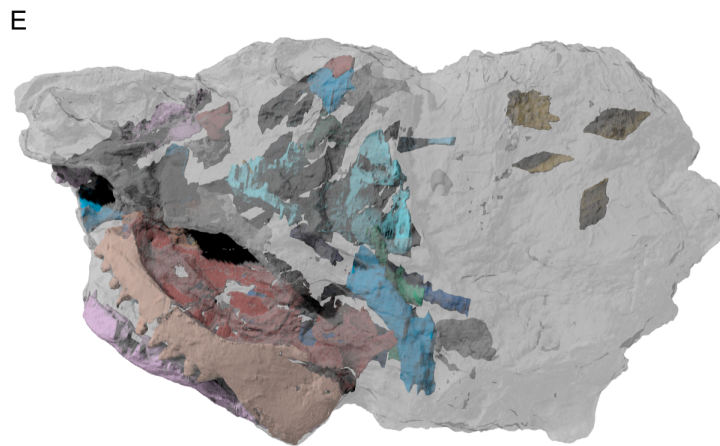
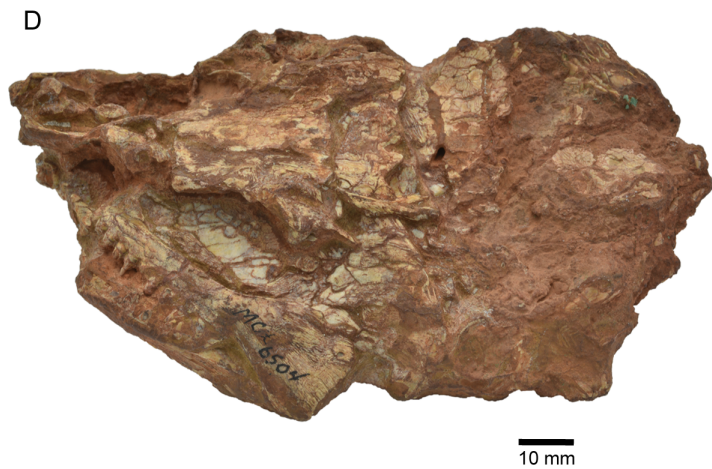
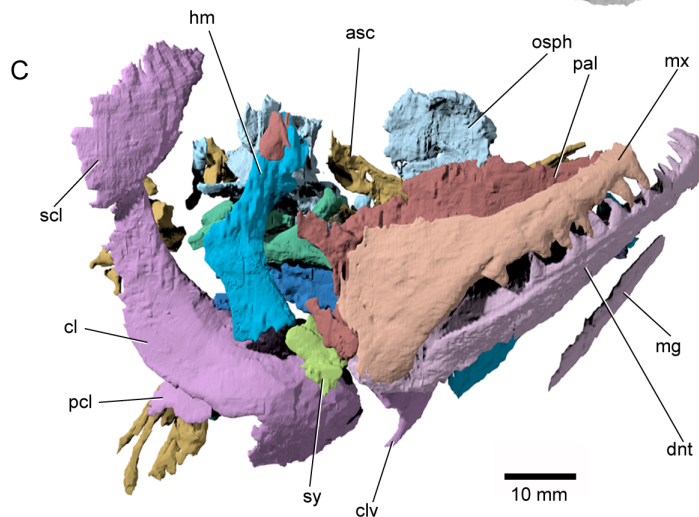
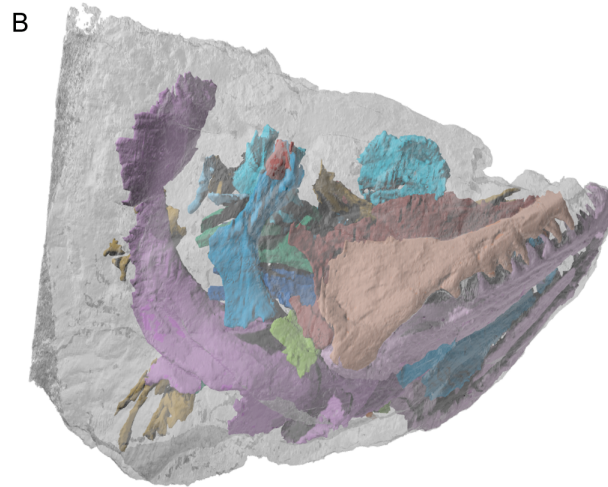


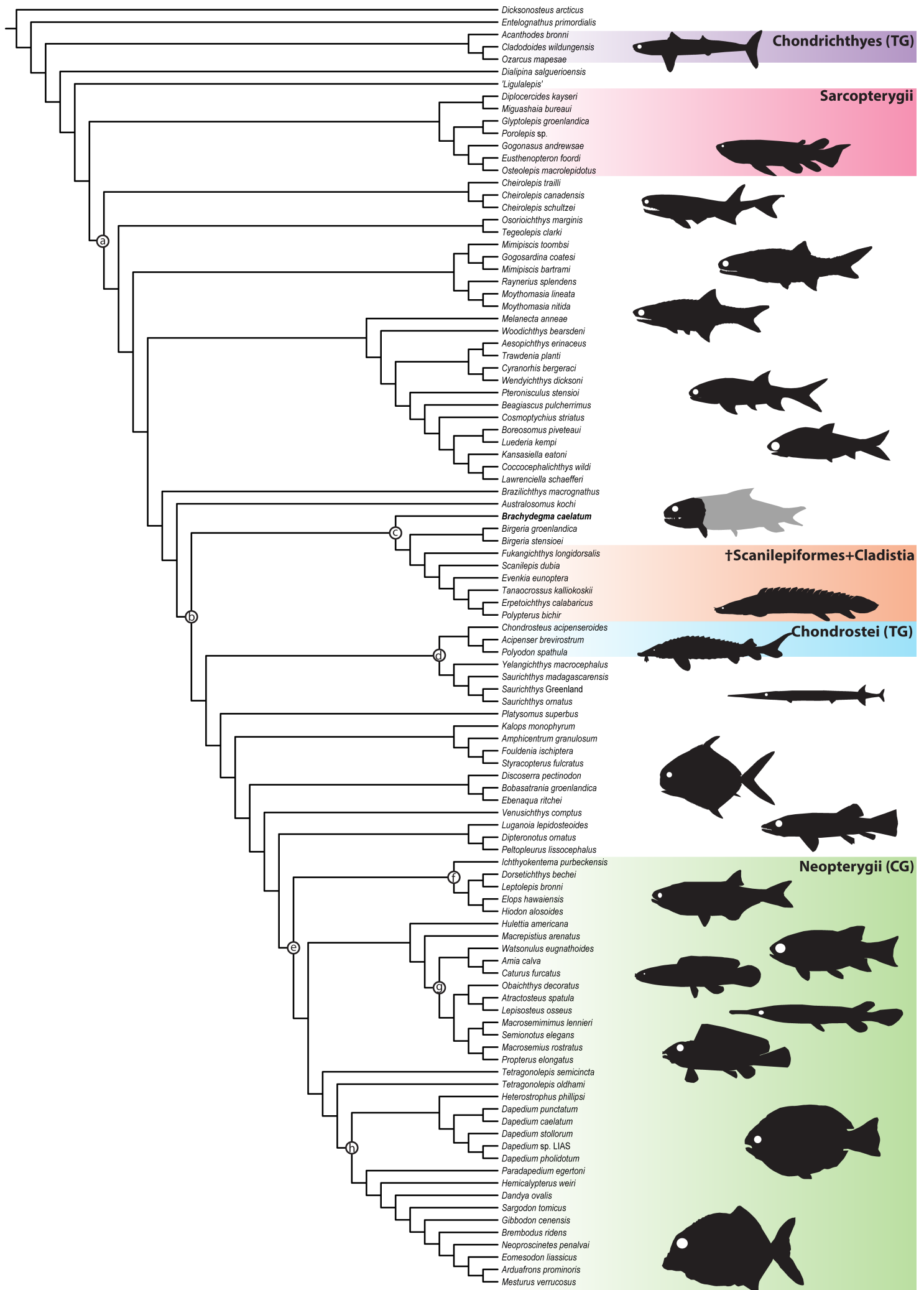
B



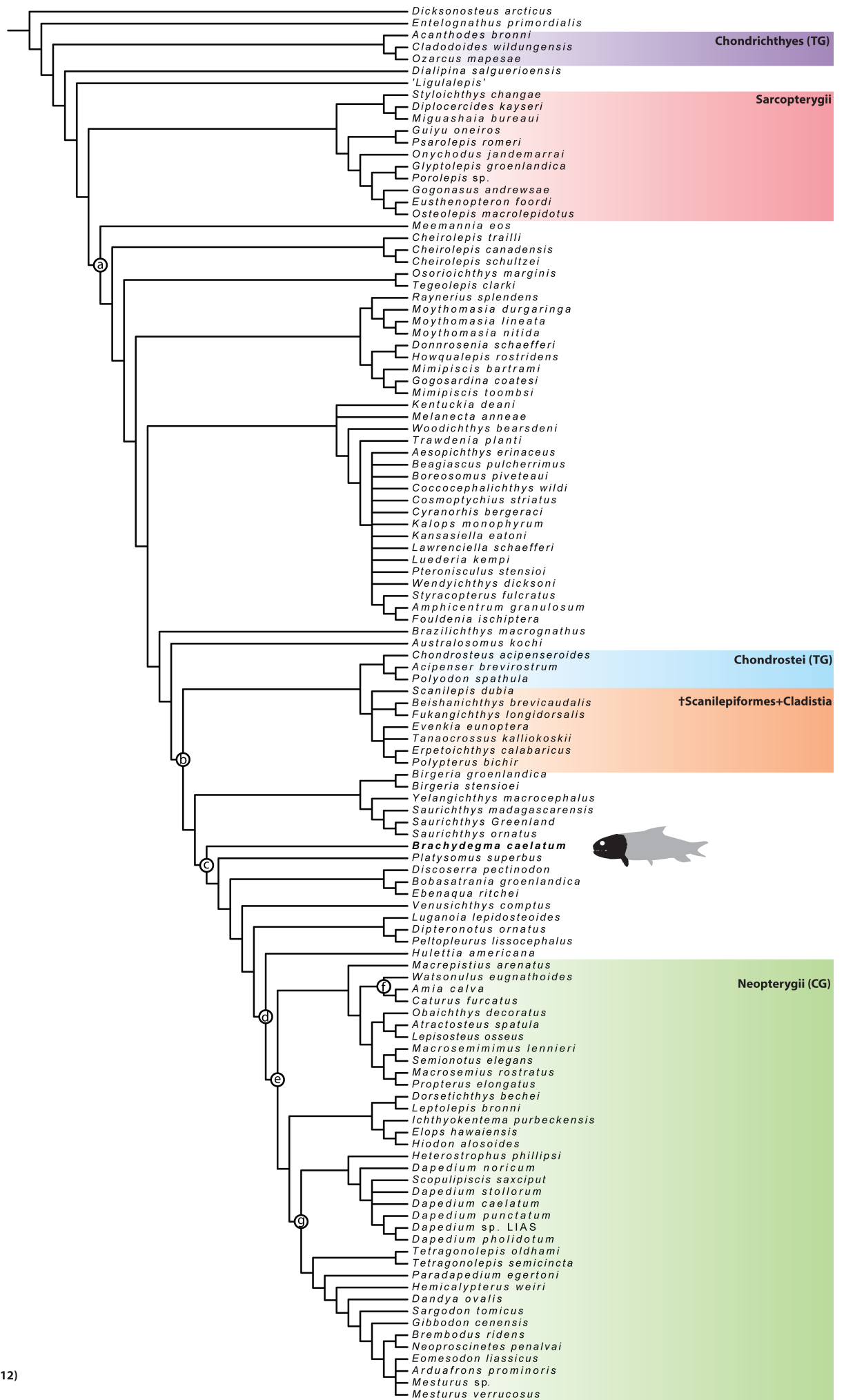
10 mm



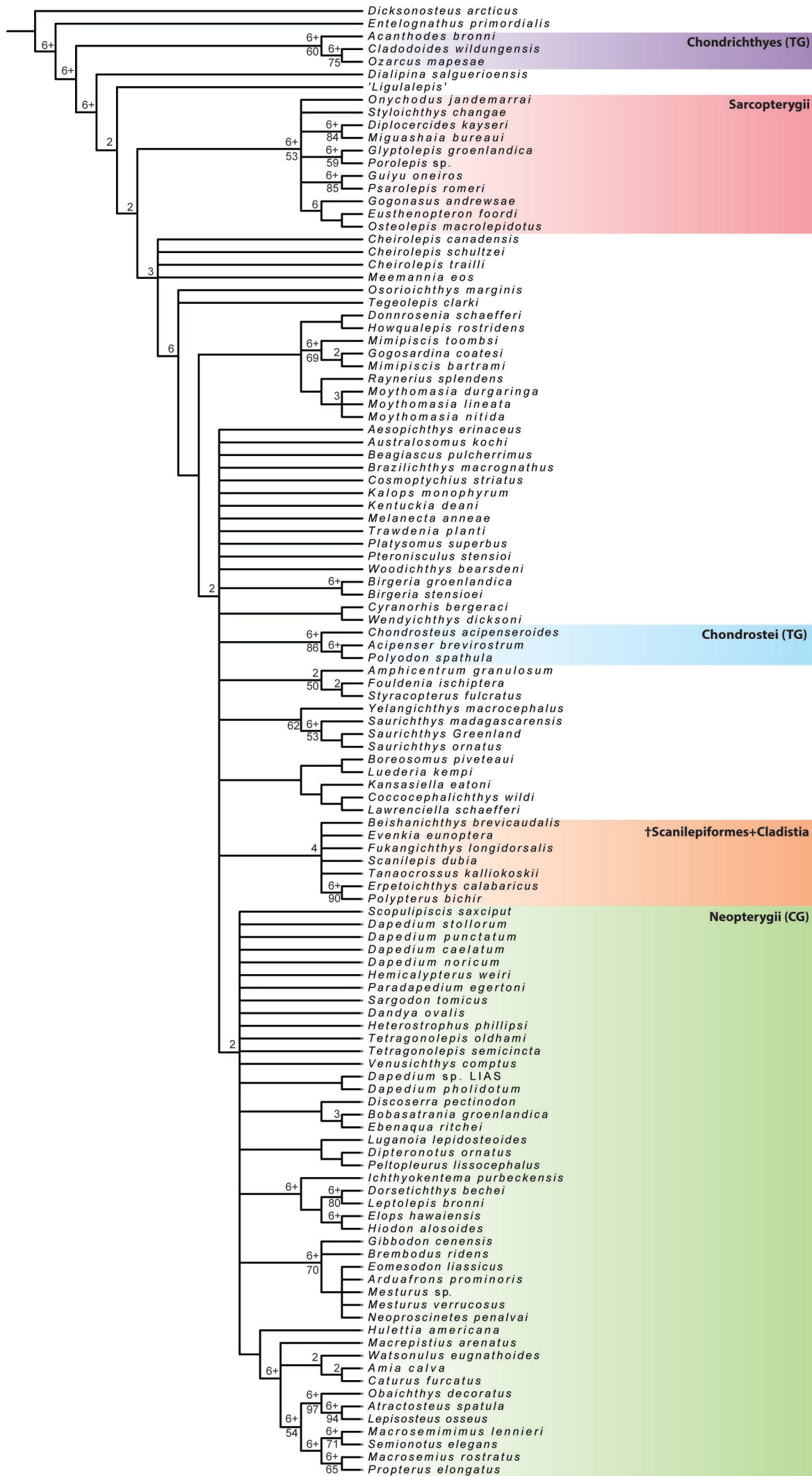


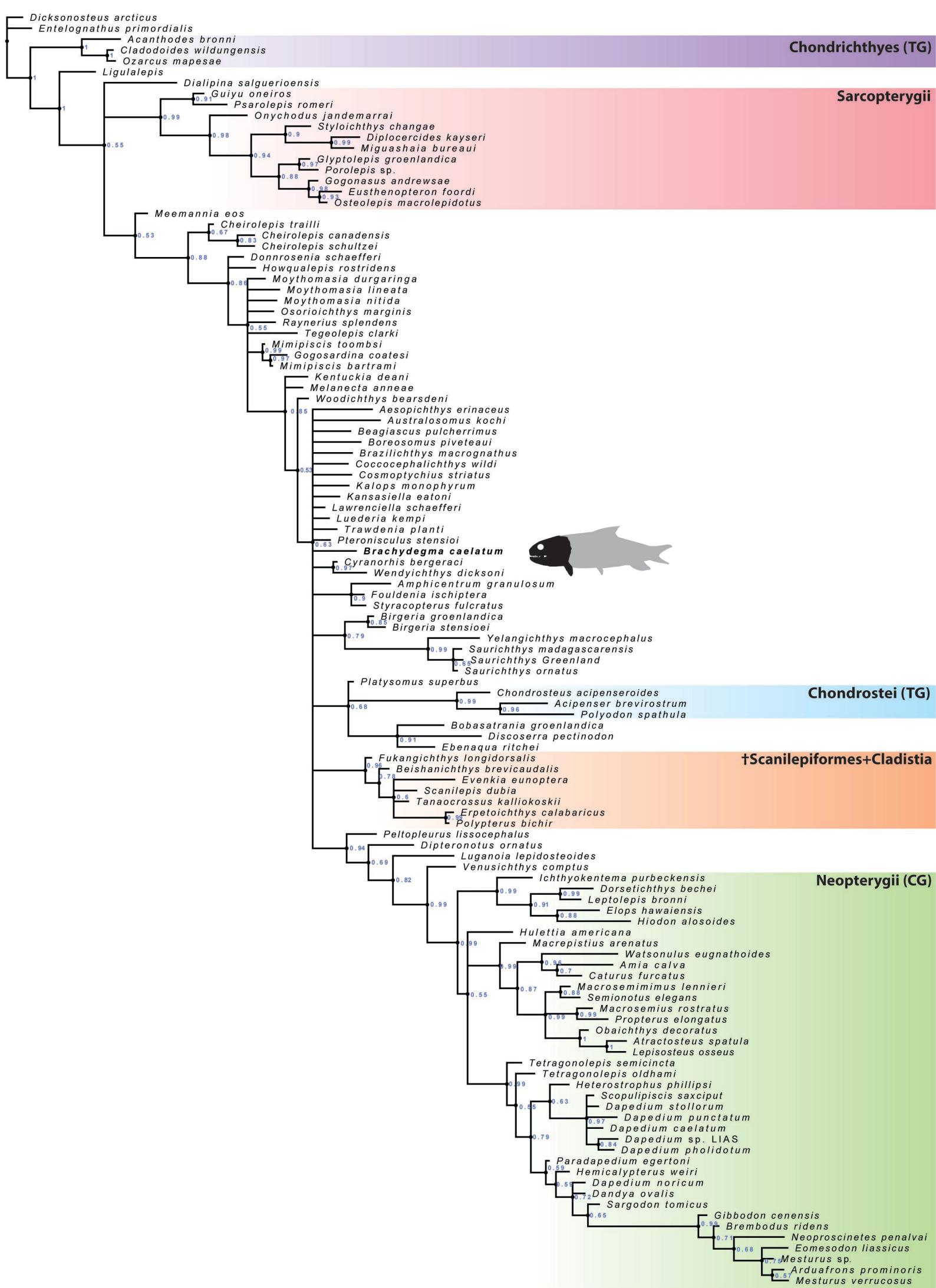






Implied weights (K=12)







†*Pteronisculus gunnari* (NHMD\_73588\_A)



10 mm



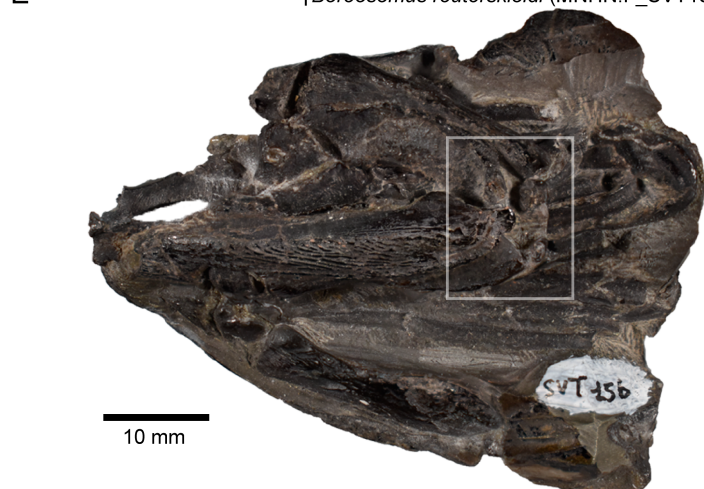
†parasemionotid (NHMD\_74424\_A)



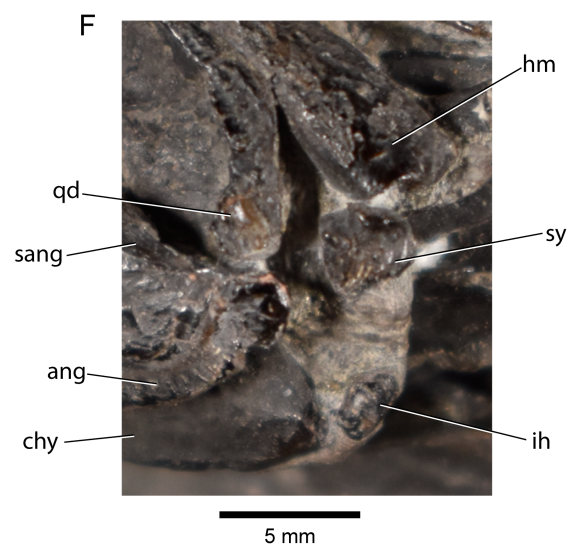
10 mm



†*Boreosomus reuterskioldi* (MNHN.F\_SVT15b)



10 mm



5 mm